EXPERIMENTALLY CHARACTERIZED EMBEDDED MCKIBBEN MUSCLES AS A NASTIC MATERIAL FOR BIOMEDICAL APPLICATIONS

A Thesis

by

OMOTAYO F. EWUMI

Submitted to the Office of Graduate Studies of
Texas A&M University
in partial fulfillment of the requirements for the degree of

MASTER OF SCIENCE

August 2007

Major Subject: Mechanical Engineering

EXPERIMENTALLY CHARACTERIZED EMBEDDED MCKIBBEN MUSCLES AS A NASTIC MATERIAL FOR BIOMEDICAL APPLICATIONS

A Thesis

by

OMOTAYO F. EWUMI

Submitted to the Office of Graduate Studies of
Texas A&M University
in partial fulfillment of the requirements for the degree of

MASTER OF SCIENCE

Approved by:

Chair of Committee,	Terry Creasy
Committee Members,	John Criscione
	Roger Morgan
Head of Department,	Dennis O'Neal

August 2007

Major Subject: Mechanical Engineering

ABSTRACT

Experimentally Characterized Embedded McKibben Muscle as a Nastic Material for Biomedical Applications.

(August 2007)

Omotayo F. Ewumi, B.S., University of Wisconsin - Madison

Chair of Advisory Committee: Dr. Terry Creasy

This study presents the experimental results that characterize a nastic sheet material's performance. We defined nastic sheet as a McKibben muscle designed from a foundation that would be embedded as an array in an elastomer matrix. The goal is to be able to utilize the embedded McKibben sheets in the biomedical industry as an improvement to the synthetic devices and/or processes. One mechanism that might produce these improvements is to mimic the biological materials that form functional organs, biological structures, and active tissues. Linking human technology and natural structures is and will continue to be important to society for several reasons. It would improve: (1) the lifestyle of humans in regards to artificial parts that mimic human parts (which will allow us to live longer), (2) artificial limb functionality, and (3) comfort and aesthetics.

The objective is focused on characterizing and evaluating McKibben muscles as an embedded muscle sheet by building McKibben muscles and testing them alone and in sheets with one, two, three, and five muscles. The sheets would be known as a single, double, triple and quintuple embedded sheet. Another objective is to determine the performance penalty that embedding puts on the material.

The experiments performed used several different approaches, such as analytical models, tensile test analysis, and prototype construction of the specimens. All specimens were designed to have a constant final length of 120mm, being embedded in a polyurethane matrix. We characterized the fundamental performance of a McKibben muscle and each specific embedded sheet. We measured the specimens' work-density and quantified the inactive matrix's impact on work-density.

Based on the results, several improvements were suggested on the fabrication of the specimens. The experiment shows positive potential outcome that could be utilized in the biomedical field, but the results would improve with the suggestions provided in the study. A sample of the results - the actual work-density for both the single and double-embedded sheets showed an increase to 7.82% and 2.96% consecutively. Once the specimens are removed from the mold, the McKibben muscle automatically tries to retract to its initial state while the polyurethane matrix tries to stay at its initial state.

DEDICATION

TO:

MY PARENTS: JOSEPH AND ANU EWUMI

MY SIBLINGS: YETUNDE, SEGUN, LANRE AND TOYIN EWUMI

AND ALL MY FRIENDS

ACKNOWLEDGEMENTS

I would like to thank God for giving me the wisdom, strength and understanding to accomplish one of my goals. I also would like to thank God for giving me the patience to learn and surrounding me with great people.

I would like to acknowledge Dr. Terry Creasy for accepting my offer as my academic advisor and providing guidance with my research quest at Texas A&M University. Dr. Creasy has been a great inspiration by improving my research and technical skills by providing several projects that were teaching tools. I would also like to thank Dr. Creasy for having a very functional lab that prevented the students from being dependent on other people. Dr. Creasy has an exceptional way of encouraging his students, especially when we are frustrated or nervous – they are very comforting.

I would also like to acknowledge the other members of my academic committee: Dr. John Criscione and Dr. Roger Morgan. Dr. Criscione, thank you for being patient with teaching and guiding me with the biomedical terminologies and applications. Dr. Morgan, thank you for being a great professor in polymers. To my committee team, thank you very much for being cooperative with me and each other.

I acknowledge the Mechanical Engineering department machine shops and labs. I would like to send my thanks to Mike Walker, Jim Sajewski, and Johnny Hallford for generously allowing me to use the equipment in the machine shops and labs to perform my testing.

(DARPA), I would like to send my thanks for providing the project and financial

support for performing my research. I want to acknowledge the undergraduate students who worked effortlessly to build parts for my research, Josh Stuart and Jennifer Glaess, and my colleague Sang Jin Lee for patiently providing me the training I needed to perform tests and conduct research. I would like to thank Pranay Asthana for taking his precious time to assist me with the specimens. It was greatly appreciated. I also want to thank friends, Ryan Mathus, Nana and Wara Serry-kamal, Ayodeji Alajo, Joanne Bartholomew, Ndidi Beckley-Lines, Leah Newman, Tobi Omonogun, Seun Olatubi, Catalina Afanador, Dayo Fawibe, Perpertual Amoah, Arshella McIntosh, Bola Onipede, Ron Fuller, and more for continuously encouraging, motivating, and supporting me in my research work. Thanks to Texas A&M University for giving me this opportunity for pursuing one of my dreams and meeting new friends.

Lastly, I want to thank my parents, Joseph and Anu Ewumi, and my siblings, Yetunde, Segun, Lanre and Toyin Ewumi, Yetunde Oloyede, and my extended family, who have always been there to encourage and motivate me while I pursued one of my goals.

TABLE OF CONTENTS

CHAPTER Page

Page

LIST OF FIGURES

FIGURE Page

FIGURE Page

FIGURE Page

FIGURE Page

FIGURE Page

FIGURE Page

FIGURE Page

FIGURE Page

FIGURE Page

FIGURE Page

LIST OF TABLES

CHAPTER I

INTRODUCTION

Nastic biomedical materials might be a great contribution to society. For example, a product that shrinks to pass through a small surgical opening and expands back to its original form would reduce surgery's impact on a patient. Nastic biostructures could assist or replace natural organs and tissues with active materials. One possible device is a muscular sheet. The human muscle is an intricate system; it is so intricate that we do not entirely know how it works. Aristotle, 384-322 B.C., wrote a book entitled "Parts of Animals, Movement of Animals, and Progressions of Animals" to describe muscle actions.[1] Aristotle described how animal groups must be separated into types—such as birds, which have wings—to better understand each group's characteristics. Aristotle described why each animal behaves differently--such as humans with two limbs walk while fish with fins swim.[2] A Roman citizen named Galen, 131-201 A.D., described muscles in his essay "De Motu Musculorum." During the 15th century engineer and scientist Leonardo da Vinci, , 1452-1519 A.D., , procured bodies from the grave and described the muscular and nervous systems.[2] From Aristotle to da Vinci, philosophers and scientists have tried to describe and understand muscle characteristics. [1]The human body has over 600 muscles; these muscles respond electrically and

---

This thesis follows the style of *Journal of Biomedical Materials Research Part B: Applied Biomaterials.*

chemically. [3,4] Muscle tissue produces force to cause body motion or internal organ movement. There are three muscle tissue classes: cardiac muscle, visceral muscle, and skeletal muscle. Chapter II will provide more in-depth information on human muscle functions. Current research has taken the field further; we now design artificial materials to mimic human muscle.

An American atomic physicist, Joseph L. McKibben, invented the McKibben muscle to augment his daughter's arm movement—she had reduced function from poliomyelitis disease [5]. Poliomyelitis, known as polio, is an acute viral infectious disease. The disease attacks the spinal cord and weakens the motor neurons that control the muscles. The McKibben muscle is a rubber tube surrounded by a braid made from strong fibers. The McKibben muscle is a pneumatic artificial muscle that mimics human skeletal muscle. The McKibben muscle contracts when actuated and extends under an external force – for example when you extend your arms your muscle bicep extends as your tricep contracts. When your arm goes into flexion the muscle action reverses: the bicep contracts as the tricep extends. Since it functions by internal pressure, the McKibben is a synthetic nastic actuator.

Nastic motion is a plant's reversible motion during reaction to an external stimulus. Cell growth does not accompany a plant's nastic movements; this allows the plant to respond continuously to the repeated stimuli. Nastic movements occur in two forms such as nyctinastic and siesmonastic movements.[6]. In depth information about nastic concepts appears in Chapter II – this thesis focuses on the seismonastic form. This happens when leaves fold or bend in response to touch, shaking, or electrical, thermal, or

chemical stimulus. [7] This research uses the McKibben muscle with internal pressure to provoke the material to change in a nastic motion.

This thesis presents the experimental results that characterize a nastic sheet material's performance. We define nastic sheet as arrayed McKibben muscles embedded within an elastomer matrix. The experiment test several model arrays– we built products with one-to-five McKibben muscles embedded in a polymer matrix. This sheet changes shape and provides actuation when subjected to internal pressure. The embedded sheets are subjected to an internal pressure similar to blowing up a balloon, the products shape will change from its original shape. Nastic engineering materials were proposed by the Defense Advanced Research Projects Administration (DARPA) as biomimetic systems that combine structure and active functions [8]. Nastic materials might find use in biomedical and structural applications.

1.1 MOTIVATION

Synthetic organs, orthotics, and prosthetics are internal or external devices that assist human living or movement. These devices need improvements that ease installation, optimize function, and enhance cosmetics. [9, 10] One mechanism that might produce these improvements is to mimic the biological materials that form functional organs, biological structures, and active tissues. Biomimetics is the study of "the structure and function of biological systems as models for the design and engineering of materials."[11] It also means trying to design artificial materials to mimic biological characteristics. Biomimetics follows the idea that replicating natural structure flexibility in engineering structures can reduce the gap between human

technology and natural structures [12]. Linking human technology and natural structures is and will continue to be important to society for several reasons: (1) it would improve the human lives because artificial parts can allow us to have longer and more capable lives, (2) artificial limb functionality, and (3) comfort and aesthetics.

1.2 OBJECTIVES

Anything to help improve human mobility benefits society because it allows people to enjoy each day. The research goal is to determine a nastic sheet material's performance as an active material.

This work had these objectives:

- to fabricate and characterize many McKibben muscles and measure their performance;
- to embed McKibben muscles in an elastomer matrix and characterize the sheet's fundamental performance when they contain one, two, three, and quintuple embedded muscles;
- to measure McKibben sheet material work density and quantify the inactive matrix's impact on work density;
- to determine the performance penalty that embedding puts on the material.

We fabricated McKibben muscle to control how the muscle was built and to obtain consistent performance during the experiments. We needed this control because this research requires many specimens. After characterizing the McKibben muscle, we would/should be able to determine what limitations the polyurethane matrix placed on

the McKibben muscle. Characterizing the various sheet sizes allowed us to examine the differences between sheets. These objectives set a foundation for future research with this material.

1.3 SCOPE OF THESIS

This thesis focuses on characterizing and evaluating McKibben muscles as an embedded sheet muscle by building McKibben muscles and testing them alone and in sheets with one, two, three, and five muscles. After characterizing the McKibben muscle, we would/should be able to determine what limitations the polyurethane matrix placed on the McKibben muscle. Characterizing several sheet sizes, would allow us to examine the difference between sheets. The work is primarily experimental and includes data analysis.

Subsequent chapters present specific things: Chapter II holds the literature review; the review provides more in-depth background information on the areas that relate to the research, such as shape changing materials in general and the McKibben muscle in particular. Chapter III introduces the present work. Chapter IV describes the preparations used to make specimens for experiments. Chapter V details the experimental procedures. Chapter VI shows the analytical work. Finally, Chapter VII provides conclusions from the work.

CHAPTER II

BACKGROUND AND HISTORY

Shape changing materials appear in plant and animal species and researchers have worked to copy these functions in synthetic materials. This chapter summarizes the natural and synthetic active materials in general, and it presents McKibben muscle history in particular.

2.1 SHAPE CHANGING MATERIALS

Shape-changing materials refer to any product, species or material that changes its shape in either direction from its original shape. For example, Worms are a shape changing species, their body shape changes as they move or glide along. This is due to their circular and longitudinal muscles that contract while their volume stays constant. [13] The materials can change shape due to several different factors such as mechanical stimuli, chemical stimuli, environmental source and much more. Shape changing material can be defined in two different forms such as a natural or synthetic form.

2.1.1 Natural Shape Changing Materials

This section discusses shape-changing materials that are natural. In this thesis the term natural refers to products from natural, living systems. For example, the Samanea Saman tree—also known as rain tree—has the Nyctinastic movement. Nyctinastic is the plant's sleeping movement; the leaf folds together while the whole leaf droops down as night approaches.[7] The leaf rises up with sunlight.

2.1.1.1 MUSCLE TISSUE

Muscle tissues have mechanical and chemical constituents that play an integral role in muscle function. These characteristics reflect comparable characteristics that would be evaluated in synthetic muscles.

The human body has over 600 muscles.[3] Muscle tissues are embryonic germ cells that have the ability to shorten or contract in an effort to effect body movements. The germ cells operate like an elastic tissue or band. Muscle tissue produces force to cause body motion or internal organ movement; electrical and chemical responses exist in muscles. [4] There are three muscle tissue classes: cardiac muscle, visceral muscle, and skeletal muscle. Cardiac muscle is unique because it is only found in the heart where it controls rhythmic beating. The cardiac muscle is an involuntary muscle and has similar characteristics as the other two; it is an involuntary muscle--like smooth muscle--and contains fibers like skeletal muscle. Muscles that are not controlled by the brain are referred to as involuntary muscles. The visceral muscles are elongated cells called fibers, which include several myofibrils. Myofibrils are located parallel to each other inside the fibers. Visceral muscles are smooth muscles; they contract slowly for a long period. Smooth muscles are involuntary in nature and are located in the stomach, intestines, uterus, and blood vessels. Skeletal muscles anchor to a bone because they move the skeletal bones. Myofibrils are located inside the skeletal muscle, and are smaller filaments; these are the actin and the myosin filaments. The myosin filaments are dark in color while the actin filaments are light. The filament arrangement generates a stripped or striated appearance. [14]

Skeletal muscles always work in pairs that pull in opposite directions—skeletal muscles are voluntary muscles that balance forces from the pair. This makes skeletal muscles the most used muscle class. The skeletal muscle has three contractions: concentric, isometric, and eccentric. Concentric contractions perform work on the body and on objects external to the body. Isometric contraction generates a force without moving the limb. An eccentric contraction generates contractive force as an external action extends the muscle. [15] The eccentric and concentric contractions illustrate that muscles are active whether they lengthen or shorten. An electrical impulse from motor nerves stimulates contraction in skeletal muscles – this causes calcium to move in to and out of the muscle. Calcium is used to transfer information between nerve fibers, muscles are categorized as a nerve fiber. Calcium intake is important to humans; if a diet lacks calcium, the muscle will take it from the bones. Glycogen is the storage bank for the muscle in order to store energy for later.

Henry Gray indicated that "The tension of a muscle is, however [varies] during the course of contraction [it] continually [decreases] during contraction. It is at a maximum at the beginning and gradually decreases." [16] Gray's statement was illustrated in several experiments we performed with regards to force and work vs. distance or time The embedded sheets' tensile characteristics match Gray's theory due to muscle contractions. Woo's theory states that the force generated by the muscle depends on the muscle's length and velocity. [10] Woo's statement does support our force-displacement results on the McKibben muscle and embedded sheets. The contractile system is a highly ordered structure that supports physiological functions. [17] The

contractile system, which is part of the embedded sheets, follows the same pattern as human muscles; this was also noted by Caldwell.

An important factor for determining muscle mechanical efficiency is force variations with speed. [18,16] We performed experiments to verify whether speed variation is a factor for force calculations – similar experiments were performed by Suzuki and Ishwata; Lupton and Hill. [17,19]

2.1.1.2 STRUCTURAL TISSUES

The structure tissue section provides in depth descriptions on plant movement. One plant movement is nastic action, which we want emulate in the embedded McKibben sheets. Nastic materials mimic plant structural tissues, as plants are subjected to external pressure; it changes its shape or movement from original state. Nastic materials are also subjected to internal pressure to follow the same characteristics as a plant.

Plant movements have two forms: tropistic and nastic. Tropism is an organism's involuntary response to an external stimulus; the organism moves its parts either by bending or turning in response to external stimuli. Tropism has three different actions: phototropism is sunlight-influenced plant growth, gravitropism is gravity-influenced plant growth, and thigmotropism is mechanical-energy influenced plant growth [6]. Nastic motion is a plant's response to an external stimulus. This thesis focuses on plants' nastic ability. Nastic could be an irreversible growth form or a reversible movement response. Cell growth does not accompany nastic movements; this allows the plant to respond continuously to the repeated stimuli. Nastic movements occur in two

forms such as nyctinastic and siesmonastic movements. Nyctinastic is the plant's sleeping movement; the leaf folds together while the whole leaf droops down as night approaches. The leaf rises up with sunlight. The Samanea Saman tree—also known as rain tree—has this movement. Another nastic movement form is called seismonastic motion, which happens when leaves fold completely or bend in response to a touch, a shake, or an electrical, thermal, or chemical stimulus. Seismonastic movement is also noticeable when the plant is low on water. Mimosa pudica is a perennial plant that performs the seismonastic movement. Mimosa pudica is a native plant in Brazil and have adopted in other countries. Mimosa is from the Greek word meaning to mimic and pudica is Latin meaning to shrink or retire. [7]

The nyctinastic mechanism is currently in debate. There are several discrepancies in the early plant movement theories. In the 19th century, as scientists observed the mimosa's movement, the previous hypothesis that plants has nerves and muscle tissues similar to animals were rejected. [20] Experiments proved that mechanisms other than turgorism contribute to leaf movement in nycitinastic plants; the mechanisms differ for each plant family. [21]

Temperature, light, pH, salinity, and electrical charge are typical environmental stimuli. The mimosa's pulvinus, which is its motor organ, is located between the stem and the petiole, which is the leaf stalk. It also has secondary pulvini for each leaflet. The pulvini are what characterize the drooping movement the leaves show following mechanical stimulus. The driving force is turgor pressure loss, which is the outward force exerted upon the cell wall by the water contained in the cell. Turgor is tension in

the cell membrane caused by water contained in the cell. [22]

Another natural tissue structure example is the worm. Worms that fall into the categories acoelmate, nemerteans, and turbellariana can change their shapes. This shape-changing role is due to the circular and longitudinal muscles. Nematodes have high internal hydrostatic pressure. Contracting their longitudinal muscles increases turgor pressure because the worm's volume is constant. [13] Worms and plants are structural tissue, which is why we consider them here to describe how we might mimic their characteristics

2.1.2 Synthetic Shape Changing Materials

This section presents shape-changing materials that are synthetic. The term synthetic refers to materials created by humans.

2.1.2.1. SHAPE MEMORY ALLOYS

Shape memory alloys (SMAs) are synthetic materials that have been designed with the ability to return to its original state after undergoing thermal process. The embedded McKibben sheet is emulating shape memory alloy characteristics. The embedded McKibben sheet changes shape when responding to an internal force and returns to its original state after the force is removed. To better understand different phase changes in shape memory alloys, the remaining paragraphs provide in-depth information.

"The term shape memory alloy (SMA) is applied to that group of metallic materials that demonstrate the ability to return to some previously defined shape or size

due to thermal procedure." [23] Shape memory alloys are also known as smart materials—although they possess no data processing ability. Reji John's description for smart materials, "the ability to respond to changes in pressure, temperature, moisture, pH or electric and magnetic fields." [24] Shape memory alloys have undergone substantial development during the last 70 years. The following paragraph provides a brief history.

Otsuka and Wayman discovered shape memory alloys in the early 1930s, while Chang; Read and Olander observed how gold-cadmium alloy's (Au-Cd) reversibility from plastic deformation and pseudoelastic behavior.[25] Au-Cd composition was one example of shape memory alloys that had the characteristics of shape memory alloys Other material compositions that could go through several phase changes such as copper-zinc (Cu-Zn), copper-tin (Cu-Sn) and copper-aluminum-nickel (Cu-Al-Ni) were discovered in the late 1930's and early 1950s. Greninger, Mooradian, Kurdjumov and Khandros, scientists during this timeframe, discovered those properties respectively.

Utilizing shape memory alloys in the medical industries was a breakthrough discovery in the late 1960s and early 1970s. Buechler and co-workers at the US Naval Ordinance Laboratory discovered the shape memory effect in nickel-titanium (Ni-Ti) alloy, patented it, and named it Nitinol. Nitinol contains 50% Ni and 50% Ti. [26] Over the years several researchers and scientists were able to utilize Nitinol in the medical fields. For example, Johnson and Alicandri surgically implanted Ni-Ti bone plates into beagles and determined its biological effects. Simon et all utilized Nitinol as a blood filter, which is a vascular device to prevent artery blockage to the lungs via a blood clot. [27] Dental appliances such as braces were designed from Nitinol by Dr.

Andreasen from the University of Iowa in 1975. [28] Other Nickel-titanium breakthroughs in the medical field were discovered by Cutright et al. in 1973 [29], Iwabuchi et al. in 1975 [17], and Castleman et al. in 1976 [30]. Applying embedded McKibben sheets in the medical industry would be an addition and improvement to what has already been discovered; it would provide a different material in addition to being more aesthetically pleasing. The following paragraphs describe shape memory alloys' phases.

SMAs can undergo an apparent permanent plastic strain and then return to their original shape when subjected to a thermal process. SMAs generate high forces if the alloy is constrained during the thermal process. An SMA has two crystallographic phases: austenite, and martensite. Austenite is stable at high temperatures and meta-stable at low temperatures. Martensite is the stable, low temperature phase and applied stress can induce the martensitic transformation in undercooled austenite.

Smart memory alloys are used in aerospace and biomedical applications. In the aerospace industry smart memory alloys control vibration in slender structures like solar panels. [31, 32] SMA robotic actuators mimic human muscle movement. [33, 34] Smart memory alloys are studied as external embedded actuators in composite materials. [35]

The biocompatibility is important if the alloys are implanted—for example, as cardiovascular devices [36]—or used in surgical instruments. [37] The alloy must not produce allergic reactions inside the body, nor can it release any ion into the blood stream. [38]

SMA behavior is controlled by three parameters: stress, strain, and temperature. [39] The most common shape memory alloys are copper-zinc-aluminum (CuZnAl), copper-aluminum-nickel (CuAlNi), and nickel-titanium (NiTi). Nickel-titanium shape memory alloy has three different forms; two forms are temperature dependent. The three structures are martensite, which exists at low temperature; austenite, which exists at high temperature; and stress-induced martensite, which is superelastic. When the material is in its martensite form it is soft, ductile, and deformable. Simon created a cardiovascular device used to filer clot from the blood, the device enters the patients body a martensite state then changes to its original state afterwards in its stress-induced martensite form it is highly elastic and similar to rubber in its austenite form the material is hard and similar to titanium. Nickel-titanium's shape change is temperature-dependent. When extended beyond its maximum elastic strain, nickel-titanium deforms in plastically by slip, which is irrecoverable, i.e., there is no memory effect. A one-way shape memory effect happens when nickel-titanium returns to its original shape at the martensite form. The two-way shape memory effect occurs when the nickel-titanium takes on an alternate shape upon cooling. Composite SMA products discovered by Rayhenan. [40, 41, 42] Stalmans and Humbeeck noted some shape memory alloy advantages like high power-to-weight ratios, reversible strains, and high stresses. [43] The embedded McKibben sheets are similar in character with the one-way shape memory effect; it has not yet been determined if the experiment would work as a two-way shape memory effect.

2.1.2.2. SHAPE MEMORY POLYMERS

Understanding the difference between shape memory alloys and shape memory polymers will allow us to determine what characteristics we would like the embedded McKibben sheet to mimic.

Shape memory polymer is a new field, especially in the biomedical industry. Shape memory polymers are similar to shape memory alloys, but they have larger deformations. Shape memory polymers are materials that can take a secondary shape due to an external stimulus such as temperature or sunlight. Shape memory polymers can increase to four times their original size or shape. [21] Other shape memory polymer advantages are that polymers are inexpensive, bio-degradable, and bio-compatible. Shape memory polymers are like rubber and glass; this is a unique combination. [44] When the shape memory polymer is heated below its glass transition (T_g) level the SMP is hard as glass while the SMP's temperature above the T_g level will be soft as rubber.

What allows shape memory polymers to change drastically? There are different shape memory polymers. A light-activated shape memory polymer resulted when researchers added photosensitive agents to the polymer network. When the shape memory polymer absorbs light it can change its shape. A few commercialized shape memory polymers are Veriflex, Memori, and Calo-Mer. In 1984 Veriflex was introduced in the United States from Japan. Veriflex is a polymer that thermal stimuli affect. Calo-Mer is a thermoplastic shape memory polymer stimulated thermally; however, Calo-Mer has no covalent crosslinks.[45]

Currently the medical industry is the primary shape memory polymer consumer because of the polymers' historical background. In 2001 Lendlein and Langer reported on biodegradable shape memory polymers. [46] Professor Robert Langer and his German colleagues discovered the shape memory polymer that is induced by light. [47] These discoveries led to smart sutures that tie themselves into a knot in spaces too confined for manual tying.

2.1.2.3. OTHER ACTIVE MATERIALS

There are other synthetic materials such as electroactive polymers (EAP), shape memory actuators, hydrogels, ceramics, and others.

Electroactive polymer/metal composites change dimensions when activated by small DC voltage. Another smart gel was the artificial muscle surface wipers and robotic arm mover. [24] The electroactive polymers are interesting because they can mimic biological muscles—especially when large strains are desired. Polymer is increasingly becoming a common material to be used in different industries. Other electroactive polymers that produce large displacements are the ion exchange membranes, gels, perfluorinated sulfonic polymers, self assembled mono-layered polymers, electrostrictive, electrostatics, and piezoelectrics polymers. [48] Bor Jang showed that functional polymers can improve a system – modulators, modifiers, self-generators. Bong confirms that polymer is being utilized for more than its initial concept. [49] A polymer that is a modulator has the capacity to regulate or adjust a system– meaning that the polymer is being used to create a change as an improvement or opposite direction in to the system its being applied to. A polymer that is a modifier has

the capacity to make a difference to a system, on either extreme. To utilize a polymer as a modifier is important because it can be used to improve or decrease characteristics. For example, if we would like to increase the work efficiency in a system, it improved with a contracted polymer that is a self-generator has the ability to evolve into itself. A self generator polymer would have the ability to return to its initial state without any external force – this can be used for applications where the initial and final states are different.

A familiar shape-memory polymer application is the memory foam pillow. The pillow conforms to the individual's body but returns to its original shape once the individual moves.

2.1.2.4. MACHINE AUGMENTED COMPOSITES

A new material in the shape memory family is the machine-augmented composites. Machine augmented composites (MAC) are matrices embedded with an array of simple machines. The simple machine in the matrix could be a fluid-filled tube or any material that can be expanded from external stimuli. The flow through the simple machine dissipates energy that causes the machine-augmented composites to have dynamic characteristics.[50, 51] This is important because it can drastically increase or decrease a specific characteristic in a short period. Machine augmented composites were first introduced by Gary Hawkins in 2002. [52]

2.2 MCKIBBEN MUSCLES

The McKibben muscle is a pneumatic artificial muscle designed to mimic human muscle, i.e., it is a biomorphic device. A biomorphic device resembles a biological

structure in shape or characteristics.

The McKibben muscle has an inner rubber tube with a braided sleeve as an outer shell with the ends tightened down – it can use either gas or liquid as the flowing fluid. As the McKibben muscle is pressurized, the inner rubber tube expands longitudinally and transversely, as a result, the rubber tube creates tension against the braided sleeve, which also expands. As the braided sleeve expands, the helix angle between each strands increases and the length decreases; this creates a contraction force. – contraction force supplies work, for example you can supply working utilizing a McKibben muscle to an external source. [53, 5] In the article written by Yoseph Bar-Cohen, two McKibben muscles were placed in antagonism (one muscle contracts concurrently the other relaxes and vice versa) method to act as the arms muscle. They found three parameters that define the muscle's static behavior. These are its initial length, its inner radius, and its initial braid angle; from these parameters the muscle's maximum force, radial size, and contraction length range are obtained easily. [54]

The McKibben muscles is used as a pneumatic actuator because it has a smooth and natural movement similar to human movement plus it has a high force to weight ration – also inexpensive.[55] The McKibben muscle has been considered to be an actuator. When a device can convert energy into a mechanical form it is termed actuation. The McKibben muscle has good actuator characteristics. For example, it generates high force per volume, and it is compact. [54, 56] The rubbertuator, a pneumatic actuator is a reinvented McKibben muscle that Bridgestone Tire Company introduced in the 1980s. The rubbertuator was design with spring characteristics and is

light weight. The rubbertuator is a rubber tube with intertwined fiber cord sleeve and metal fittings at each end. The rubbertuator was designed to be used in robotic application, to mimic human hand movement. [57]

When the inner rubber bladder or tube is pressured it uses this pressure to push the inner surface against the outer shell and this will allow volume to increase The actuator will shorten because the braided shell's fiber angles enable a scissors motion; this is reflected in the experiment as internal pressure is added to the McKibben muscle. The graphical results show that the rising tension paths are consistent but the tension falling paths are different, a goal we are plan to achieve is to determine why and what causes this trend.. The tension-length cycle reflects hysteresis, meaning will the material return to its original state and did it create a lag in the system, due to coulomb friction. This is caused by the contact between the inner bladder and the outer shell, plus the braided fibers.[58]

This article written by Bertetto and Ruggiu in 2004, "Characterization and modeling of Air Muscles" focuses on characterizing the McKibben muscle and designing a straight-fiber muscle using finite element analysis (FEM). The straight fiber muscle is designed similarly to the Pleated pneumatic muscle by Daerden, etc. The results from the experimental and numerical tests agreed. This shows that the straight fiber muscle can pull in five times the force produced by the McKibben muscle. [59] Klute and Hannaford, developed a modeling system to determine a McKibben muscle's fatigue life, the modeling system was focused on the rubber tube.[60] Other testing and characterizations were performed on the artificial muscles in 1993 [61], in 2003 [62],

and 2003. [63]

A new Pneumatic Artificial Muscle (PAM) was created and named the Pleated Pneumatic Artificial Muscle (PPAM) – is an improved McKibben Muscle. PAMs are contractile and linear motion devices operated by gas pressure. As the membrane is inflated or deflated, the device bulges out or slims down respectively. The pleated pneumatic artificial muscle prevents dry friction between the tube and the braid and reduces hysteresis, which is a McKibben weakness. The PPAM concept is that once it is pressurized laterally the outer pleated material will unfold outwardly without friction from the tube--this suggests actuation with no or low hysteresis. [64] The pleated pneumatic artificial muscle has been investigated for automation and robotic (Bipedal Robots) applications. [65, 66, 67]

The Shadow air muscle, which is a commercial McKibben muscle, is a device that provides a pulling force and behaves similarly to a biological muscle. The pneumatic cylinders produce a small force over a long movement; the Shadow air muscle produces a higher force over a short movement with low air pressures – this shows that the shadow air muscle is an improvement over the pneumatic cylinders because in a short period a change will occur. [68]

2.2.1 Examples of McKibben Muscle Use

The Air-bug, which is a six-legged walking machine, was a cooperative development with FESTO and uses its fluidic muscles – currently the majority of fluidic muscles are used in robotic applications. The Air-bug was displayed at the Hannover Fair in 2001. Airbug is a six-legged walking machine that uses FESTOs fluidic muscles – each joint had (2) muscles working in antagonistitc process.[69,70] Other robotic applications are reported by Bar-Cohen, Y. [71], Caldwell [72], and biological applications by Klute et al. [73], Caldwell et al.[74] This article focused on designing and testing a light-weight powered orthosis for the human lower limb that was able to provide torque to the planar (2-dimensional movements) and dorsi (ability to bend backwards and forward) flexion while walking. The orthosis was designed from a carbon fiber shell, hinge joint and two artificial pneumatic muscles. The artificial pneumatic muscles have an inner latex tube, a braided polyester sleeve as the shell, plastic pneumatic fittings for the end caps and nozzles, with air hose clamps from McMaster-Carr. The results showed that the orthosis was very comfortable to wear without interfering with walking. [75] Their pneumatic artificial muscle concept will have a membrane that will expand radially and contract axially when inflated, while generating high pulling forces along the longitudinal axis. To prevent hysteresis and friction, they utilized a sleeve that was radially laid out like a pleated sleeve. Hysteresis is the lagging effect between a change such as an increase or decrease in power or source or the response to the source. Pneumatic artificial muscles only generate force when shortened; therefore, they designed the robot with a bi-directional joint that has two

muscles opposing one another. [67]

The experiments conducted focused on the McKibben muscle built in-house using latex rubber tube with a polyethylene terephthalate (PET) braided mesh sleeve. The experiments also involve an array of McKibben muscles being embedded in a polyurethane matrix.

The next chapter focuses on current projects related to the McKibben muscles.

CHAPTER III

PRESENT WORK

The McKibben artificial muscle an ongoing interest because scientists and researchers are developing uses beyond the original concept. In addition, continuing material improvement increases the products performance

The project documented in this thesis uses an embedded McKibben array in a polymer sheet as a nastic material for biomedical uses. The McKibben muscle sheets components include the inner elastomer tube, the rigid polymer braided sleeve, and the elastomer matrix. The McKibben muscle was broken down into individual components to measure each component's properties such as the tensile strength, stress, strain and Young's modules. Once the McKibben muscle was characterized, the next several experiments focused on embedded McKibben muscles. This thesis focused on a pre-stretched McKibben muscle that was embedded in a polyurethane matrix in different assemblies such as: single embedded muscle, double embedded, triple embedded and quintuple embedded McKibben sheets. Equipment used for the assessments were self-built – built encasing mold for the embedded sheets, built holding devices, trying to create a consistent control over the specimens and the testing. CNC machines were programmed to cut the mold used to embed the McKibben muscles into the polymer matrix. Lathes cut the plugs used in the McKibben muscles. Tensile test equipment in the mechanical engineering department was used to test each specimen. Special clamps were purchased holding device to hold specimens and some components to build

McKibben muscles.

The subsequent chapters will cover detail aspects of the experiment, such as material preparation for each component of an embedded McKibben muscle, experimental procedures of all analyses performed, as well as the presentation and analysis of the results and the conclusions.

CHAPTER IV

MATERIAL PREPARATION

This chapter describes the components used to build the McKibben muscles and embedded sheets. To enable new specimen construction, the material suppliers and specification are summarized for each component.

4.1. ELASTOMER TUBE

McMaster Carr sells this elastomer tube as part number 5234K241. The elastomer tube is latex rubber. Latex material will allow the part to spring back to the original shape after it has been bent, stretched, and compressed. It is also a flexible, smooth, and resilient material. It is an unreinforced single-line tube with outer diameter 4.7625 mm (0.1875 in), inner diameter 3.175 mm (0.125 in), and wall thickness 0.7938 mm (0.03125 in). The tube's color is translucent and amber in color. The elastomer tube is safe at a 0.138 Mpa (20 psi) when the temperature is 21.1 °C (70 °F). Its operating temperature is between -17.8 and 70 °C (0 and 158 °F). This particular elastomer tube resists abrasion and it is very soft; and its durometer rating is 35A. The elastomer tube's tensile strength rating is 27.6 Mpa (4000 psi) with 850 % elongation-to-failure.

The vendor sells this elastomer tube in 7.620 m (25-ft) spools. Specimens had an active, i.e. inflatable, section 40 mm (1.57 in) long. Tubes are 8 to 10 mm (0.32 to 0.39 in) longer outside of the active region; this extra tubing holds the aluminum fittings. A

paper sheet with lines marked 40 mm (1.57 in) apart with extra length for the aluminum tubes acted as a cutting guide. The tube, which was under only enough tension to straighten it without stretching it, was positioned over the guide and cut at the lines on the paper. Figure 1 shows a latex tube sample.

Figure 1. Latex rubber tube purchased from McMaster Carr.

4.2. ELASTOMER MATRIX

The flexible, polyurethane-elastomer matrix came from Freeman Manufacturing and Supply Company (FMSC), located in Avon Ohio. This matrix is soft with 40A Shore hardness. We purchased the one-gallon kit (FMSC Type 1035, product code 055401, Part A lot number 65091, and Part B lot number 55188). This kit has a one-to-one mixing ratio by either weight or volume. Part B contains nonhazardous polyol, diethyl toluene diamine, di(methylthio) toluene diamine. Part A contains polyurethane polymer and bis(2-ethylhexyl) phthalate. This polyurethane elastomer gels in 30

minutes when the temperature is 22.2 °C (72 °F). The demold time is 16 hours at 22.2 °C (72 °F). This polyurethane has a tensile strength at 3.102 Mpa (450 psi) and a 9.81 x 10^{-4} m^3/kg (27.2 in^3/lb) volumetric yield.

This soft polyurethane elastomer is the embedding matrix in building the specimen. The matrix is mixed after the McKibben muscle is placed in the mold because the polyurethane elastomer has a short gel time. Figure 2, shows dogbone specimens made from the flexible polyurethane specimen and Figure 3, illustrates polyurethane's chemical structure.

Figure 2. Elastomer matrix built into a dumbbell shape for testing.

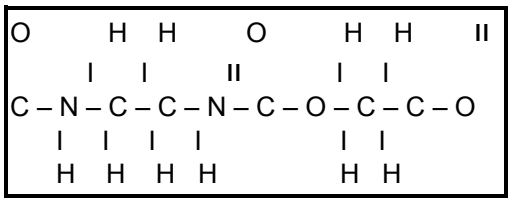

Figure 3. Polyurethane's chemical structure.

4.3. RIGID POLYMER BRAID

The polymer braid that sheathed the tube came from McMaster Carr (general purpose braided polyethylene-terephthalate (PET), part number 9284K511, FLEXO sleeving by Techflex Incorporated Spartam, New Jersey). PET is a thermoplastic polyester. This braid—when in its natural, relaxed condition—has a 3.175mm (0.125 in) inner diameter. The braid covers tubes or wires with a nominal diameter between 2.3813 to 6.35 mm (0.09375 to 0.25 in). The standard spool holds 100 feet. Its operating temperature is at 125 °C (257 °F). The braid was designed to be flexible and durable; in addition it dissipates heat and moisture through its openings. This braid resists chemical attack and abrasion because it is a polyester material.

The braided polyethylene terephthalate sleeve used to build the McKibben specimen uses at least 125 mm (4.92 in) length with some extra 20 to 40 mm (0.79–1.57 in) in length for fittings and loops. To create consistency, we measure out the length on paper that is used as a gauge before cutting it. A hot knife is used to cut the braided sleeve without it fraying. Figure 4, shows the braided PET mesh sleeve and figure 5, illustrates Polyethylene terephthalate's chemical structure.

Figure 4. Braided PET mesh sleeve purchased from McMaster Carr.

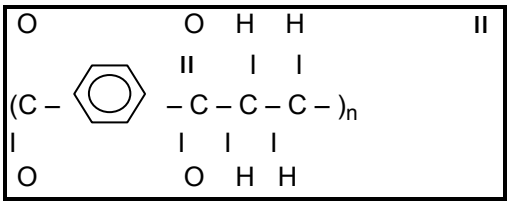

Figure 5. PET's chemical structure.

The aluminum rod was purchased from McMaster Carr, with an outer diameter of 3.175mm (0.125 in). The aluminum rod is cut into small sizes of about 4-6 mm (0.16-0.24 in) for the fittings utilizing the lab's bandsaw. Utilizing the minilathe in the lab, the small aluminum rod is ground further down with a groove in the middle to fit both the latex rubber tube and the black plastic tube. Two undergraduate students built aluminum fittings ahead of time to be more efficient. Figure 6, is an example of the aluminum solid fitting.

Figure 6. Aluminum solid fitting built in-house.

The black plastic tubing used for making the McKibben muscle is nylon 6 material, purchased from McMaster Carr (part number 5173K53, black color). The tubing is rigid, impact resistant, and withstands vacuum of 759.46 mm (29.9 in) Hg at 21.1 °C (70 °F). This nylon is nontoxic and it can resist most chemicals. This tubing's allowable use temperature ranges from -40 to 121.1 °C (-40 to 250 °F). The nylon 6 tubing has a tensile strength of 62 Mpa (9000 psi) and an elongation to failure of 250 percent. This tubing has a 3.5052 mm (0.138 in) inner diameter and a 4.7625 mm (0.1875 in) outer diameter; therefore, the tube wall thickness is 0.635 mm (0.025 in). The black nylon 6 tubing was cut into convenient lengths as shown in figure 7. Since the tube is rigid, longer give more flexibility and make the plumbing of the material easier.

Figure 7. Black nylon 6 tubing purchased from McMaster Carr.

The double-pinch clamps are zinc plated steel hose and tube clamp, (McMaster Carr part number 6541K34). These clamps can join tubes and fittings with a diameter between 5 and 7mm (0.2033 and 0.2813 inches). Figure 8 is a photograph of two double-pinch clamps. These clamps slide over the tube and a fitting, which may be a union or a terminating fitting. A special pinch tool plastically deforms the 'ears' on either side of the clamp to reduce the clamp's diameter and put the tube and fitting into a compressive seal.

Figure 8. Zinc plated double pinch hose and tube clamp purchased from McMaster Carr.

4.4. MCKIBBEN MUSCLE

One McKibben muscle can be built from the following materials:

1. one 40 mm (1.57 in) or longer elastomer tube
2. one 125 mm (4.92 in) or longer braided polyester mesh sleeve
3. two 4-6 mm (0.16-0.24 in) aluminum fittings; one with a through hole; these were purpose-made in the Creasy laboratory; aluminum fitting with "through hole" will be called pressure supply fitting and without the hole will be called end seal fitting
4. one plastic tube can be any length, use for guiding the compressed nitrogen into the McKibben muscle will be named pressure supply tube
5. two double pinch hose clamps

The McKibben Muscle is built using the following steps: (section 23)

On a paper sheet we marked the target length for the latex elastomer tube and the braided polyester mesh sleeve – this would be used to verify the length before the final build. The second step, would be to cut or lay out all materials that are used. Then assemble the pressure supply fitting to one end of the black plastic tube – to make sure that the air flows through and into the McKibben muscle. If you run into problems, the plastic tubing can be heated to soften and must quickly assemble before it cools. Another option would be to make sure the aluminum fittings are slightly smaller than the plastic tube's inner diameter for a tight fitting.

Fourth step, place one end of the latex elastomer tube over the pressure supply tube and the pressure supply fitting subassembly created in third step. Fifth step, involves that the braided polyester mesh sleeve must have a small hole cut into it, to allow the pressure supply tubing to pass through it – the pressure supply tube should not pass through the other end of the braided polyester mesh because it would prevent the creation of loop needed. To assemble the braided polyester sleeve with the assembly in step 5, slide the free end of the plastic tube into the braided sleeve until it comes out of the hole on the other end

Seventh step, the end where the hole is on the braided sleeve, we have some of the material left. This material is used to create a loop at that end. This loop must be held in place with one of the double pinch hose clamps. The clamp can be assembled from either end of the sub-assembly; it needs to hold the loop end of the braid to the braided polyester sleeve to the latex elastomer tube to the pressure supply tube to the pressure supply fitting. Note: Crimping tool is used to tighten the double pinch hose clamps.

Ninth step, the other end of the sub-assembly, where the end seal fitting is located needs to be slowly pushed with the latex elastomer tube to almost the end of the braided polyester sleeve. This should be the opposite end of the plastic tube. As the end seal fitting gets closer to the end, the gage length of the muscle needs to be confirmed when stretched with the measurement on the paper; this is before we clamp the other end with the last double pinch hose clamp. Tenth step, there should be some more material that is left after the 125 mm (4.92 in) length has been reached. The remaining material is

shaped into another loop for that side and held in place to the braided polyester sleeve and the end seal fitting with the double pinch hose clamp.

Eleventh step, once the muscle has been completely assembled, verify that the extended gage length is 125 mm (4.92 in). The achieved gage length is the distance between the inside of the hose clamp (gage length can be characterized differently). Final step, once the McKibben muscle has been built, we test every muscle by using an air compressor in the lab to check for leaks. Figure 9, shows a McKibben muscle.

Figure 9. An example of a McKibben muscle built in-house.

4.5. EMBEDDED MCKIBBEN MUSCLE

An embedded muscle is when a McKibben muscle is embedded in a different material that would allow alter the specimen's property. In this experiment we embed the McKibben muscle into a flexible polyurethane matrix to investigate what properties were diverged.

A single McKibben muscle is constructed from these materials:

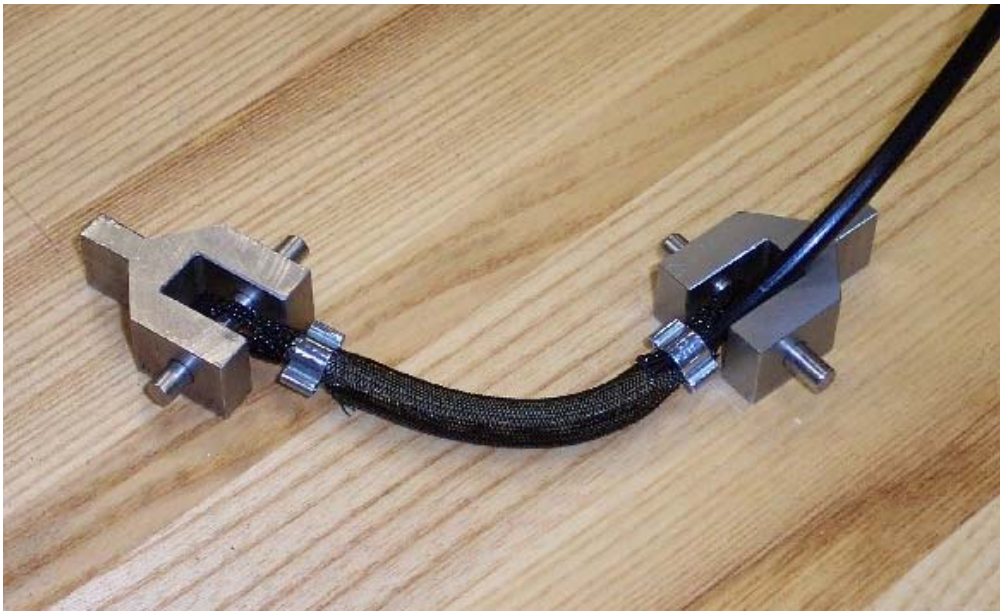

Figure 10. A complete McKibben muscle with clamps.

All molds were made of machinable wax material and designed on Solidworks software, then transferred to the lab's CNC machine to be built.

A Single Embedded McKibben Muscle is constructed by following these steps - We performed this experiment as specified in section 23; however we had to add extra steps to complete the construction of a single-embedded McKibben sheet. After following the instructions in section 23, we have to allow the muscle to be free of the polyurethane matrix, we coat the McKibben muscle in silicone paste – making sure the holes in the braid are filled also. At this point, we can mix the polyurethane elastomer at 1 to 1 ratio by weight. We pour some of the polyurethane elastomer into the mold to make sure that the McKibben muscle is fully covered. Secondly, the McKibben muscle is placed into the mold where the loops would be attached to two aluminum rods that are more than 125 mm (4.92 in) in-between them – this process is easier with four hands or

have the mold clamped down. This shows that the McKibben muscle would be completely stretched to its extended gage length, while the polyurethane elastomer matrix is at its neutral stage. Finally, the remaining polyurethane elastomer matrix is poured over the McKibben muscle to completely cover the top and fill-in all gaps or bubble.

The polyurethane elastomer matrix has a gel time of 30 minutes, so you will need to work fast. If you run into any problem that will cause the matrix to gel, you can mix-up another batch and add that to the mold without any discernable interface between the batches. If the polyurethane batch that was mix did not completely cover the specimen, quickly mix another batch to pour over the specimen. Demold time per McMaster Carr was 16 hours, if I made the specimen today it would be demolded the next day. We did find out that if the specimen was left in the mold for over 48 hours, the specimen would initially not respond as it should – meaning it should curl but if the specimen is left outside the mold for about the same period it would respond as it should. Once the embedded McKibben muscle has been removed from the mold, the specimen is ready to be tested. Figure 10, illustrates a single embedded McKibben muscle. Figure 11, is an example of a single embedded muscle, while figure 12 is the equipment setup used for testing.

Figure 11. An example of a single embedded muscle built in-house.

Figure 12. Instron 4411 with computer and compressed nitrogen bottle.

CHAPTER V

EXPERIMENTAL PROCEDURE(S)

The objective of this section is to describe and define the experimental testing procedures performed in each area.

5.1. TENSILE TEST OF ELASTOMER TUBE

The internal elastomer tube inside the McKibben muscle is made from latex rubber. The latex rubber tube was characterized mechanically with a tensile test procedure. Instron 4411 apparatus located in a Texas A&M University Mechanical Engineering lab was used to perform the series of tests. The Instron 4411 apparatus connects to a computer that stores data. Four testing samples were used to perform the failure and cyclic test with gauge length ranging from 30 -58 mm (1.18 – 2.28 in). Gauge length was measured from the distance in-between material grip on equipment without tension. Sandpaper was used on the tube ends to prevent slippage from the grips. Three samples were used for the failure test procedure; instructions are for a single sample:

Instruction 2: Grip both sample ends without tension in the gage section. Zero the extension and force readings on the Instron 4411. Set the speed rate at 25.4mm/min (1 in/min) with a five Hertz data acquisition rate. Clear the LabView software and enter test notes into the database. Start the DAQ for several seconds before starting the crosshead. Then the specimen fails, stop the DAQ system and then stop the crosshead.

Save the data to storage media. Calculate the extended displacement that would be used for the cyclic test by following these calculations:

a. (ε) Strain (%):

$$\left(\frac{lf}{li}\right)*100 \qquad \textbf{(12)}$$

Where, l_i = initial gage length

l_f = final gage length (failure displacement)

b. Find 90 percent of strain (%):

$$strain\ g \Rightarrow \left(\frac{90}{100}\right) * strain \qquad \textbf{(13)}$$

Where, $strain_g$ = 90 percent of strain

c. Extended displacement (mm):

$$le \Rightarrow \left(\frac{li * straing}{100}\right) \qquad \textbf{(14)}$$

Where, l_e = extended gage length

One sample was used for the cyclic test procedure; instruction is per sample:

Instruction 3: Each end of a sample was placed in-between the material grip without tension. The extension and force readings on the Instron 4411 apparatus should be cleared. The speed rate was entered at 25.4mm/min (1 in/min) with a sample rate of five Hertz. The Instron 4411 software is cleared and information is entered into the database. Always start the software before the Instron 4411 apparatus to run test: to verify that data is captured by the software, there should be some waves showing on the database graph. During the first cycle, as the top grip moves upward measure the gage length distance to correspond to 125mm (4.92 in) as extended gage length. Place hard stop at the location of the extended gage length. Once the grip reaches the hard stop, allow some time for the latex rubber to perform its stress relaxation behavior before returning to original position. Step 8 will be repeated three times to acquire four cycles of the latex rubber tube. After the 4^{th} cycle, stop the database and Instron 4411 and save data to storage location.

Another test that was performed was to determine, when the stress relaxation for the latex rubber stabilizes. This experiment was conducted to determine if time was a factor to consider when conducting future experiments that would utilize the rubber tube:

We performed this experiment as specified in instruction 3, however data acquired for all tests were in English units that were converted into metric units. Equation conversions:

$$N \Rightarrow (lbs * 4.4482216)$$

$$mm \Rightarrow (in * 25.4)$$

Instron 4411 software acquires data for time, displacement and load. The subsequent chapter will illustrate results from all test noted above.

5.2. TENSILE TEST OF ELASTOMER MATRIX

McKibben muscles were embedded in an elastomer matrix of flexible polyurethane known as FMSC 1035. Tensile test was performed on Instron 4411 at Texas A&M University mechanical engineering 360 lab. The tensile test consists of the failure analysis and cyclic test of the polyurethane specimen. Two procedures from American Society of Testing and Materials (ASTM) were used; ASTM D 4482-06: Standard Test Method for Rubber Property – Extension Cycling Fatigue and ASTM D 412-98a: Standard Test Methods for Vulcanized Rubber and Thermoplastic Elastomers – Tensions.

There are several shapes that could be used for testing such as ring specimen, straight specimen and dumbbell (also known as dogbone) specimen. ASTM D4482-06 and ASTM D 412-98a both recommend the dumbbell specimen for the tensile-strain cycle.

Procedure of dumbbell specimen built from polyurethane elastomer: To determine dumbbell dimensions, we used the standard size recommended by the ASTM standards. Use solidworks 2005 to design a dumbbell mold made from wax – designed five dumbbells in a row. Transferred the solidworks drawing to the CNC machine to build dumbbell mold. Once wax mold has been built, mix polyurethane batch to make

dumbbell specimen and pour into mold. The polyurethane mixture is a one to one ration by weight or volume – used weight. Polyurethane has a thirty minute cure time and a sixteen hour de-mold time. To be accurate and consistent, gage length was marked on the dumbbell before it was remove from the mold

Procedure of polyurethane dumbbell specimen failure test: Each tab of the polyurethane dumbbell specimen was placed in-between the material grip without tension. The extension and force readings on the Instron 4411 apparatus was zeroed. The speed rate was entered at 50.8mm/min (2 in/min) with a sample rate of five Hertz. The Instron 4411 software is cleared and information is entered into the database. Always start the software before the Instron 4411 apparatus to run test: to verify that data is captured by the software, there should be some waves showing on the database graph. Once specimen has reached its ultimate elongation point, stop software before the Instron apparatus. Save data to storage location. Calculate the extended displacement that would be used for the cyclic test by following these calculations:

a. (ε) Strain (%):

$$\left(\frac{lf}{li}\right) * 100 \qquad (12)$$

Where, l_i = initial gage length

l_f = final gage length (failure displacement)

d. Find 90 percent of strain (%):

$$strain\ g \Rightarrow \left(\frac{90}{100} \right) * strain \quad (13)$$

Where, $strain_g$ = 90 percent of strain

e. Extended displacement (mm):

$$le \Rightarrow \left(\frac{li * straing}{100} \right) \quad (14)$$

Where, l_e = extended gage length

9. Failure test is performed on three different specimens to get a range of data. The data with the smallest extended displacement value is used for the cycle test.

The cyclic test procedure for the polyurethane dumbbell specimen, instruction is per sample: Each tab of the polyurethane dumbbell specimen was placed in-between the material grip without tension. The extension and force readings on the Instron 4411 apparatus should be cleared. The speed rate was entered at 50.8mm/min (2 in/min) with a sample rate of five Hertz. The Instron 4411 software is cleared and information is entered into the database. Always start the software before the Instron 4411 apparatus to run test: to verify data is captured by the software, there should be some waves showing on the database graph. During the first cycle, as the top grip moves upward measure the gage length distance to correspond to extended gage length. Place hard stop at the

location of the extended gage length. Once the grip reaches the hard stop, allow some time for the polyurethane to perform its stress relaxation behavior before returning to original position. Step 8 will be repeated three times to acquire four cycles of the polyurethane dumbbell specimen. After the 4^{th} cycle, stop the database and Instron 4411 and save data to storage location. Data acquired for all tests were in English units that were converted into metric units. Equation conversions:

$$N \Rightarrow (lbs * 4.4482216)$$

$$mm \Rightarrow (in * 25.4)$$

Instron 4411 software acquires data for time, displacement and load. The subsequent chapter will illustrate results from all test noted above. Figure 13, is an example of a wax mold for the polyurethane dumbbell. Figures 14-15, displays how the polyurethane is shaped into a dumbbell.

Figure 13. Polyurethane dumbbell mold made from wax.

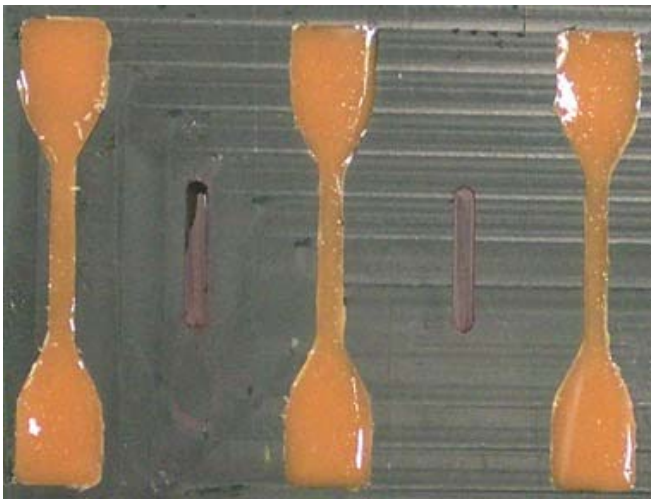

Figure 14. Creation of the polyurethane dumbbell.

Figure 15. Final product of the polyurethane dumbbell.

Figure 16. Testing procedure of the polyurethane dumbbell per ASTM standard.

Figure 16, shows a sample testing procedure for the polyurethane dumbbell.

5.3. TENSILE TEST OF RIGID POLYMER BRAID

The rigid polymer braided tube used for the McKibben's outer shell is a polyethylene terephthalate (PET) mesh sleeve. Our primary concern was to determine the failure characteristics of the polyethylene terephthalate mesh sleeve. In order to test the maximum force needed to pull-out or break the PET braided mesh sleeve from the polyurethane matrix, we performed a fiber pull-out test. The pull-out test is when a piece of fiber is embedded to a specific depth into the polymer matrix, and then the fiber is clamped on one end while the polymer matrix is clamped on the other end. The fiber is mechanically pulled from the matrix to find the maximum force needed to pull or break the whole fiber from the matrix. This experiment was conducted to assist in understanding the bonding characteristics between the fiber and the matrix. Instron 4411

apparatus at Texas A&M University Mechanical Engineering 360 lab was used with a different gripping device. A cylindrical gripping device with a slot opening in the middle was used for the rope test. The method is to wrap the rope around the cylindrical edge and in-between the slot several times, the rope around the cylindrical edge would put tension on the grip to close the slot tightly on the material inside.

The following is the procedure used for the polyethylene terephthalate (PET) braided mesh sleeve failure test: The sample length of polyethylene terephthalate braided mesh sleeve should be more than 125 mm (4.92 in), would need extra length to wrap around both cylindrical grips several times – four pieces would be needed. To confirm both end of the sleeve are tightly wound up to the grip, we placed rubber bands around the sleeve and the grips. At this point, you would need to characterize where the gage length would be measured – we chose our gage length to start and end in the middle of each cylindrical grip. Make sure tension does not exist on the sleeve where the gage length is located. The extension and force readings on the Instron 4411 apparatus are to be cleared. The speed rate was entered at 25.4mm/min (1 in/min) with a sample rate of five Hertz. The Instron 4411 software is cleared and information is entered into the database. Always start the software before the Instron 4411 apparatus to run test: to verify data is captured by the software, there should be some waves showing on the database graph. Once specimen has reached its ultimate elongation point, stop software before the Instron apparatus. Save data to storage location – to be repeated three more times. Data acquired for all tests were in English units that were converted into metric units. The following are the equation conversions:

$$N \Rightarrow (lbs * 4.4482216)$$

$$mm \Rightarrow (in * 25.4)$$

Instron 4411 software acquires data for time, displacement and load. The subsequent chapter will illustrate results from all tests noted above. Figure 17, shows the rope test procedure on the braided mesh.

Figure 17. The braided polyethylene terephthalate mesh failure analysis per rope test.

5.4. TENSILE TEST OF MCKIBBEN MUSCLE

A failure test was performed on the McKibben muscle several times; unfortunately we could not fail the McKibben muscle – with the limitations on the

testing equipment we could not reach the failure point of the McKibben muscle. Due to pressure manifold limitation, we could only pressure the McKibben muscle to 1.38 Mpa (200 psi) – McKibben muscle was still intact. A tensile test was performed on the McKibben muscle using Instron 4411 apparatus at Texas A&M University Mechanical Engineering 360 lab. The McKibben muscle was design to have an extended gauge length to be 125 mm (4.92 in), measured in-between double pinch clamps.

Materials and equipments needed to perform tensile test on McKibben muscles included:

1. A bottle of compressed nitrogen
2. Pressure manifold
3. Holding devices to be used with Instron 4411 grips. Holding device was designed and tested using solidworks 2005 and built by Brandan, Inc.
4. Plastic hose used between compressed nitrogen cylinder and manifold

The tensile test procedure for the McKibben muscle, instruction is per sample: Place open-loop ends of the McKibben muscle into the holding device. Place holding device into the material grip of Instron 4411 . Attach the open of the nylon 6 black tube on the McKibben muscle to the pressure manifold. Attach the plastic white hose to both the manifold and the compressed nitrogen cylinder, then open bottle of compressed nitrogen. The extension and force readings on the Instron 4411 apparatus should be cleared. The speed rate was entered at 25.4mm/min (1 in/min) with a sample rate of five Hertz. The Instron 4411 software is cleared and information is entered into the database. Always start the software before the Instron 4411 apparatus to run test: to verify data is

captured by the software, there should be some waves showing on the database graph. During the first cycle, as the top grip moves upward measure the gage length distance to correspond to extended gage length. Place hard stop at the location of the extended gage length. Once the grip reaches the hard stop, allow some time for the specimen to perform its stress relaxation behavior before returning to original position. The initial complete cycle is performed without pressure added to the McKibben muscle and cycled four times. The following cycles will perform differently from the initial cycles. The McKibben muscle will begin unstretched without any pressure, and then the muscle is stretched until it reaches it pre-determined length – at that point pressure is added to the McKibben muscle. Stress relaxation takes place at this point, so there is some waiting period. The waiting period is also used to make sure that the pressure determined is stabilized in the muscle. Compressed nitrogen continuously flows into the McKibben muscle while the muscle is returned to the original unstretched position. Nitrogen pressure ranges used are 0.2 Mpa (29 psi), 0.4 Mpa (58 psi), 0.48 Mpa (70 psi), and 0.69 Mpa (100 psi). 1.38 Mpa (200 psi) pressure range was used for a tensile test. Note: compressed nitrogen was removed after and before each pressure range. At each pressure range, the McKibben muscle was cycled once but to confirm consistency a few were cycled two to three times. After each cycle, stop the database and Instron 4411 and save data to storage location. Data acquired for all tests were in English units that were converted into metric units. The equation conversions are:

$$N \Rightarrow (lbs * 4.4482216)$$

$$mm \Rightarrow (in * 25.4)$$

Instron 4411 software acquires data for time, displacement and load. The subsequent chapter will illustrate results from all tests noted above. Figures 18-19, displays a single McKibben muscle when its actuated & unactuated.

Figure 18. McKibben muscle installed into the holding fixture.

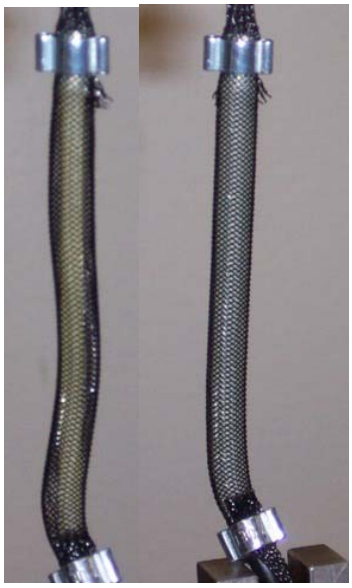

Figure 19. Examination of the McKibben muscle during non-actuation and actuation process.

5.5. TENSILE TEST OF MUSCLE SHEET

A tensile test was performed on different specimens of McKibben muscle sheets using Instron 4411 apparatus at Texas A&M University Mechanical Engineering 360 lab. This procedure is to observe how different arrays of McKibben muscles react in an embedded sheet. The McKibben muscle was designed to have an extended gauge length to be 125 mm (4.92 in), measured in-between double pinch clamps – this requirement corresponds to the McKibben muscle sheets. Other tests had to be performed before the McKibben muscle sheets were tested such as a pull-out and stability test.

The pull-out test procedure is used to determine the bonding strength of the polyurethane matrix to the polyethylene terephthalate (PET) braided mesh sleeve. This information determines how much of the polyethylene terephthalate sleeve needs to be embedded into the polyurethane matrix before it fails. The best failure point would be that the polyethylene terephthalate braided sleeve fails before the polyurethane matrix. The testing procedure is as follows:

Used ALGOR, finite element analysis (FEA) software, to design and test pull-out apparatus – we created several simulations to determine the failure point. Used solidworks 2005 to design and CNC to build wax mold for matrix. Two different molds were created to perform this test. One mold was to hold the matrix, while the other mold was to create a polyurethane rod that was equivalent to the inside diameter of the polyethylene terephthalate braided sleeve. The rod is to keep the polyethylene terephthalate braided sleeve round, not to be crushed by the surrounding matrix. The polyurethane rod has to be created first to insert into the polyethylene terephthalate

braided mesh. Polyurethane batch is mixed to be poured into matrix mold with the filled polyethylene terephthalate braided sleeve in the determined location. Two designs were created with the polyethylene terephthalate braided sleeve half-way and fully immersed into the polyurethane matrix. Specimens that were designed with polyurethane matrix has a thirty minute gel time and sixteen hours de-mold time. A c-shaped holding device was designed in solidworks and built by Brandan enterprise, inc – to prevent the matrix from slipping and squeezed in material grip. The pull-out specimen is strung through the c-shaped holding device. On Instron 4411 equipment, the polyethylene terephthalate braided sleeve is held directly by the top grip. The c-shaped holding device is held in place by the bottom grip. The extension and force readings on the Instron 4411 apparatus should be cleared. The speed rate was entered at 25.4 mm/min (1 in/min) with a sample rate of five Hertz. The Instron 4411 software is cleared and information is entered into the database. Always start the software before the Instron 4411 apparatus to run test: to verify data is captured by the software, there should be some waves showing on the database graph. Once specimen has reached its ultimate elongation point, stop software before the Instron apparatus. Save data to storage location. Figures 20-22, displays testing & design procedures on the matrix and braided mesh.

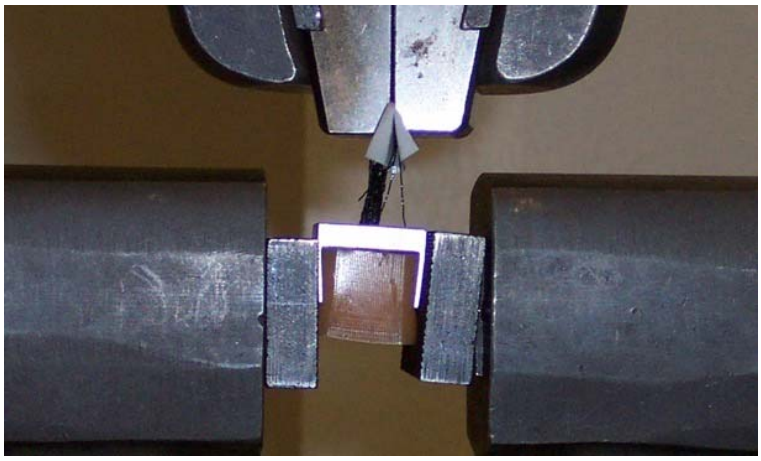

Figure 20. Experimentation of the pull-out test.

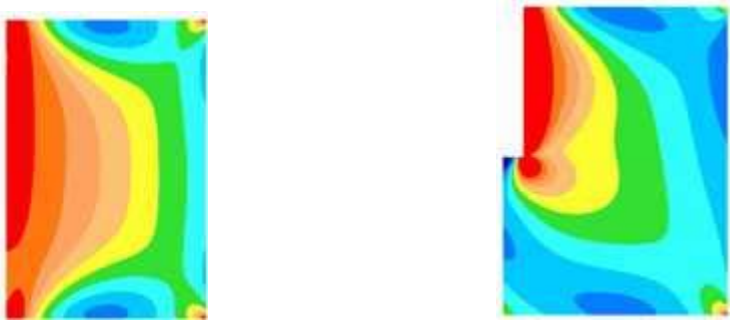

Figure 21. Testing analysis of concept for the pull-out test.

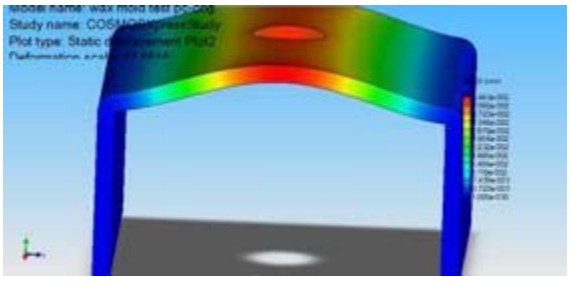

Figure 22. Testing analysis of the pull-out fixture.

The stability test corresponds to how the speed on the Instron 4411 influences the data acquired. This procedure was to confirm that at different rates the information acquired was not influenced. Minitab software was used to analyze the data from Instron 4411. The procedure is as follows:

Each specimen of the McKibben muscle sheet was tested different speed rate. The speed rate ranges were 25.4mm (1in), 12.7mm (0.5 in), 6.35mm (0.25 in), 3.175 mm (0.125 in), 1.588 mm (0.0625 in) per minute. Previous cyclic method was used for this application. Each specimen were only tested at the extreme of the pressure ranges; 0 and 0.69 MPa (100 psi). Save data to storage location. Use Minitab software to analyze data

Materials and equipment needed to perform tensile test on McKibben muscles included (Figures 23-24, displays the design concepts on the holding fixture):

1. A bottle of compressed nitrogen
2. Pressure manifold
3. Holding devices to be used with Instron 4411 grips. Holding device was designed and tested using solidworks 2005 and built by Brandan, Inc.
4. Plastic hose used between compressed nitrogen cylinder and manifold
5. Wax molds for embedding McKibben muscles in polyurethane matrix. Molds were designed with solidworks 2005 and built with the CNC machine
6. 15 mm aluminum rods to use with molds
7. Silicone grease by Dow Corning
8. McKibben muscles - 125 mm (4.92 in) extended gage length

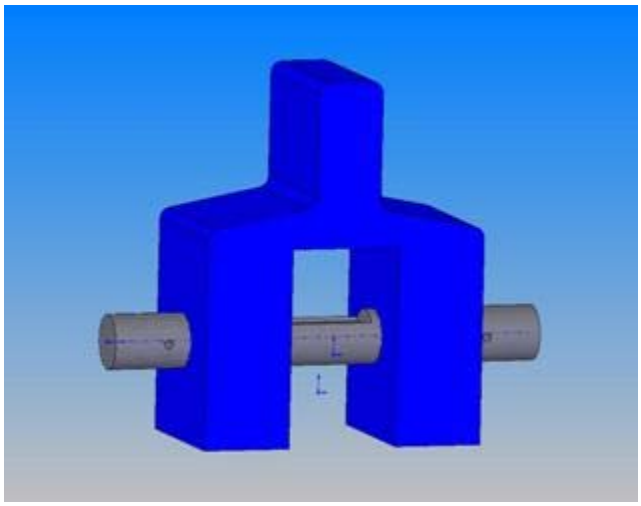

Figure 23. Design of holding fixture for the McKibben and single embedded sheet utilizing solidworks.

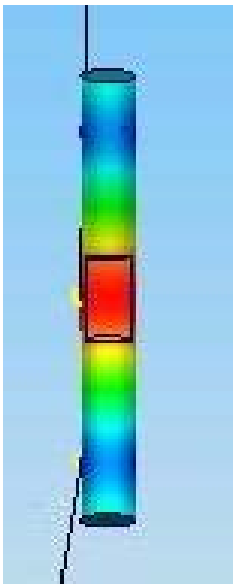

Figure 24. Test analysis of the holding fixture rod by solidworks.

5.5.1. Single Embedded McKibben

Building instructions for a single embedded McKibben sheet: McKibben muscle should be completely coated with Dow silicone grease with a brush. Put two aluminum rods into the hole of the single embedded McKibben sheet wax mold. Mix-up the batch of polyurethane matrix by weighing out one to one pound of Part A and Part B. About 88.96-133.45 N (20-30 lbs) is needed or this application. Fill the wax mold to about one-third of its volume. Using forceps, place the McKibben muscle into mold by locating the open-loops on the muscle over the aluminum rods – the mold is designed to use the extended gage length of the McKibben muscle. The McKibben muscle is fully stretched to 125 mm (4.92 in) (4.92 in). Try to rotate double-pinch clamp into square slot in the mold, this keeps the muscle leveled.

Slowly, pour the remaining polyurethane matrix over and around the McKibben muscle. The elastomer is poured slowly to prevent bubble build ups Polyurethane has a gel time of 30 minutes with a sixteen hour de-mold time. Once the single embedded McKibben sheet is removed from the mold, use blade to remove excess material around the edges. Completely, clear holes with blade to ease installation of clamps. Due to polyurethane's color, we would have to re-characterize a new initial gage length. The new initial gage length is the distance in-between the insides of the double-pinch clamps.

The tensile test procedure for the single embedded McKibben sheet: Place open-loop ends of the single embedded McKibben sheet into the holding device. Place holding device into the material grip of Instron 4411. Attach the open of the nylon 6

black tubes on the McKibben muscle to the pressure manifold. Attach the plastic white hose to both the manifold and the compressed nitrogen cylinder, then open bottle of compressed nitrogen. The extension and force readings on the Instron 4411 apparatus should be cleared. The speed rate was entered at 25.4 mm (1 in/min) with a sample rate of five Hertz. The Instron 4411 software is cleared and information is entered into the database. Always start the software before the Instron 4411 apparatus to run test: to verify data is captured by the software, there should be some waves showing on the database graph. During the first cycle, as the top grip moves upward measure the gage length distance to correspond to extended gage length. Place hard stop at the location of the extended gage length. Once the grip reaches the hard stop, allow some time for the specimen to perform its stress relaxation behavior before returning to original position.

The initial complete cycle is performed without pressure added to the single embedded McKibben sheet and cycled four times. The following cycles will perform differently from the initial cycles. The single embedded McKibben sheet will begin unstretched without any pressure, and then the sheet is stretched until it reaches it pre-determined length – at that point pressure is added to the single embedded McKibben sheet. Stress relaxation takes place at this point, so there is some waiting period that is needed. The waiting period is also used to make sure that the pressure determined is stabilized in the sheet. Compressed nitrogen continuously flows into the McKibben sheet while the muscle is returned to the original unstretched position. Nitrogen pressure ranges used are 0.2 Mpa (29 psi), 0.4 Mpa (58 psi), 0.48 Mpa (70 psi), and 0.69 Mpa (100 psi). Note: compressed nitrogen was removed after and before each pressure

range. At each pressure range, the single embedded McKibben sheet was cycled once but to confirm consistency a few were cycled two to three times. After each cycle, stop the database and Instron 4411 and save data to storage location.

Figure 25. Manufacturing process of single embedded sheet.

Figure 26. Examples of single embedded sheet.

Figure 27. Single embedded sheet examination process.

Figures 25-27, displays different stages of building a single embedded sheet.

5.5.2. Double Embedded McKibben

Building instructions for a double embedded McKibben sheet: McKibben muscles should be completely coated with Dow silicone grease with a brush. Put four aluminum rods into the hole of the double embedded McKibben sheet wax mold. Mix-up the batch of polyurethane matrix by weighing out one to one pound of Part A and Part B. About 88.96-177.93 N (20-40 lbs) is needed for this application. Fill the wax mold to about one-third of its volume. Using forceps, place the McKibben muscles into mold by locating the open-loops on the muscle over the aluminum rods – the mold is designed to use the extended gage length of the McKibben muscle. The McKibben muscle is fully stretched to 125 mm (4.92 in) (4.92 in). Try to rotate double-pinch clamp into

square slot in the mold, this keeps the muscle leveled. Slowly, pour the remaining polyurethane matrix over and around the McKibben muscle. The elastomer is poured slowly to prevent bubble build ups. Polyurethane has a gel time of 30 minutes with a sixteen hour de-mold time. Once the double embedded McKibben sheet is removed from the mold, use blade to remove excess material around the edges. Completely, clear holes with blade to ease installation of clamps. Due to polyurethane's color, we would have to re-characterize a new initial gage length. The new initial gage length is the distance in-between the insides of the double-pinch clamps.

The tensile test procedure for the double embedded McKibben sheet: Place open-loop ends of the double embedded McKibben sheet into the holding device. Place holding device into the material grip of Instron 4411. Attach the open of the nylon 6 black tubes on the McKibben muscle to the pressure manifold. Attach the plastic white hose to both the manifold and the compressed nitrogen cylinder, then open bottle of compressed nitrogen. The extension and force readings on the Instron 4411 apparatus should be cleared. The speed rate was entered at 25.4mm/min (1 in/min) with a sample rate of five Hertz. The Instron 4411 software is cleared and information is entered into the database. Always start the software before the Instron 4411 apparatus to run test: to verify data is captured by the software, there should be some waves showing on the database graph. During the first cycle, as the top grip moves upward measure the gage length distance to correspond to extended gage length. Place hard stop at the location of the extended gage length. Once the grip reaches the hard stop, allow some time for the specimen to perform its stress relaxation behavior before returning to original position.

The initial complete cycle is performed without pressure added to the double embedded McKibben sheet and cycled four times. The following cycles will perform differently from the initial cycles. The double embedded McKibben sheet will begin unstretched without any pressure, and then the sheet is stretched until it reaches it pre-determined length – at that point pressure is added to the double embedded McKibben sheet. Stress relaxation takes place at this point, so there is some waiting period that is needed. The waiting period is also used to make sure that the pressure determined is stabilized in the sheet. Compressed nitrogen continuously flows into the McKibben sheet while the muscle is returned to the original unstretched position. Nitrogen pressure ranges used are 0.2 Mpa (29 psi), 0.4 Mpa (58 psi), 0.48 Mpa (70 psi), and 0.69 Mpa (100 psi). Note: compressed nitrogen was removed after and before each pressure range.

At each pressure range, the double embedded McKibben sheet was cycled once but to confirm consistency a few were cycled two to three times. After each cycle, stop the database and Instron 4411 and save data to storage location.

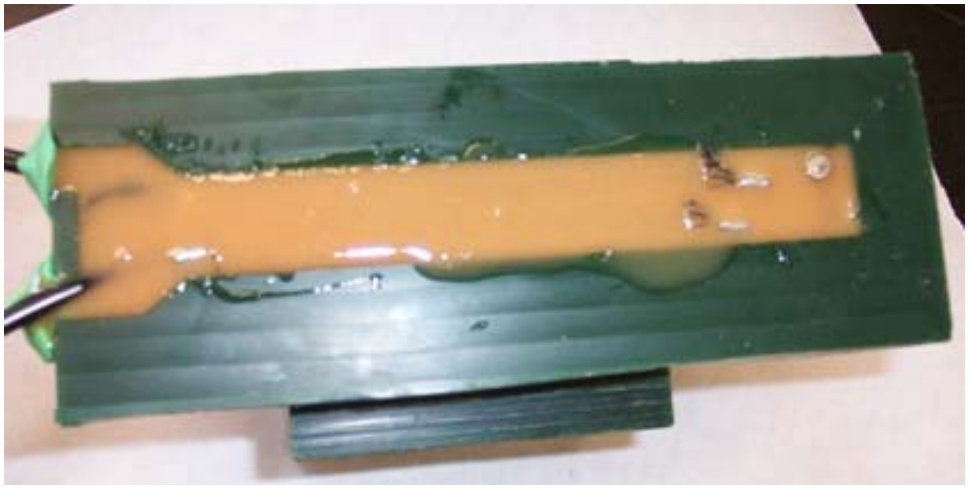

Figure 28. Fabricating a double embedded sheet.

Figure 29. This double embedded muscle sheet shows that the muscles bend the sheet as they contract passively.

Figure 30. Double embedded sheet experimentation.

Figures 28-30, displays different stages of building a double embedded sheet.

5.5.3. Triple Embedded McKibben

Building instructions for a triple embedded McKibben sheet: McKibben muscles should be completely coated with Dow silicone grease with a brush. Put four aluminum rods into the hole of the triple embedded McKibben sheet wax mold. Mix-up the batch of polyurethane matrix by weighing out one to one pound of Part A and Part B. About 88.96-222.41 N (20-50 lbs) is needed for this application. Fill the wax mold to about one-third of its volume. Using forceps, place the McKibben muscles into mold by locating the open-loops on the muscle over the aluminum rods – the mold is designed to use the extended gage length of the McKibben muscle. The McKibben muscle is fully stretched to 125 mm (4.92 in) (4.92 in).

Try to rotate double-pinch clamp into square slot in the mold, this keeps the muscle leveled. Slowly, pour the remaining polyurethane matrix over and around the McKibben muscle. The elastomer is poured slowly to prevent bubble build ups. Polyurethane has a gel time of 30 minutes with a sixteen hour de-mold time. Once the triple embedded McKibben sheet is removed from the mold, use blade to remove excess material around the edges. Completely, clear holes with blade to ease installation of clamps. Due to polyurethane's color, we would have to re-characterize a new initial gage length. The new initial gage length is the distance in-between the insides of the double-pinch clamps.

The tensile test procedure for the triple embedded McKibben sheet: Place open-loop ends of the triple embedded McKibben sheet into the holding device. Place holding device into the material grip of Instron 4411. Attach the open of the nylon 6 black tubes

on the McKibben muscle to the pressure manifold. Attach the plastic white hose to both the manifold and the compressed nitrogen cylinder, then open bottle of compressed nitrogen. The extension and force readings on the Instron 4411 apparatus should be cleared. The speed rate was entered at 25.4mm/min (1 in/min) with a sample rate of five Hertz. The Instron 4411 software is cleared and information is entered into the database. Always start the software before the Instron 4411 apparatus to run test: to verify data is captured by the software, there should be some waves showing on the database graph

During the first cycle, as the top grip moves upward measure the gage length distance to correspond to extended gage length. Place hard stop at the location of the extended gage length. Once the grip reaches the hard stop, allow some time for the specimen to perform its stress relaxation behavior before returning to original position. The initial complete cycle is performed without pressure added to the triple embedded McKibben sheet and cycled four times. The following cycles will perform differently from the initial cycles. The triple embedded McKibben sheet will begin unstretched without any pressure, and then the sheet is stretched until it reaches it pre-determined length – at that point pressure is added to the triple embedded McKibben sheet. Stress relaxation takes place at this point, so there is some waiting period that is needed. The waiting period is also used to make sure that the pressure determined is stabilized in the sheet. Compressed nitrogen continuously flows into the McKibben sheet while the muscle is returned to the original unstretched position. Nitrogen pressure ranges used are 0.2 Mpa (29 psi), 0.4 Mpa (58 psi), 0.48 Mpa (70 psi), and 0.69 Mpa (100 psi). Note: compressed nitrogen was removed after and before each pressure range. At each

pressure range, the triple embedded McKibben sheet was cycled once but to confirm consistency a few were cycled two to three times. After each cycle, stop the database and Instron 4411 and save data to storage location.

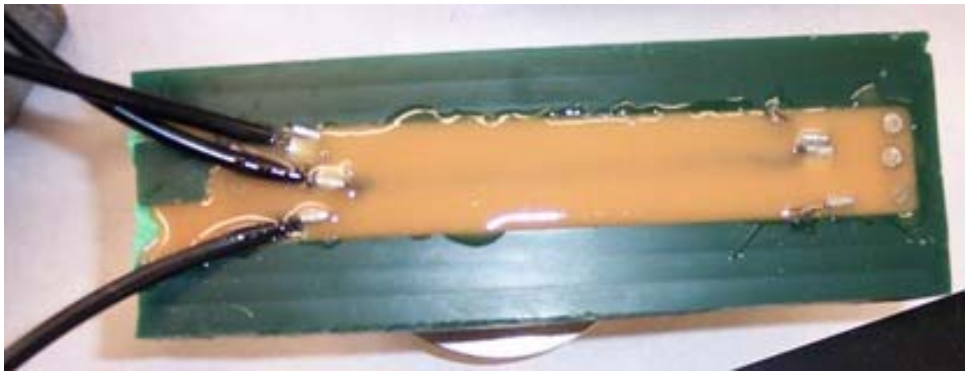

Figure 31. Triple embedded sheet construction.

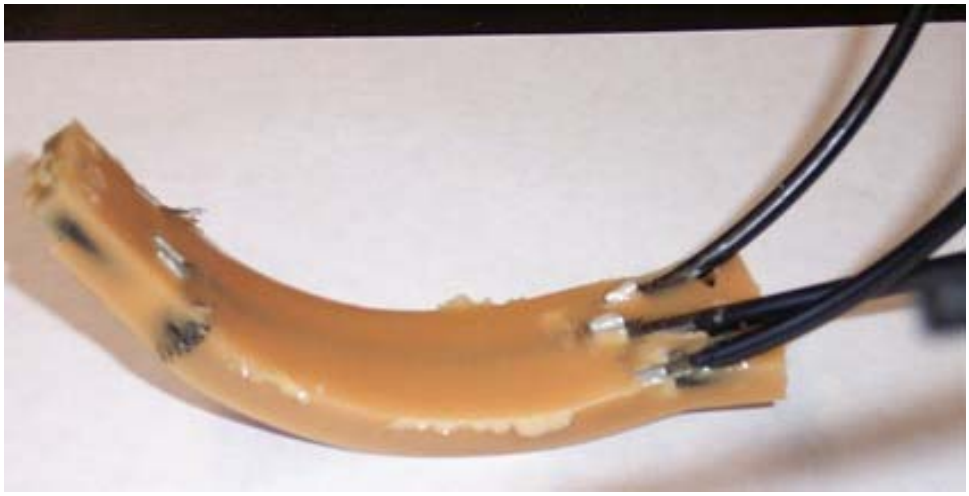

Figure 32. Finished product of triple embedded sheet.

Figure 33. Triple embedded sheet testing process.

Figures 31-33, display different stages of building a triple embedded sheet.

5.5.4. Quintuple Embedded McKibben

Building instructions for a quintuple embedded McKibben sheet: McKibben muscles should be completely coated with Dow silicone grease with a brush. Put four aluminum rods into the hole of the double embedded McKibben sheet wax mold. Mix-up the batch of polyurethane matrix by weighing out one to one pound of Part A and Part B. About 88.96-266.89 N (20-60 lbs) is needed for this application. Fill the wax mold to about one-third of its volume. Using forceps, place the McKibben muscles into mold by locating the open-loops on the muscle over the aluminum rods – the mold is designed to use the extended gage length of the McKibben muscle. The McKibben muscle is fully stretched to 125 mm (4.92 in). Try to rotate double-pinch clamp into square slot in the mold, this keeps the muscle leveled. Slowly, pour the remaining polyurethane

matrix over and around the McKibben muscle. The elastomer is poured slowly to prevent bubble build ups. Polyurethane has a gel time of 30 minutes with a sixteen hour de-mold time.

Once the quintuple embedded McKibben sheet is removed from the mold, use blade to remove excess material around the edges. Completely, clear holes with blade to ease installation of clamps. Due to polyurethane's color, we would have to re-characterize a new initial gage length. The new initial gage length is the distance in-between the insides of the double-pinch clamps.

The tensile test procedure for the quintuple embedded McKibben sheet: Place open-loop ends of the quintuple embedded McKibben sheet into the holding device. Place holding device into the material grip of Instron 4411. Attach the open of the nylon 6 black tubes on the McKibben muscle to the pressure manifold. Attach the plastic white hose to both the manifold and the compressed nitrogen cylinder, then open bottle of compressed nitrogen. The extension and force readings on the Instron 4411 apparatus should be cleared. The speed rate was entered at 25.4 mm/min (1 in/min) with a sample rate of five Hertz. The Instron 4411 software is cleared and information is entered into the database. Always start the software before the Instron 4411 apparatus to run test: to verify data is captured by the software, there should be some waves showing on the database graph.

During the first cycle, as the top grip moves upward measure the gage length distance to correspond to extended gage length. Place hard stop at the location of the extended gage length. Once the grip reaches the hard stop, allow some time for the

specimen to perform its stress relaxation behavior before returning to original position. The initial complete cycle is performed without pressure added to the quintuple embedded McKibben sheet and cycled four times. The following cycles will perform differently from the initial cycles. The quintuple embedded McKibben sheet will begin unstretched without any pressure, and then the sheet is stretched until it reaches it pre-determined length – at that point pressure is added to the quintuple embedded McKibben sheet. Stress relaxation takes place at this point, so there is some waiting period that is needed. The waiting period is also used to make sure that the pressure determined is stabilized in the sheet. Compressed nitrogen continuously flows into the McKibben sheet while the muscle is returned to the original unstretched position. Nitrogen pressure ranges used are 0.2 Mpa (29 psi), 0.4 Mpa (58 psi), 0.48 Mpa (70 psi), and 0.69 Mpa (100 psi). Note: compressed nitrogen was removed after and before each pressure range. At each pressure range, the quintuple embedded McKibben sheet was cycled once but to confirm consistency a few were cycled two to three times. After each cycle, stop the database and Instron 4411 and save data to storage location.

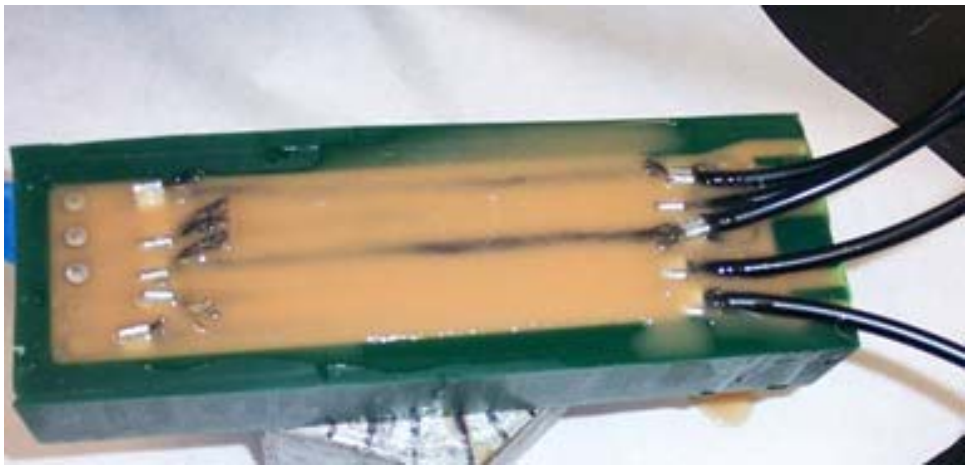

Figure 34. Quintuple embedded sheet creation.

Figure 35. Final quintuple embedded sheet.

Figure 36. Quintuple embedded sheet testing procedure.

Figures 34-36, displays different stages of building a quintuple embedded sheet.

Data acquired for all tests were in English units that were converted into metric units for analysis. Equation conversions:

$$N \Rightarrow (lbs * 4.4482216)$$

$$mm \Rightarrow (in * 25.4)$$

Instron 4411 software acquires data for time, displacement and load. The subsequent chapter will illustrate results from all test noted above.

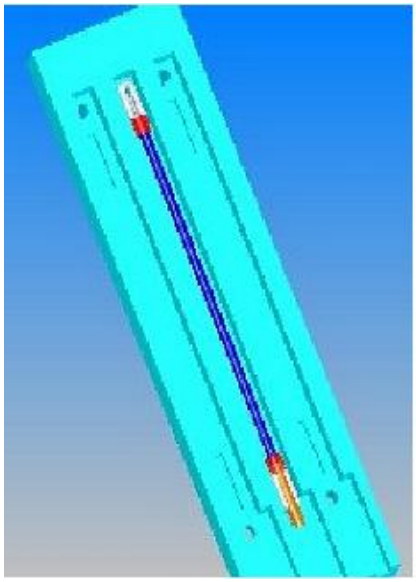

Figure 37. McKibben assembly embedded in an elastomer matrix. Active region of the McKibben muscle does not bond to the matrix.

Figure 37, displays part fo the design preparation of the wax mold and the embedded sheets using solidworks 2006. While figure 28, displays another option of creating an embedded sheet which differs from our original choice.

Embedding Options:

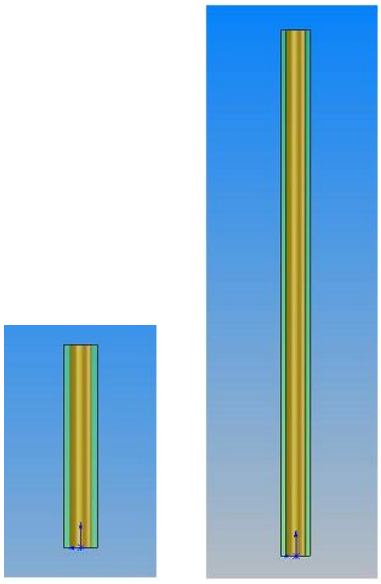

Option A Option B

Figure 38. Option A: Matrix helps activation. Option B: Matrix hinders activation.

Figures 39-40, displays the planning and testing stages of the experiment.

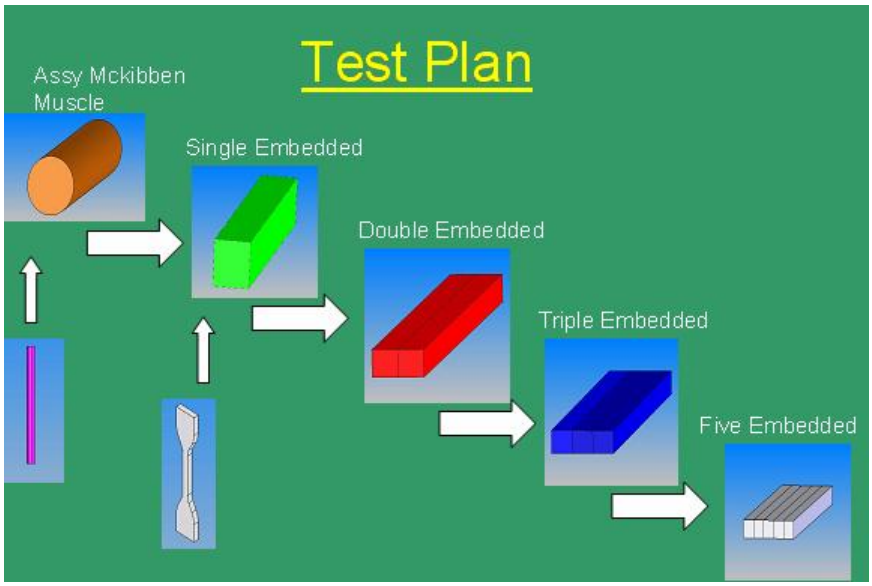

Figure 39. Test plan sequence.

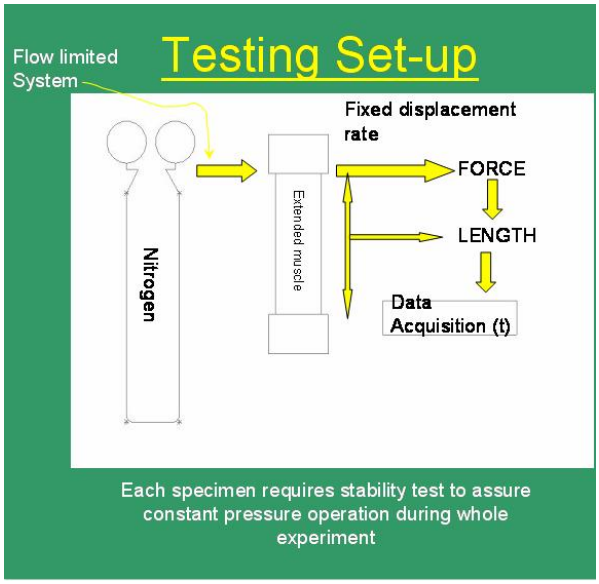

Figure 40. Testing set-up procedure.

CHAPTER VI

RESULTS

6.1. ELASTOMER TUBE RESULTS

This section presents the results from latex tube experiments. . . Testing parameters used for performing the test and results appear in Tables 1 and 2. Figure 41 displays the stress/strain behavior from three elastomer tube samples.

Table 1. Testing parameters for elastomer tubes.

Number of samples:	3
Test speed:	25.4 mm/min
Data acquisition sample rate:	5 Hz
Outer diameter:	4.75 mm
Thickness:	1 mm

Table 2. The stress and strain at failure show significant variation; therefore, the lowest strain at failure determined the limit for cyclic testing.

Specimen	Gage Length	Force at Failure	Failure Stress	Failure Strain
	(mm)	(N)	(MPa)	(%)
A	30	79.18	11.86	1278
B	46	47.51	7.10	422
C	45	42.87	6.42	808

We used three specimen lengths from the same roll to assure that there was no

length effect in the results. All specimens showed consistent behavior until they reached 300% strain, beyond that their performance differs. The experiment determined the maximum gauge length that is required for the cyclic process, by taking 90% of the failure force for the worst specimen. These experiments lead us to select Specimen B as a safe force at failure for the cyclic experiments that followed.

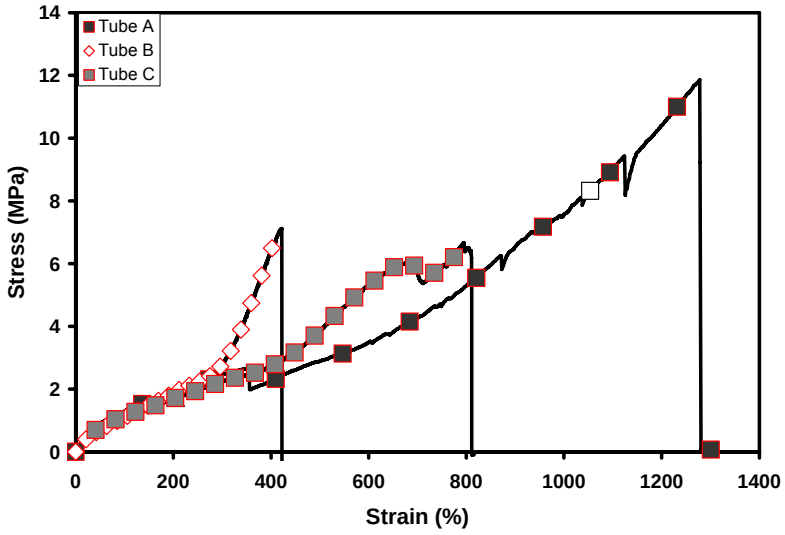

Figure 41. The stress-strain response of the tube specimens shows consistent behavior until they reach 300% strain. At higher strains the response is variable.

Figures 42-45 show the elastomer tubing's cyclic behavior. . The specimen has a 58 mm (2.28 in) gauge length and the Instron extended it until the gauge length reached 220.4 mm (8.68 in). First, Figure 42 shows four extension/return cycles conducted with the same specimen. The displacement is controlled, linear, and repeated for each cycle.

Table 3. Key data from cyclic extension of latex elastomer tube over four cycles.

Cycle	Peak Force	Strain @ Peak	Stress @ Peak
	(N)	(%)	(MPa)
1	16.72	377.3	2.50
2	16.48	374.4	2.47
3	16.36	377.1	2.45
4	16.24	377.0	2.43

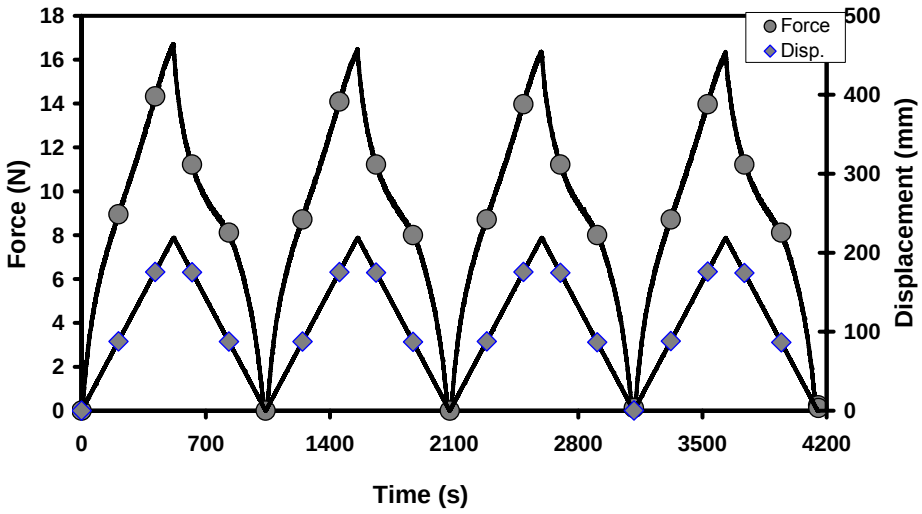

Figure 42. The controlled parameter—displacement—is controlled during the four cycles. The tensile force generated during the experiment becomes consistent for the 3rd and 4th cycles.

Figure 43 provides a detail view of changes in the peak force from cycle 1 to cycle 4. As shown, the greatest change occurs between cycle 1 and cycle 2. Within experimental error, cycles 3 and cycle 4 have a constant response. The shift change is due to stress relaxation in the rubber tube. The stress reduction after the initial extension is known as the Mullins effect; Mullin suggested that the first is unique and cannot be retraced [76], shift occurs with new elastomers and this effect must be removed from the

experiments by conditioning the samples. The stress-strain curve in Figure 44, shows how much hysteresis is created from a rubber tube during the tensile procedure. . The behavior in this image is does not show a typically-large hysteresis change after the first cycle. We suggest that the manufacturer preconditioned the tubing by stretching it prior to sale.

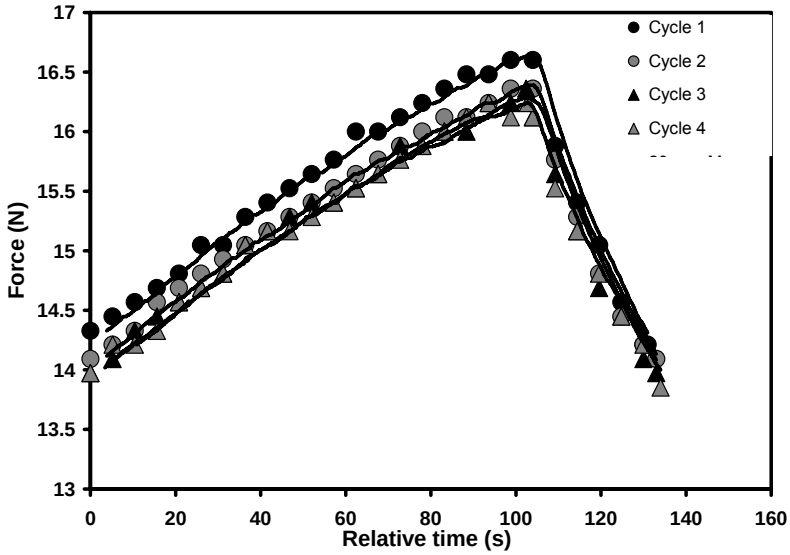

Figure 43. In this Figure each peak force occurs at a relative time of 100 s. The latex tube changes significantly after the first and second cycle; however, the third and fourth cycle agree within experimental error at 16.30 +/- 0.0849 N, which is 0.52 % and this is within excellent experimental error. This implies that the cyclic behavior of this latex should provide consistent response after three cycles to a set maximum strain.

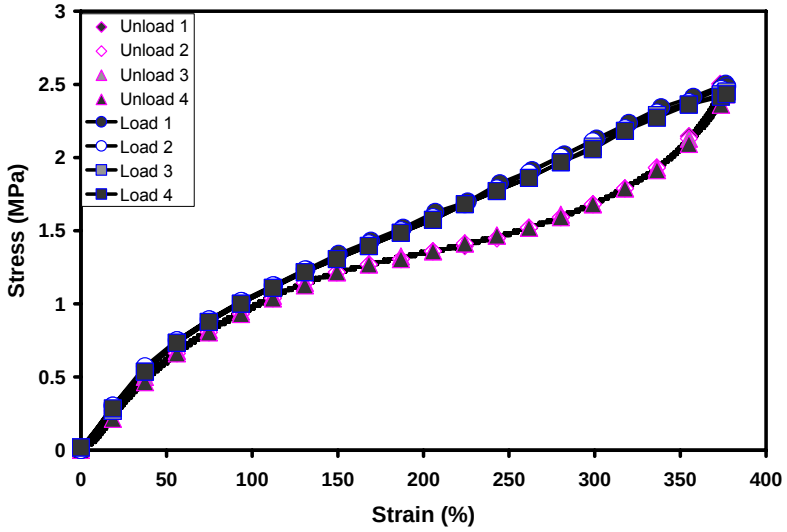

Figure 44. The hysteresis curve for the latex tube specimen shows typical energy dissipation with each cycle. Note that the baseline strain did not shift to a significant permanent strain after the first cycle. This suggests that the manufacturers subjected the tube to an initial tensile extension before they sold it. Circle and square symbols indicate the loading portion of the cycle; diamonds and triangles mark the unloading part of the cycle.

A cyclic tension test was performed to determine how much stress relaxation occurs in the elastomer tube. The test was performed by holding the maximum extension on the 1st and 3rd cycle for 1200 seconds, while the 2nd cycle was allowed to immediately cycle back to its unstretched state. Figures 45-46 show thoroughly how stress relaxation is different between the 1st and 2nd cycles. Stress relaxes less during the 3rd cycle. Figure 45, shows the force and displacement history during the experiment. The displacement, which is controlled, is consistent for both cycles and constant during the long dwell time at maximum displacement. The rubber tube's force changes with time. With the displacement data removed, Figure 46 shows that the first cycle has more stress relaxation than the third. The 3rd cycle displays a slight difference between the

initial and final peak force; however, it is more stable. The 2nd cycle will only show the initial peak force without the stress relaxation – this is to demonstrate the difference in behavior, between allowing stress relaxation or not to the elastomer specimen.

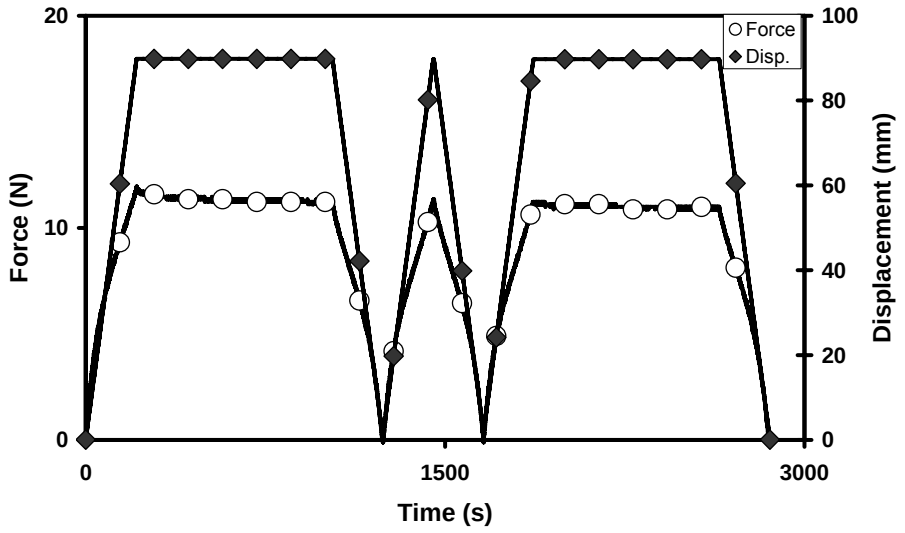

Figure 45. This graph conveys how stress relaxation influences force for an elastomer tube. It also conveys how force becomes constant over time.

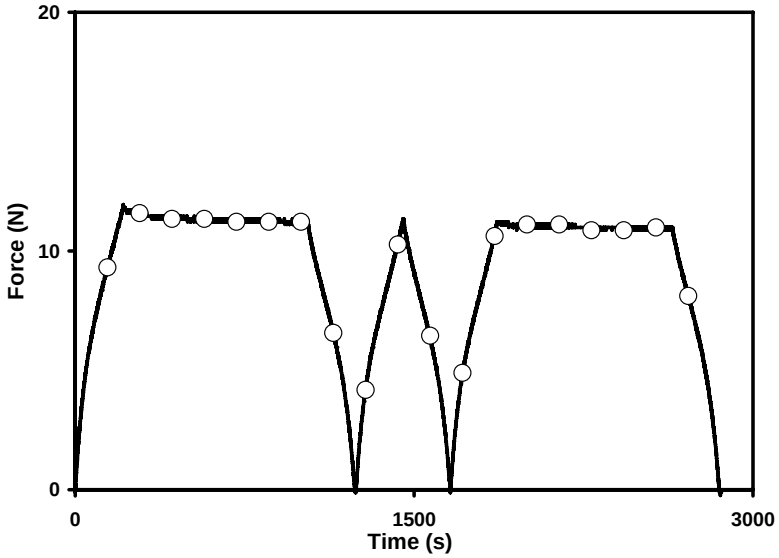

Figure 46. This graph conveys how the elastomer tube's peak for both the first and third cycle is constant.

Figure 47 shows how stress relates to cycle history and time. The stress difference between the 1st and 3rd cycle shows that cycle history affects stress.

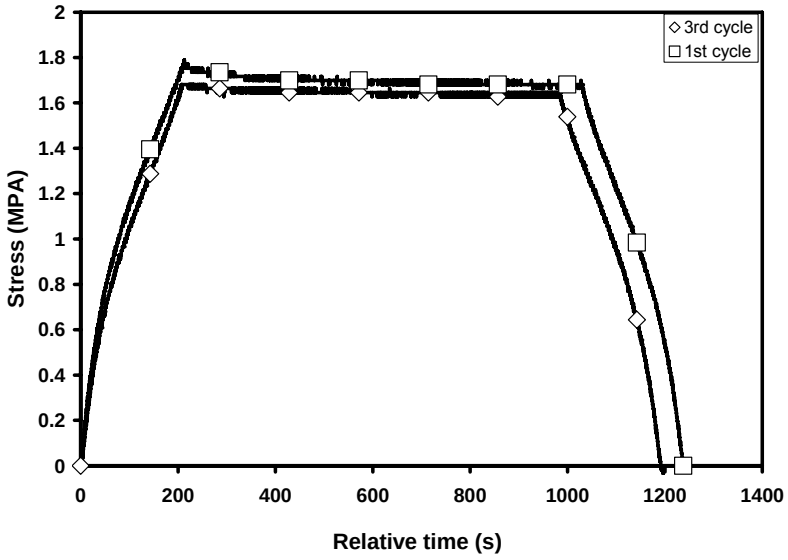

Figure 47. This graph conveys how the first and third cycle are adjacent to each other of the elastomer tube - hysteresis.

6.2. ELASTOMER MATRIX RESULTS

The Figures below display the results of both the failure analysis and the cyclic tests of polyurethane dumbbell specimens. Table 4 lists the test parameters used during these experiments and Table 5 notes key values measured.

Table 4. Testing parameter met the requirements of ASTM D 4482-06 and D 412-98a.

Number of samples:	9
Test speed:	50.8 mm/min
Data acquisition sample rate:	5 Hz
Dumbbell width:	3.175 mm
Dumbbell thickness:	3 mm
Dumbbell gage length:	22 mm
Overall length:	69 mm

Table 5. Force, stress and strain data for the polyurethane matrix.

Specimen	Force at Failure	Failure Stress	Failure Strain
	(N)	(MPa)	(%)
D1B1	7.05	0.74	1187
D2B1	8.12	0.85	1082
D3B1	10.03	1.05	1496
D4B1	7.88	0.83	1497
D1B2	8.00	0.84	946
D2B2	10.39	1.09	1464
D3B2	9.55	1.00	1310
D4B2	8.00	0.84	1472

The photographs in Figures 48 and 49 show a failed dumbbell specimen. The elastomer matrix was molded into the ASTM dumbbell. The photo shows that the dumbbell specimen failed at close to the middle of the gage section.

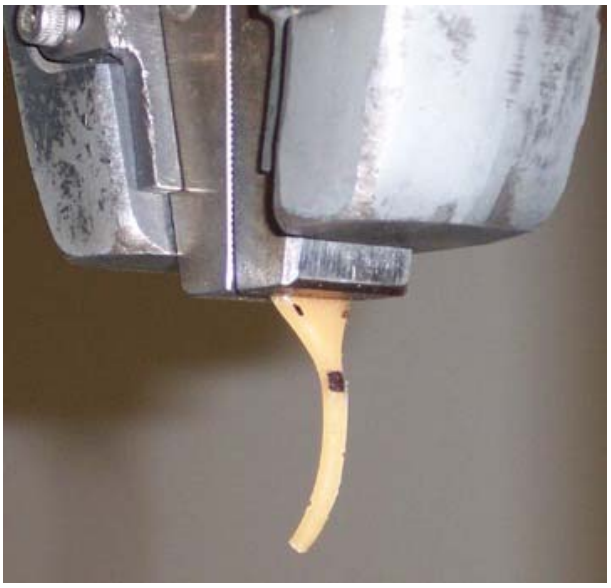

Figure 48. This picture represents the top half of one failed polyurethane dumbbell.

Figure 49. This picture represents the bottom half of one failed polyurethane dumbbell.

Figure 50 presents the force-displacement results from eight polyurethane specimens. The eight specimens come from two groups. The groups came from a single polyurethane kit; however, we mixed the kit resins and molded the specimens in two batches processed 2 days apart. Figure 50 shows a diamond symbol for one batch and a square symbol for the other. This experiment should indicate any batch dependence on specimen performance. Figure 50 show that the polyurethane dumbbells fall into two performance levels; however, these levels contain results from both batches. Five specimens had higher force-displacement response than the other three had. The low performance specimens showed consistent behavior to each other. The failure point ranged from 240 to 330 mm and 7 to 10.5 N.

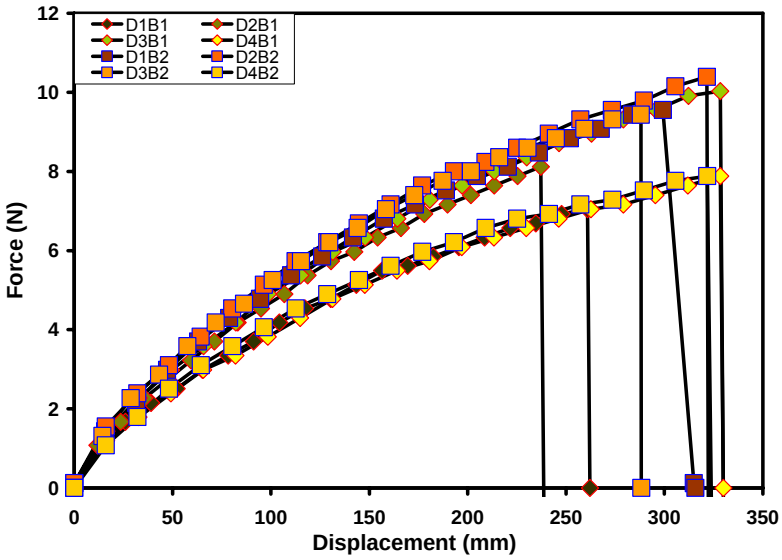

Figure 50. This graph conveys how eight polyurethane dumbbells failed of the similar dimensions.

The cyclic test used the maximum length calculated from the worst specimen at 90% of the failure at force. Average failure point to calculate the maximum length for the cycle experiment. The displacement cycle, which appears in Figure 51, shows that the specimen receives the same extension-return for each cycle. During each controlled displacement cycle the data acquisition system recorded the force generated by the specimen. Figure 51 shows that the peak force during the 1st cycle is the highest and that the peak force drops again after the 2nd cycle. The peak force becomes constant after the 3rd and 4th cycle because the specimen is conditioned to the displacement. Table 6 lists the significant values measured during the experiment.

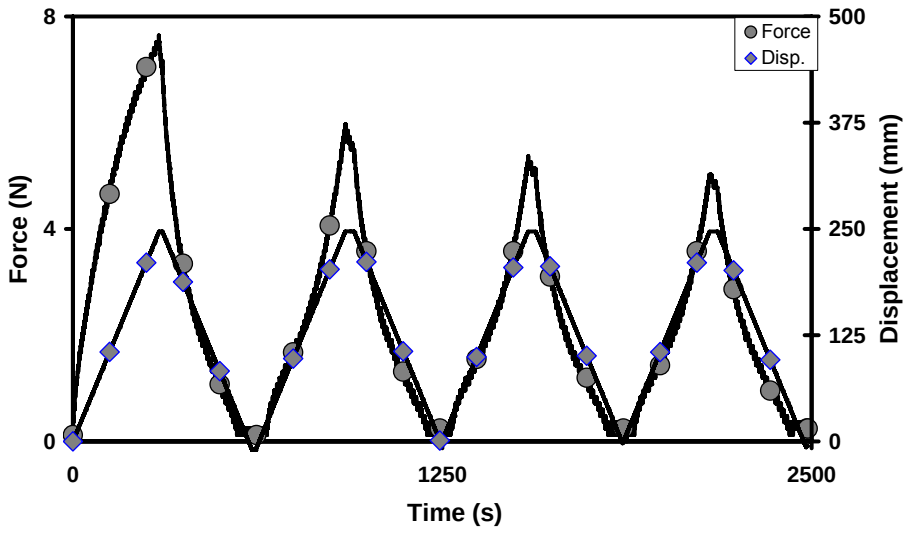

Figure 51. This graph displays the force and displacement relationship to time of the cycled polyurethane dumbbell.

Table 6. Tensile test data for the polyurethane matrix. The specimen has a gage length of 22 mm and extended gage length of 250 mm.

Cycle	Peak Force	Stress @ Peak	Strain @ Peak
	(N)	(MPa)	(%)
1	7.166	0.727	971.1
2	5.494	0.577	972.2
3	5.018	0.527	945.0
4	4.777	0.502	944.8

Figure 52 presents the unloading curves for the polyurethane. Relative time 0 represents the starting point for unloading at each cycle in Figure 51. This Figure shows that the unloading behavior changes dramatically between the first and second cycle, changes slightly between the second and third cycle, and becomes consistent—within experimental error—by the third cycle. Figure 53 shows this same data in a hysteresis plot. By the third cycle the material performance is consistent; therefore, all sheet specimens using this matrix must receive two or three cycles before we can collect data that represents its actuation behavior.

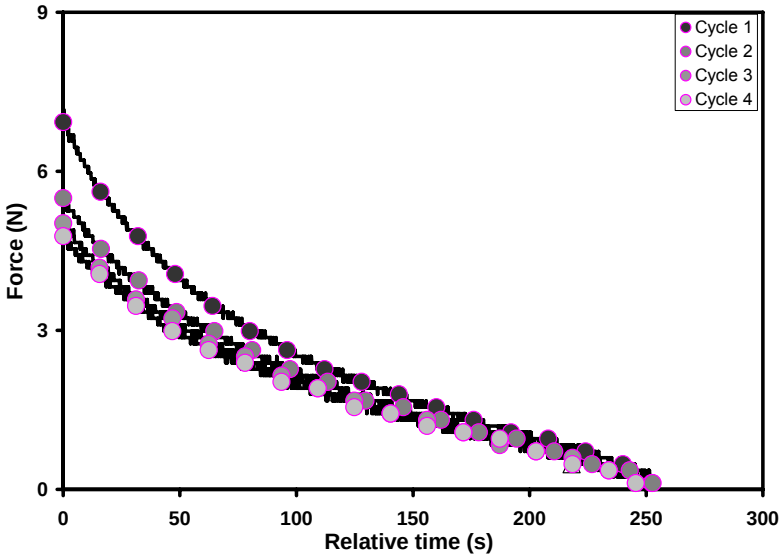

Figure 52. This graph conveys how consistent the polyurethane unloading cycle of the relative time.

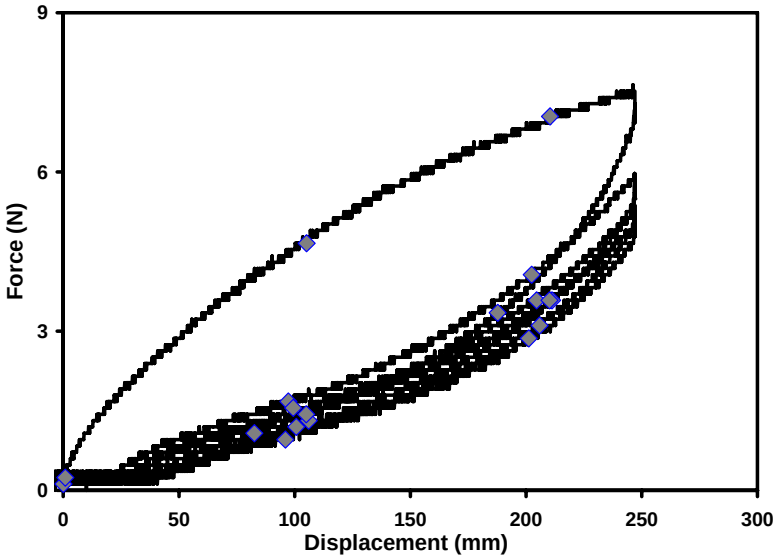

Figure 53. This graph represents the polyurethane's hysteresis – force is dependent on displacement. As shown, the second to fourth cycle never return to zero displacement.

We compare the cyclic stress strain response to the static response in Figure 54. In this Figure the cyclic data appear with triangle and circle symbols. The conditioned material shows the typical hysteresis found in elastomers and the stress/strain performance is significantly lower that obtained from an 'as-molded' specimen tested statically.

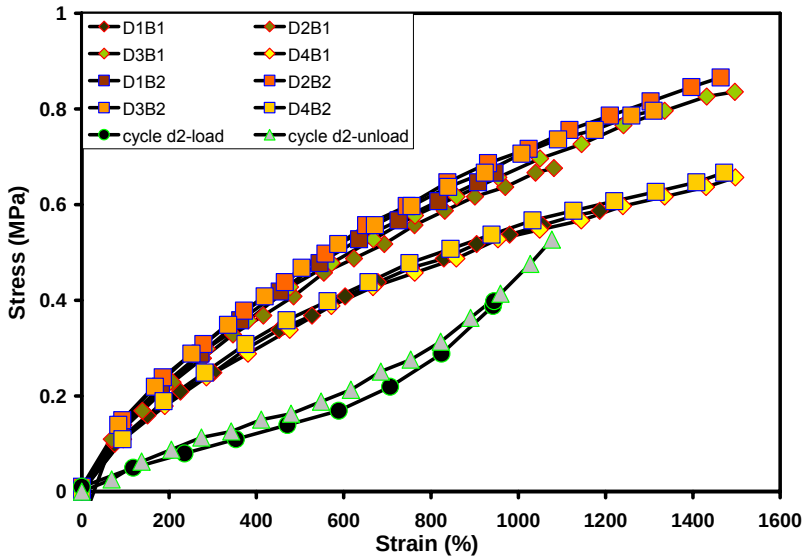

Figure 54. This graph conveys the stress-strain of the failure analysis and the cycle test. The curves of the failed dumbbells represent the simple tensile extension of fresh coupons, while the curves of the cycled dumbbell represent its fourth cycle. Note that the simple tension test fell into two classes of stress/strain response that establish the envelope of available stress/strain behavior.

6.3. POLYMER BRAID RESULTS

This section contains the results from testing the polyethylene terephthalate (PET) braided sleeve with the rope test method. This test determined the failure stress for the braid–the sleeve must not fail before the elastomer tube. Table 7 lists the

parameters for these experiments and Table 8 notes the significant data extracted from the data. Figures 55-56 display the results of the failure analysis data.

Table 7. Significant analysis of the polyethylene terephthalate.

Procedures:	Rope test
Number of samples:	4
Test speed:	25 mm/min
Data acquisition sample rate:	5 Hz
Overall diameter:	approx. 3.175 mm
Number of threads:	32
Diameter of each thread:	0.023 mm
Length of tube:	1030 mm

Table 8. Force, stress and strain of the polyethylene terephthalate braid at failure.

Specimen	Force at Failure	Failure Stress	Failure Strain
	(N)	(MPa)	(%)
1	590.3	46.97	104.0
2	600.1	47.75	130.2
3	540.0	42.97	128.1
4	624.1	49.66	105.9

The photograph in Figure 55 shows the how the PET braided mesh sleeve failed during the rope test. We used four specimens. Figure 56 shows that the specimens fell into two groups. The PET braided mesh sleeve initially fails at around 600N when about 90% of the strands fracture. Following this initial failure, the graph shows that the remaining 10% of the strands fail in small groups until all break. We chose specimens one and four as our reference because they failed at the lowest strain.

Figure 55. This picture represents a failed polyethylene terephthalate mesh sleeve using the rope test method.

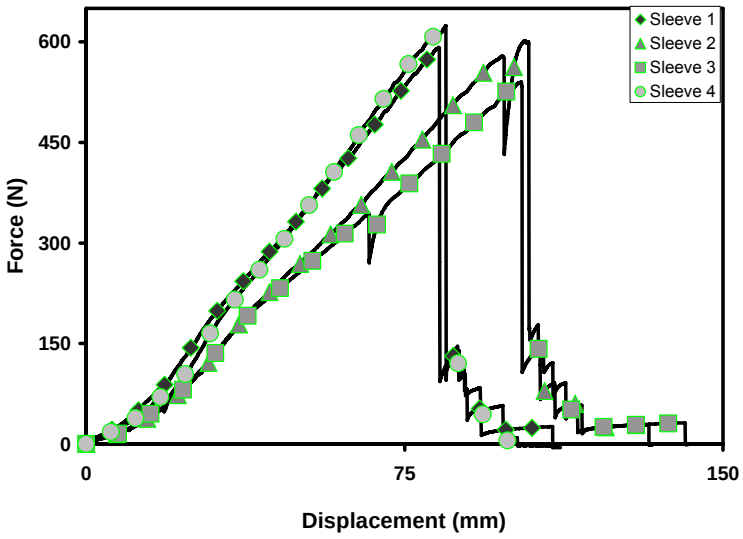

Figure 56. This graph conveys the force/displacement data of four specimens of braided polyethylene terephthalate extended to fracture.

This section shows the tensile results for all load-bearing components used to create McKibben muscles and embedded-McKibben sheets. The next sections present results for the active specimens, that is, McKibben muscles and McKibben sheets with one, two, three, and quintuple embedded McKibbens. These actuator specimens went through the same static and cyclic experiment and the graphs will be similar to those for the components.

6.4. MCKIBBEN MUSCLE RESULTS

The McKibben muscle was characterized with the tensile test methods presented above. Table 9 lists the dimensions used when the tensile data was analyzed.

Table 9. Characterized data used for testing.

Diameter	8	mm
Radius	4	mm
Gage length	55	mm
Ext gage length	125	mm

6.4.1. Tensile Test

In each experiment we used three specimens without actuation pressure, i.e., at 0 MPa, from each batch to determine if the muscles perform consistently. The detailed information presented here comes from the specimen that falls closest to the three specimen's mean performance. Table 9 shows the typical dimensions for the McKibben muscles produced here.

Figure 57 shows the force-displacement hysteresis for three McKibben muscles.

The force-displacement trends are similar but the muscles have different peak forces and displacements. The peak forces for these McKibben muscles is close to the peak force of the latex tube in Figure 42 above., This suggests that the PET sleeve has little impact on the latex tube behavior. We chose muscle 3 to represent the average performance.

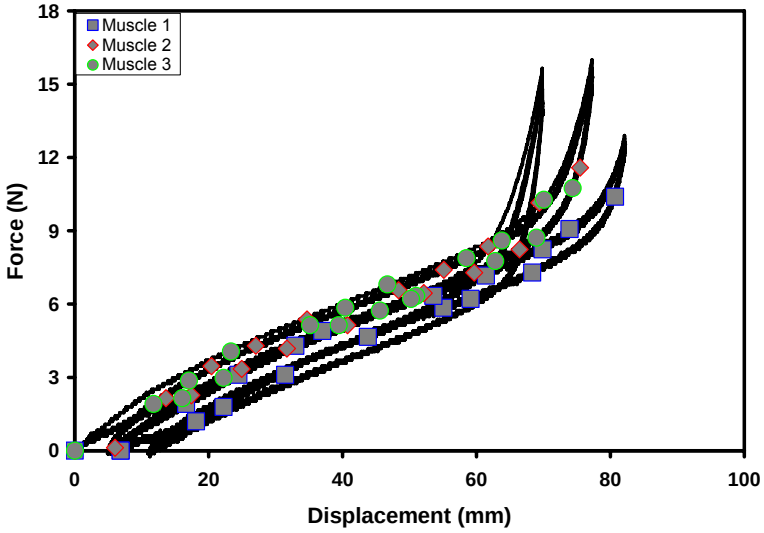

Figure 57. This graph represents force-displacement data for three unactuated McKibben muscles. The graph conveys the McKibben muscle's hysteresis.

Figures 58 – 71, display the tensile test result from muscle 3. Figure 58 displays the force-time and displacement-time data. The response shows similar characteristics to the latex tube, where the peak force decreases over time but stabilizes after the 3rd cycle. Figure 59 displays the unloading curve for each cycle adjusted so that relative time zero is at the start for unloading. The graph shows that the McKibben unloads

consistently.

Table 10. Tensile test data for the McKibben muscle.

Pressure (MPa)	*Load* (N)	*Work* (J)	*W/vol C* (MJ/m^3)	*W/vol E* (MJ/m^3)
0	14.81	0.38	0.14	0.24
0.2	21.85	0.43	0.15	0.27
0.4	31.40	0.59	0.21	0.38
0.48	37.38	0.64	0.23	0.41
0.69	50.53	0.91	0.33	0.58
1.38	105.07	1.97	0.71	1.26

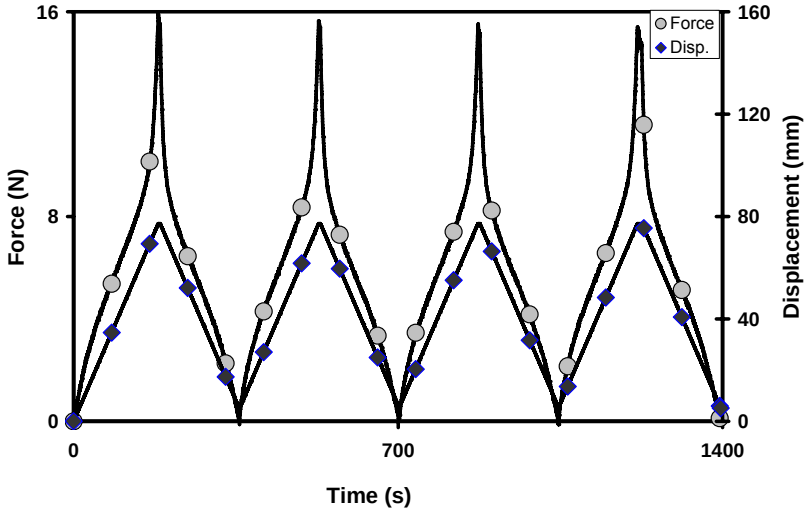

Figure 58. The data displayed is muscle three, which is the middle data at 0 MPa.

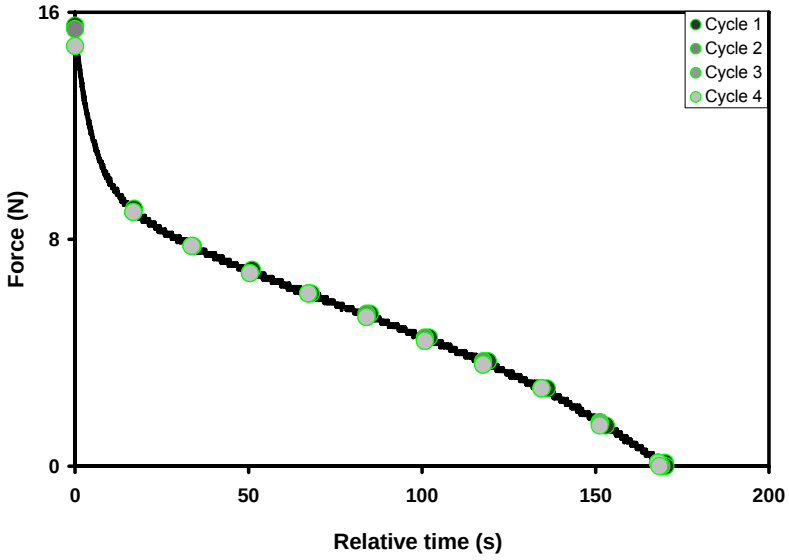

Figure 59. This graph conveys the McKibben muscle consistency for the unloading time with all cycles.

Figure 60 shows the hysteresis present in each cycle. The 1st cycle is slightly separated from the others —any preconditioning performed on the latex tube was incomplete. The remaining cycles overlap each other and the muscle performs consistently from the 3rd cycle onward.

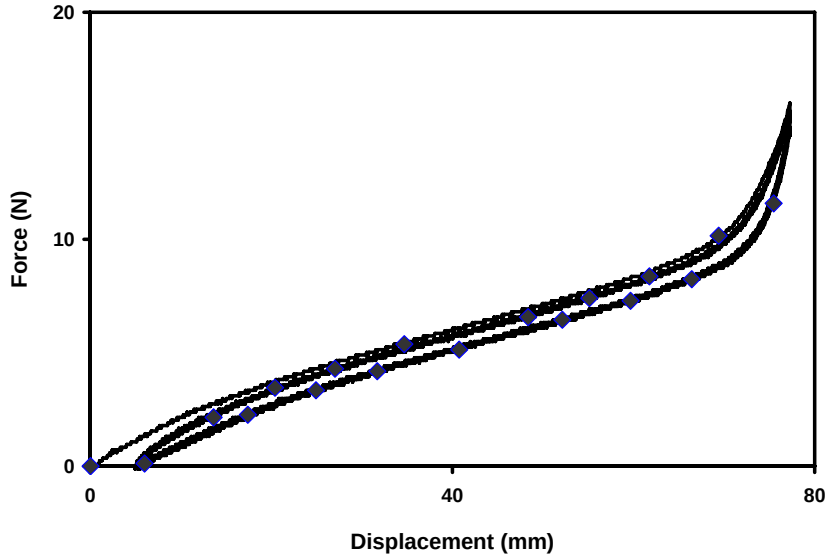

Figure 60. This graph conveys how the force is dependent on displacement. The first cycle is separated from the other cycles.

Figures 61-63 display detailed information for this McKibben muscle at pressures between 0 and 0.69 MPa. The results will illustrate how pressure affects the characteristics of the McKibben muscle.

Since the same McKibben muscle is used for every pressure; the muscle was only cycled once at each non-zero pressure. This assured that the specimen survived the experiment and provided a complete data set. Figure 61 present the experiments with the force and displacement oriented to represent actuation. At zero displacement the force is the largest possible at any pressure. As the muscle reaches its maximum displacement, the force falls to zero. The lowest curve, which has square symbols, comes from the unpressurized muscle. In this case the McKibben is only a rubber-band spring with a 14.81 N initial force that falls to zero force at about 70 mm displacement.

As we pressurize the McKibben, the initial force rises in response. The

pressurized McKibben provides additional work—the areas under the force-displacement curves in Figure 61 are obviously growing with increasing internal pressure. However, Figure 61 shows that the displacement available for actuation decreases as the internal pressure increases.

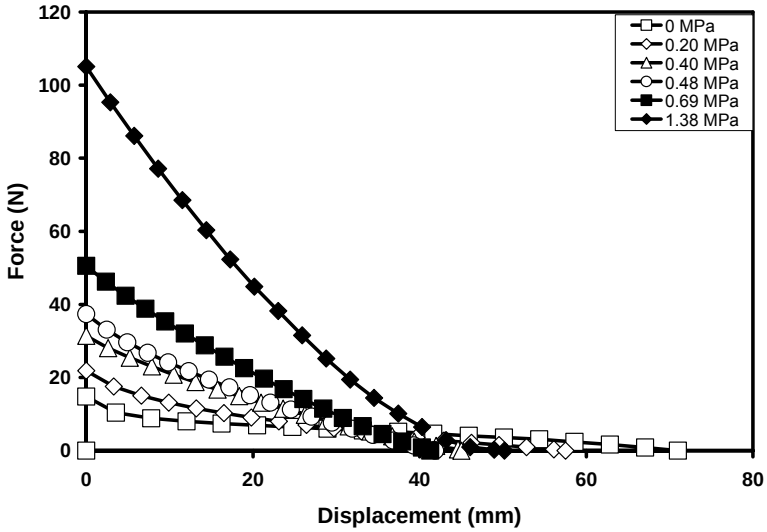

Figure 61. This graph represents the force/displacement actuation capability of the McKibben muscle at each test pressure. The force decreases as the displacement increases. However, note that the total displacement falls as actuation pressure increases.

Although the force-displacement graph shows the general response, the stress-strain graph provides the work possible with this actuator. Figure 62 shows the same behavior as Figure 61, of course; however, now the area under each curve is the work performed during actuation.

The figure (63) on page 100, the McKibben work increases with actuation pressure but the displacement decreases. The decrease is displacement must be cause by

the actuation pressure. Without pressure a McKibben muscle is just a rubber band. With internal pressure the tube expands against the braided sleeve and the braid goes into tension. When the braid fibers rotate toward the radial direction they lose their ability to generate axial force. This decreases the displacement range. For each non-zero pressure the work rises quickly with displacement and then asymptotically approaches the maximum work as the muscle approaches its maximum displacement. Finally, work output increases directly with as actuation pressure rises. Table 11 lists the force, work, and industrial work density, which is the blocked stress multiplied by free strain.

Table 11. Force, work, and work density obtained from a McKibben muscle shows that output is a direct function of actuation pressure.

Pressure	Maximum Stress (MPa)	Total Work (J)	Work Density (MJ/m^3)
0	0.25	0.35	0.325
0.20	0.47	0.45	0.4935
0.40	0.49	0.65	0.4802
0.48	0.75	0.70	0.5925
0.69	1.0	0.95	0.77
1.38	2.2	2.0	1.98

Subsequent graphs present this data as work-density because we compare actuators by their work densities. Note that these are the integrated work density rather than the product of blocked stress and free strain; therefore, the work density numbers will be smaller than those shown in Table 11. Each work density appears twice because the McKibben's volume changes significantly during its action. At first the muscle is long and thin. When the actuation ends the muscle is short and wide. Here we use both volumes to set upper and lower bounds on the integral work density. The actual integrated work density must fall between these values. Figure 63, the McKibben work increases with actuation pressure but the displacement decreases

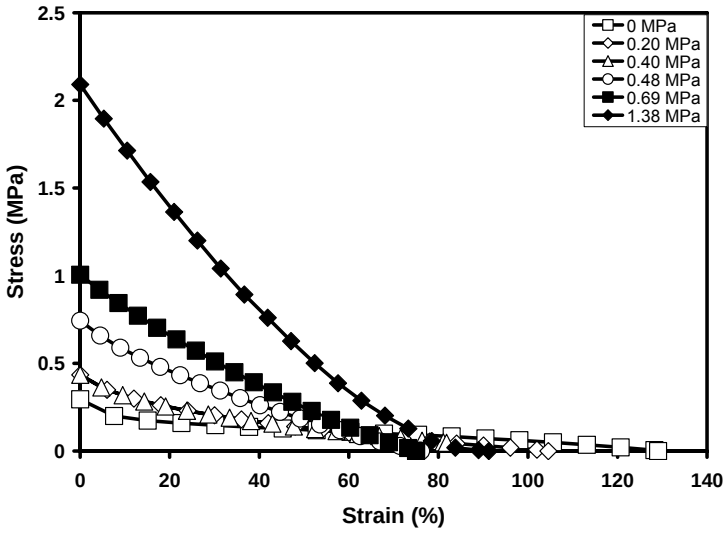

Figure 62. All pressures of the McKibben muscle are represented by the stress-strain curve. Stress is dependent on pressure.

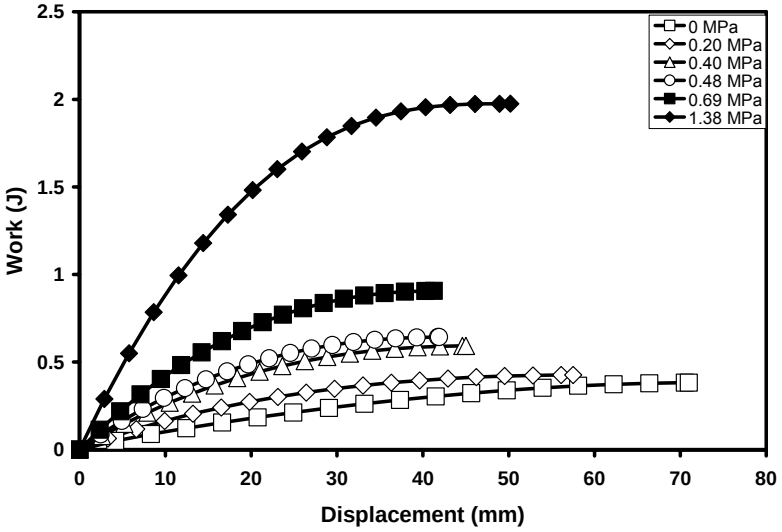

Figure 63. This graph conveys how work is dependent on actuation pressure for a McKibben muscle. Note that total work output grows with increasing actuation pressure even though the total displacement tends to decrease.

Figure 64 shows the upper- and lower-bound integrated work density curves and the blocked stress/free strain work density curve. These curves have increasing slopes; therefore, apply more actuation pressure always produces more work and work density. The only limit on output is the save operation pressure for the muscle.

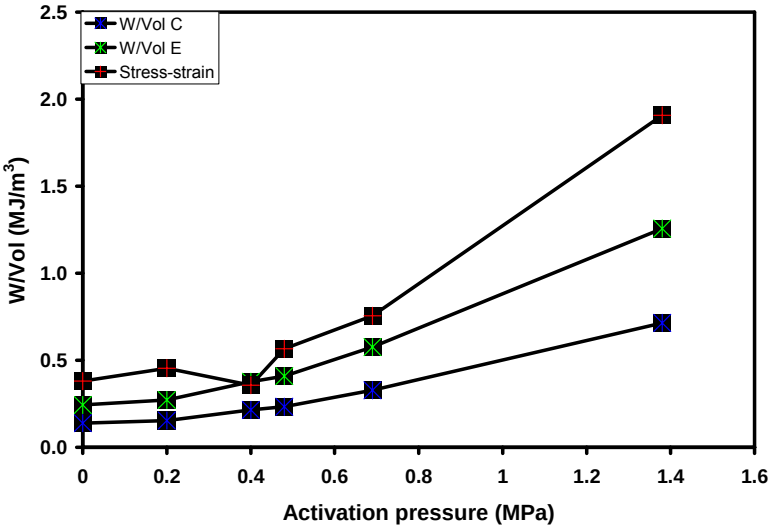

Figure 64. This is a detailed graph showing how work-density is dependent on pressure for a McKibben muscle. The trend shows that more work output is possible up to the point of failure at the activation pressure.

With the McKibben performance determined at these test conditions we faced this question: does the strain rate affect the work output? This question is significant because our experiment is affected by two rate limiting items: the apparatus' gas flow rate and the hysteresis in the elastomers. These experiments must occur with a fixed pressure in the muscle. Since the muscle volume expands dramatically during actuation, the pressure could drop if the regulator and supply tubes cannot deliver gas quickly enough at high strain rate. The next section reports the experiments performed to assure that the pressure remained constant.

6.4.2. Work Output Dependence on Strain Rate

This test was performed to determine whether actuation speed influenced the work produced. Figure 65 shows eight experiments performed at displacements

between 3.18 and 25.4 mm/min. We performed these tests at 0 MPa and 0.69 MPa actuation pressure. At 0 MPa, the results show that experiments performed at 25.4 mm/min or less produce consistent results. At 0.69 MPa, the results fall within accepted experimental error—there is no significant strain-rate effect. The work output from these experiments appears in Figure 66. The error range for both pressures was at 5.63% at 0 MPa and 2.29% at 0.69 MPa–these are within experimental error. This suggests that speeds at or below of 25.4 mm/min do not affect the outcome. The Minitab analysis shown in Figure 67 indicates that no results were outliers at either pressure.

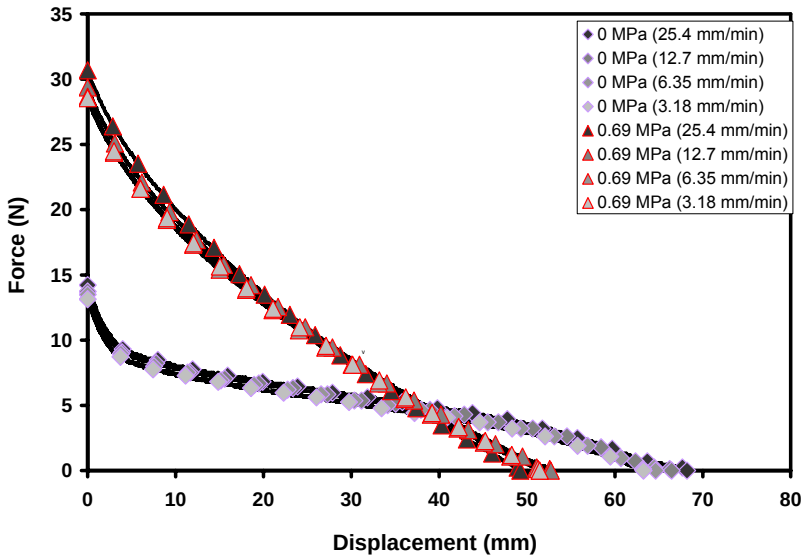

Figure 65. This graph shows that the engineering strain rate does not affect the force displacement response of a McKibben for strain rates between 0.05292 and 0.4233 min^{-1}. The tests at 0.69 MPa show that the inflation system can keep the muscle at 0.69 MPa throughout the actuation displacement.

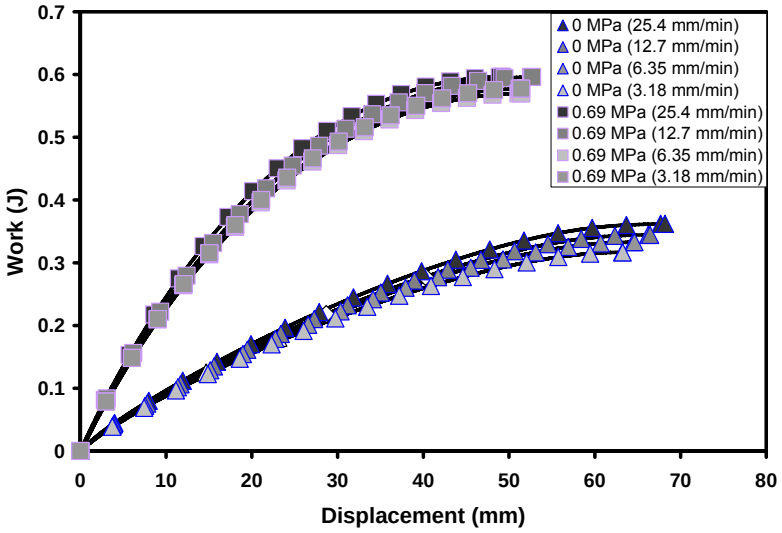

Figure 66. The average work output for un-pressurized (0 MPa) is 0.34 +/- 0.019 J and the average for muscles activated at 0.69 MPa is 0.58 +/- 0.013 J. The standard deviation for both classes is within the acceptable experimental error range at 5.63 % and 2.29% respectively, so this range of engineering strain rate has no effect. This graph conveys how speed influences work. The test is performed in two groups of 0 and 0.69 MPa.

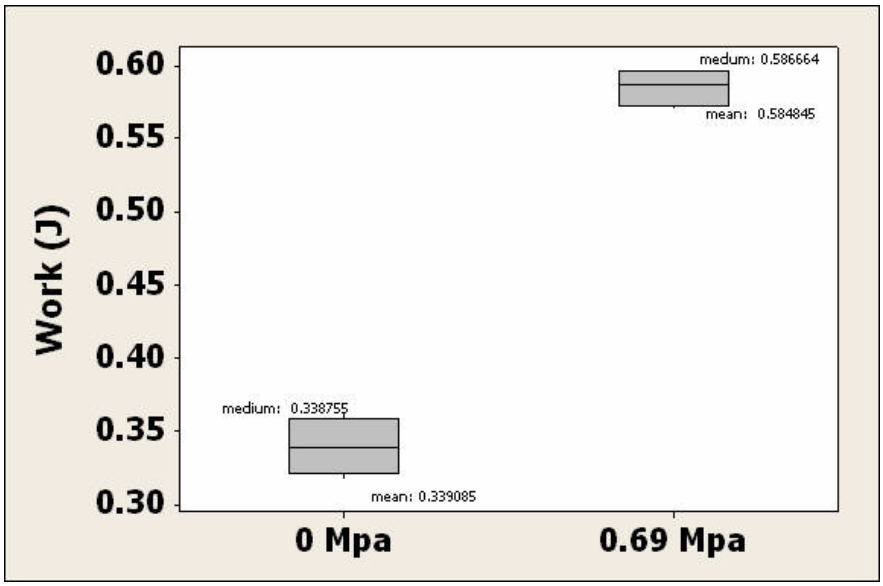

Figure 67. Statistical analysis of the work at all strain rates shows that the output is 0.34 +/- 0.019 J and 0.58 +/- 0.013 J at 0 and 0.69 MPa respectively. These deviations are within typical experimental error; therefore, the applied strain rate does not affect the work output.

Since the strain rates employed here do not affect the work output, the next experiments checked the affect that stress relaxation had on work output.

6.4.3. Work Output Dependence on Stress Relaxation

This test was performed on the latex rubber tube and the McKibben muscle. In each test, we performed three cycles of tensile extension from zero stretch to maximum stretch and back to zero stretch again. During cycle one and cycle three we held the maximum stretch for 400 to 700 seconds and recorded the stress. The Figures below show that the peak of each cycle does stabilize but only after stress relaxation has occurred. Stress relaxation still occurred in cycle three; this relaxation is consistent with

relaxation at the first cycle's end. We performed these experiments with two different McKibben muscles to determine if a change would occur from muscle to muscle. In Figure 68, the graph illustrates that stress relaxation does have an influence on the experiments conducted. The results show that once the initial peak force has been reached, the McKibben muscle has to go through a stress relaxation process due to creating an initial stretch on the latex tube. Over time, the peak force reaches a stabilized rate where stress relaxation has been completed – the displacement process proves that the result is constant. We designed the experiments with the knowledge acquired in the time stability test that all test would need to allow stress relaxation to occur before the experiments would be completed. In Figure 69, shows an up-close view of where the peak force stabilizes after stress relaxation occurs. In Figure 70, the trend proves that there is a direct correlation between the peak force and time. If R^2 is greater than 0.49 confirms that the two factors involve have a direct correlation to each other – both muscles had R^2 greater than 0.99.

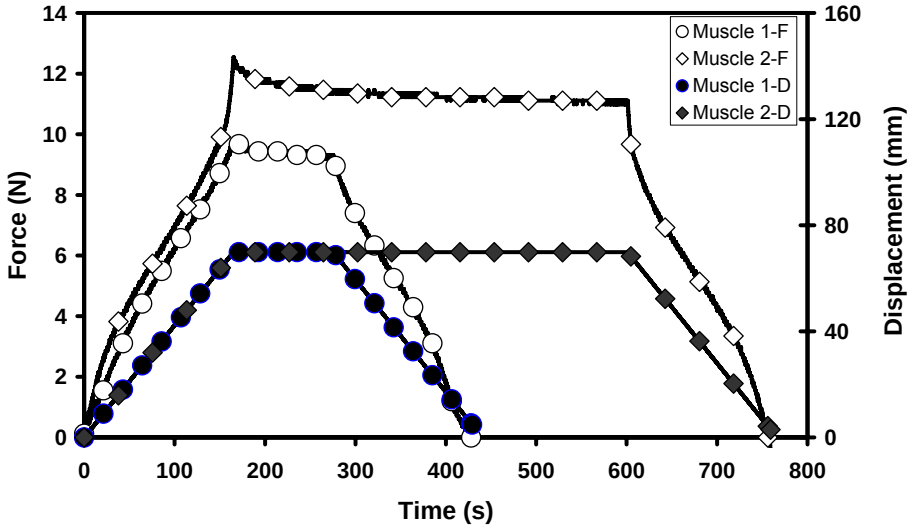

Figure 68. This graph conveys how stress relaxation influences force for a McKibben muscle. It also conveys how force becomes constant over time.

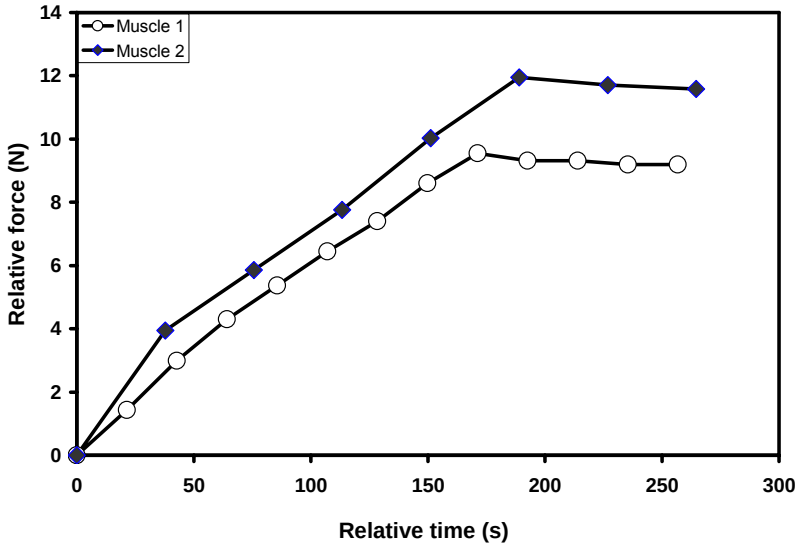

Figure 69. This graph conveys how the McKibben muscle's peak force stabilizes.

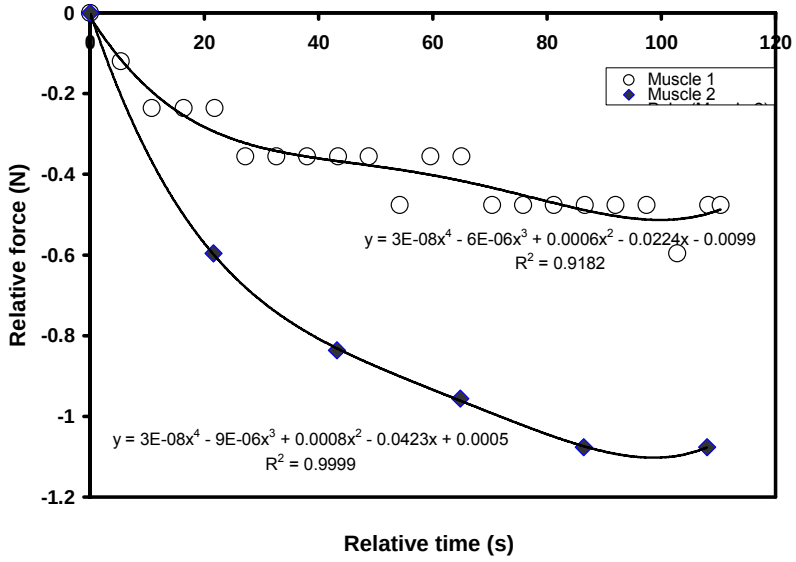

Figure 70. This is a detailed version of the elastomer tube peak, focused from the initial peak force to an area where it begins to stabilize.

6.5. RESULT OF MUSCLE SHEET

All McKibben muscle sheets were characterized by using the tensile testing method, cycle test and stability test. Each sheet is designed as an array of one, two, three or five McKibben muscles inside a polyurethane matrix. The data acquired informs us how an array of McKibbens behaves within an elastomer matrix. It will inform us how the muscle sheets behave compared to a bare McKibben muscle and how the matrix volume affects the mechanical characteristics of the muscle sheet.

Pull-out test:

A pull-out test was performed, to determine how much of the PET braided mesh sleeve would need to be embedded into the polyurethane matrix before a failure occurs within the specimen. We created a testing specimen for this experiment, where we

inserted a sample of PET braided mesh sleeve into a small square polyurethane matrix. The PET braided mesh sleeve was partially inserted into the matrix at different length. In Figure 71, the picture depicts that the PET braided mesh sleeve did not fracture, but it completely separated from the matrix. Inside of the PET braided sleeve mesh, we inserted a polyurethane matrix with the exact shape inner sleeve to prevent the sleeve from collapsing. In Figure 72, the graph illustrates the behavior of the PET braided mesh sleeve in the polyurethane matrix before and after the experiment.

Table 12. Pull-out test analysis.

Number of samples:	4
Test speed:	25.4 mm/min
Data acquisition sample rate	5 Hz
PET sleeve length:	30 mm
Matrix dimension:	19 x 19 x 15 mm

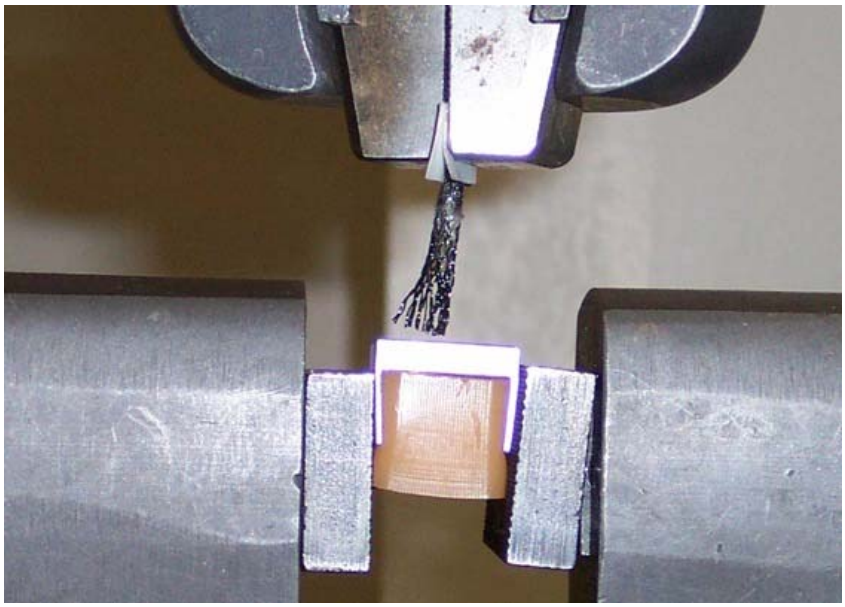

Figure 71. This picture shows the PET mesh sleeve pulled from the polyurethane matrix without fracture of the mesh.

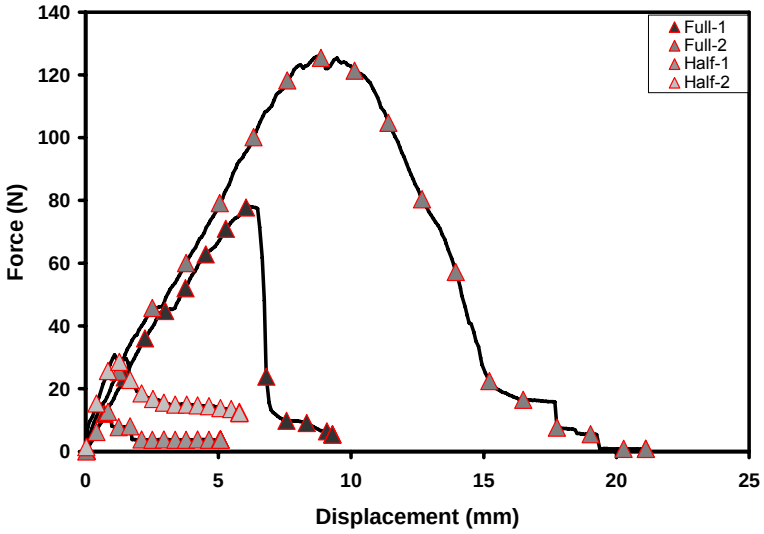

Figure 72. This graph conveys the results of the pull-out test for specimens with 15 mm and 7.5 mm embedded lengths of the sleeve in the polyurethane matrix. The braid did not fail in either test.

6.5.1. Single Embedded Sheet

Tensile Test Experiment:

Data was acquired from three single-embedded McKibben muscle specimens, and the displacement graph is shown in Figure 73. Detailed information would be displayed for the mean of the three single-embedded McKibben sheet. The force-displacement results in Figure 73, were used to show the difference between all three muscles, plus it would be easier to calculate the mean from the graph. The graph depicts that all three muscle have the similar behavior especially when the hysteresis is pronounced in the graph. Muscle one was chosen as the mean of all three sheets.

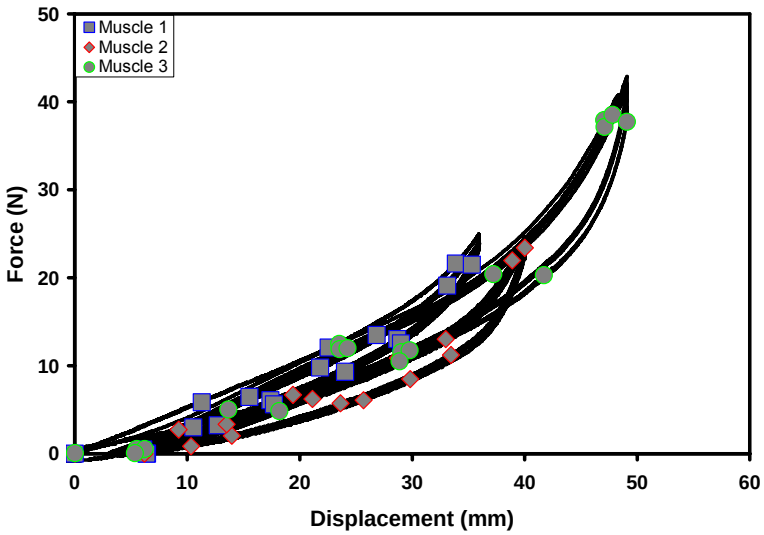

Figure 73. This graph represents force-displacement data for three single embedded muscles.

Figures 74-78, display detailed results for the average single-embedded McKibben muscle from the three tested at 0 MPa – muscle one was chosen as the mean of the three single-embedded sheets. In Figure 74, the graph provides an overall trend of the single-embedded McKibben muscle. The peak force of the single-embedded McKibben muscle has increased from the peak force of the McKibben muscle only. We performed three cycles on the specimen to acquire the true peak force that stabilizes after the 3rd cycle due to stress relaxation. In Figure 75, the graph focuses on the force-time process to illuminate the peak force changes due to stress relaxation. The force-displacement graph always illustrates if hysteresis has occurred or not, as shown in Figure 76. The lagging effect in the force-displacement graph is pronounced more than the McKibben muscle only, the 2nd and 3rd cycle do not return back to the 0 position but at 5mm. Figures 77 and 78, provide an up-close view of the characteristics of the single-embedded McKibben. Both graphs, prove that there is a consistent trend in regards to time and displacement due to the overlapping of all cycles of the unloading unactuated single-embedded McKibben muscle.

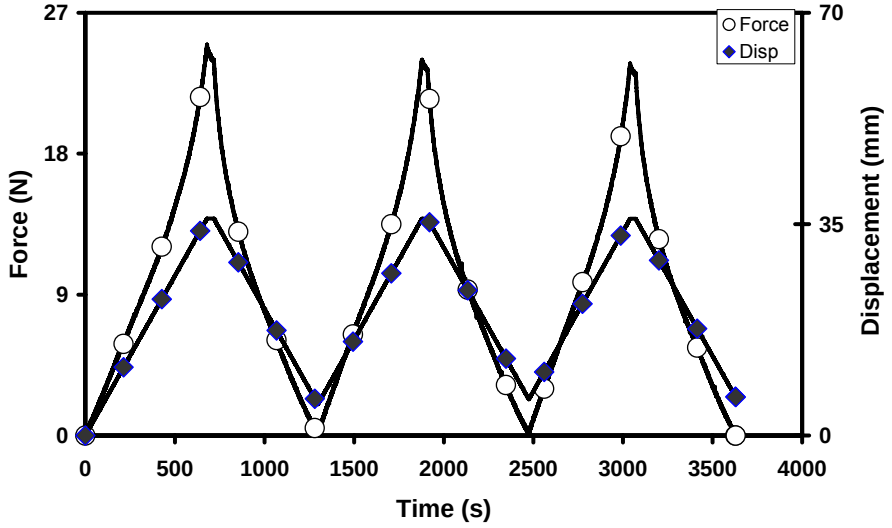

Figure 74. This is muscle one data displayed for a single-embedded muscle at 0 MPa.

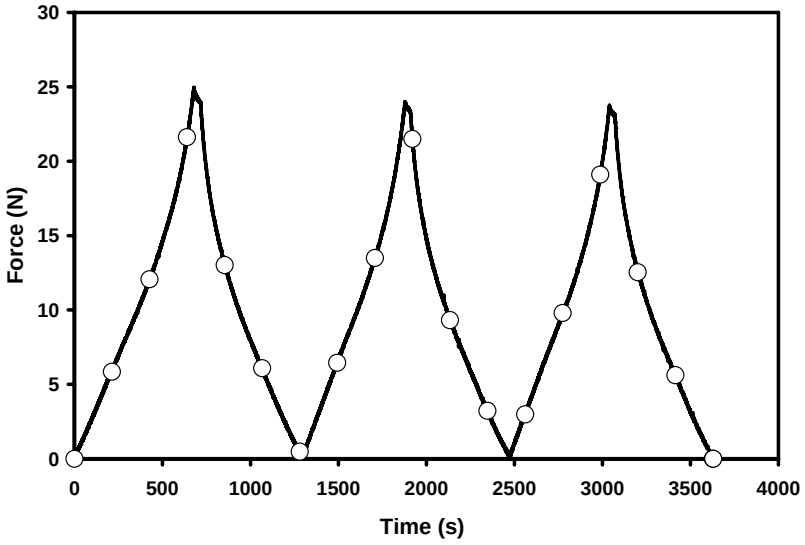

Figure 75. This graph conveys the cycle consistency of the single-embedded muscle.

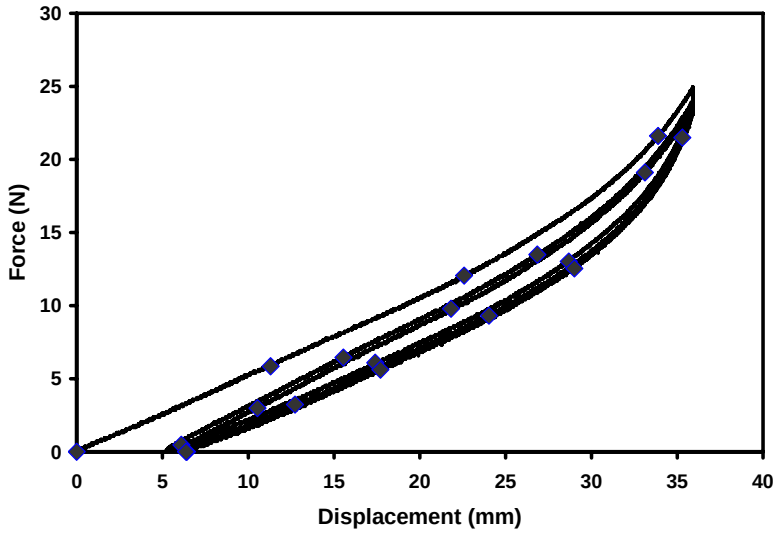

Figure 76. This graph conveys the how the force is dependent on displacement. The first cycle is separated from the other cycles.

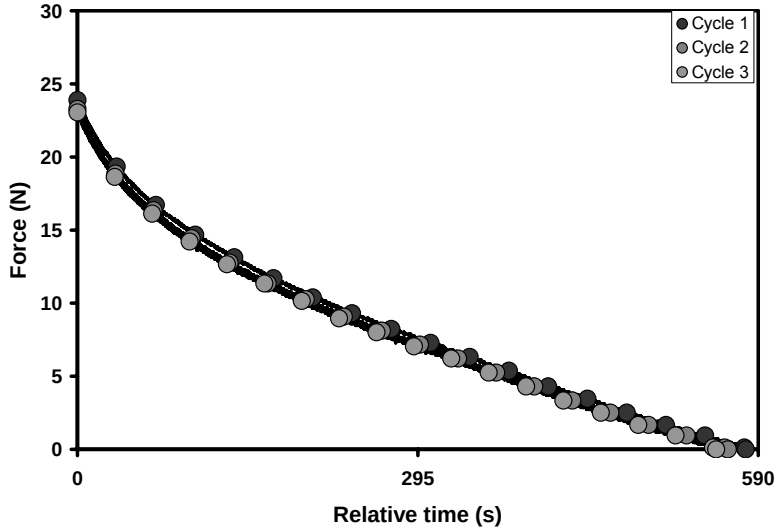

Figure 77. This graph conveys the single-embedded muscle consistency for the unloading time with all cycles.

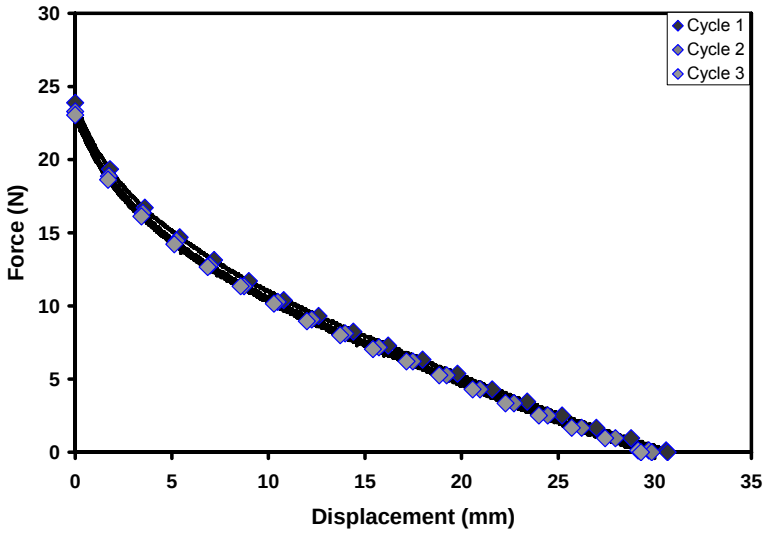

Figure 78. This graph conveys the consistency for all cycles of the unloading single-embedded muscle.

Tensile Test at Variation of Actuation Pressure:

Figures 79 - 81, display detailed information for the average single-embedded McKibben muscle at all pressures from 0 to 0.69 MPa. This experiment is to determine if we can increase the force and work output, by increasing the actuation pressure and investigate what characteristics are affected. In Figure 79, the graph depicts the results of the single-embedded McKibben sheet as the actuation pressure varies from 0 MPa to 0.69 MPa. The initial test with actuation pressure of 0 MPa is cycle three times, to allow the sheet to undergo its stress relaxation – this allows us to perform one cycle with the changes of actuation pressure. The graph shows an interesting trend with the loading actuation process, for all actuation pressure on the single-embedded McKibben sheet the loading actuation process are equivalent to each other. Otherwise, their unloading actuation process differs because as the sheet is

contracting the actuation pressure determines the muscles speed for returning to its original state. In depth detail is provided in Figures 80 and 81, the graphs show how force behaves in regards to relative time and displacement, respectively. Both graphs, display the same characteristics in regards to actuation pressure. Force is dependent on the actuation pressure in regards to relative time and displacement. In a single-embedded McKibben sheet, as the actuation pressure increases the force increases as well, but the contraction rate decreases. Similar trend is shown in the force-displacement results of the unloading actuation process that as force increases with actuation pressure the displacement increases as well. The single-embedded McKibben sheet behaves similar to the McKibben only specimen; the polyurethane matrix has been able to enhance some of its properties.

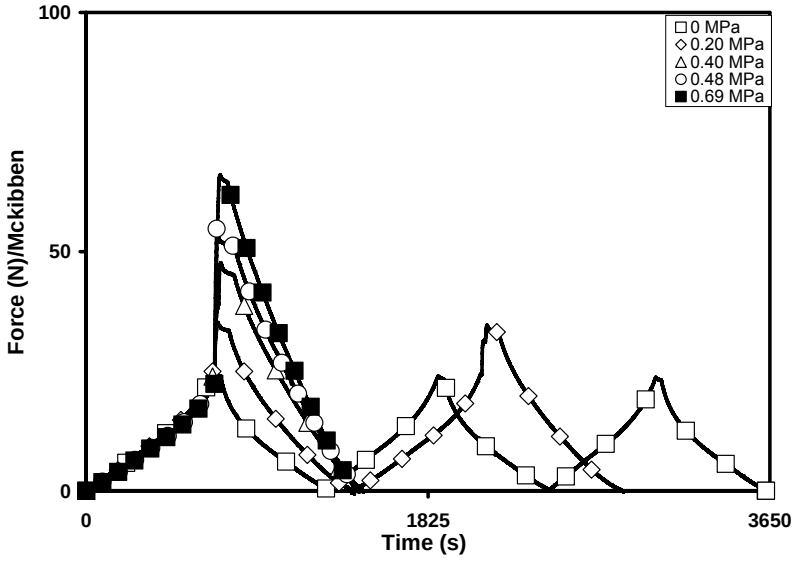

Figure 79. This graph conveys all pressures for the single-embedded muscle. It shows how force is dependent on pressure.

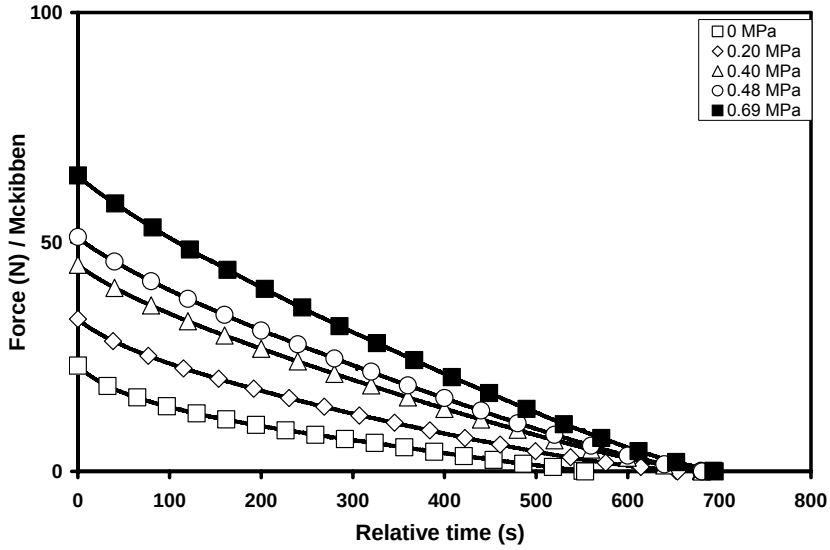

Figure 80. This graph represents the unloading of the single-embedded muscle for all actuation pressures. It conveys how force is dependent on pressure.

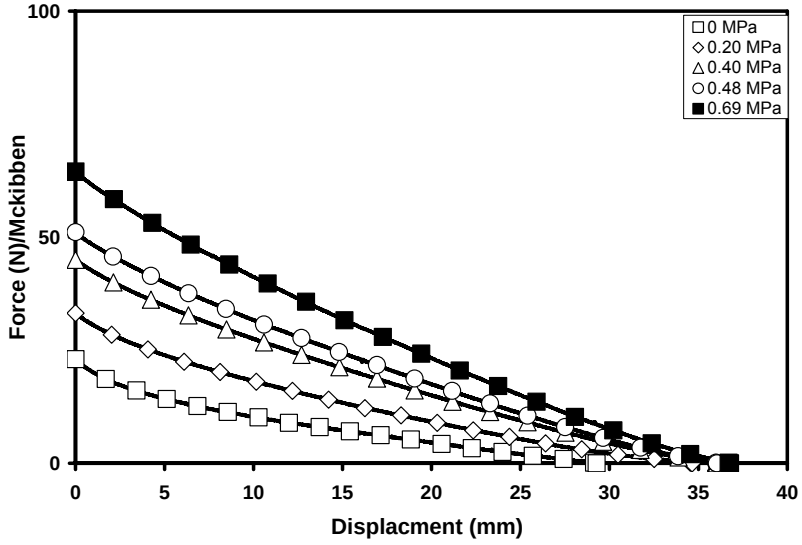

Figure 81. This graph represents the unloading of the single-embedded muscle for all pressure due to displacement. The displacement decreases as force increases.

The stress-strain results provided in Figure 82 shows similar trend as the force-displacement results. Stress is always dependent on force, while strain is dependent on displacement, as shown in the graph below. As the actuation pressure increases on the single-embedded McKibben muscle, so does the stress and strain characteristics. The work-displacement results are provided in Figure 83, it illustrates that as work increases with the actuation pressure the displacement increases. This is important depending on your goal of either increasing the work output or increasing displacement. In our case, we are interested in increasing the work output. We also calculated the work-density of the single-embedded McKibben sheet, by analyzing both the contraction and extended positions. In Figure 84, displays the result for the contraction process. It follows similar trend as the work-output, as the work-density increases with actuation pressure the displacement decreases. The curve also shows that we can increase the work-density output, but the displacement will become constant after a while. The extended process is shown in Figure 85, it follows the same trend as the work and contraction work-density output. Comparing the contraction and extended process, the work-density output differs between positions. To acquire the correct data for the work-density output, interpolation would need to be performed in-between the contraction and extended process.

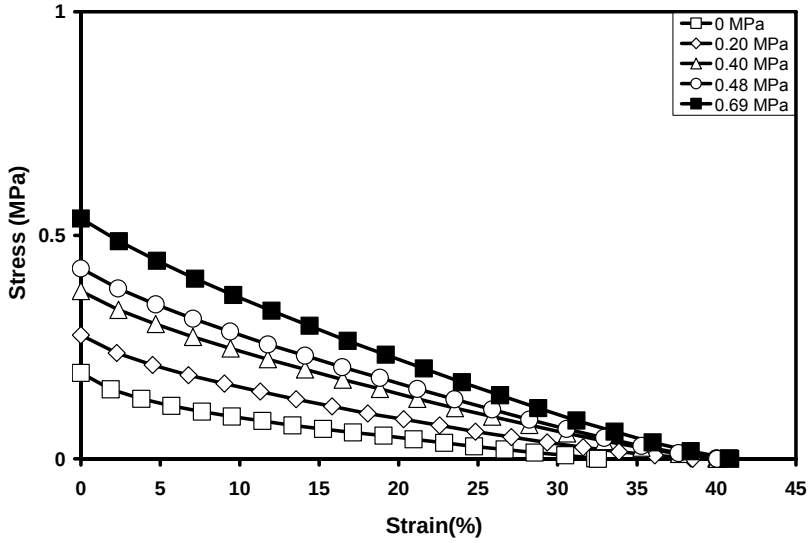

Figure 82. All pressures of the single-embedded muscle are represented by the stress-strain curve. Stress is dependent on pressure.

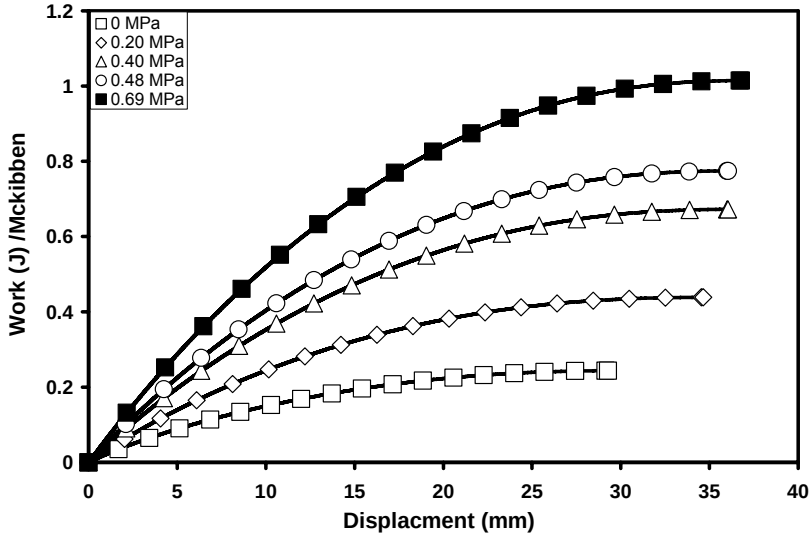

Figure 83. This graph conveys how work is dependent on pressure for a single-embedded muscle.

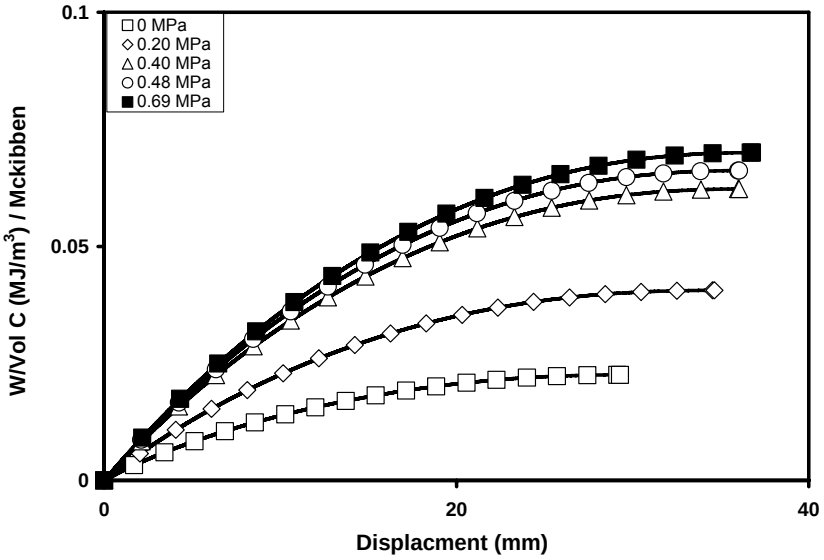

Figure 84. This graph conveys how work density is dependent on pressure of a single-embedded muscle when it contracts.

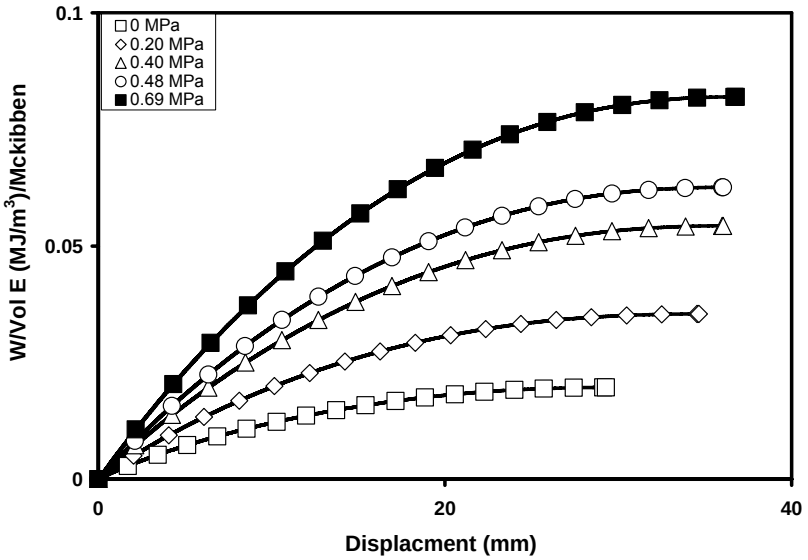

Figure 85. This graph conveys how density is dependent on pressure of a single-embedded muscle when it extends.

In Figure 86, we provided the force-actuation pressure results to illustration if there are any correlations between each factors. The results prove that if we are interested in developing a single-embedded McKibben sheet with force larger than 65 N, we just need to increase the actuation pressure accordingly - will need to note single-embedded McKibben sheet's failure point. The curve shows a positive upward trend that suggests the process would not plateau. In Figure 87, the graph has the results for both the contraction and extended work-density output. The graph illustrates that the region in-between both process is where the true work-density work output lies, while the curves represent the limitations. The work-density output follows similar trend in regards as to the force-actuation pressure characteristics. The results prove that force, work and work-density are dependent on the actuation pressure.

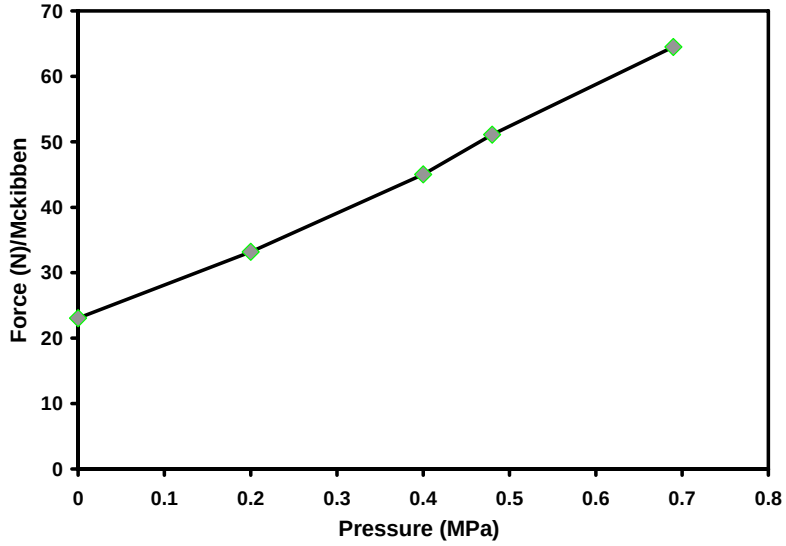

Figure 86. This is a detailed graph showing how force is dependent on pressure for a single-embedded muscle.

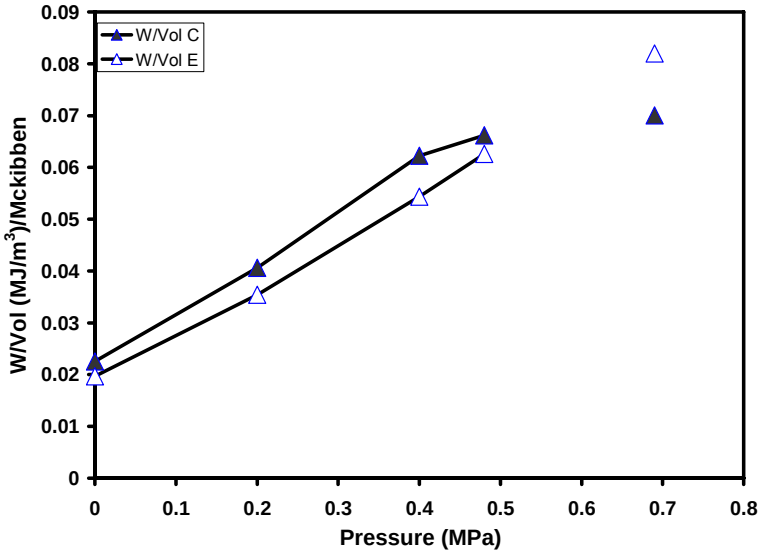

Figure 87. This is a detailed graph showing how work and density are dependent on pressure for a single-embedded muscle.

Stability Test by Variation in Speed:

The stability test by variation of speed was conducted to ensure that the experiment speed will influence the results acquired – even though it was confirmed with the McKibben muscle only, it has to be confirmed with the single-embedded McKibben sheet due to additional factor of the polyurethane matrix. In Figure 88, the force-displacement results illustrates that the strain rate due to speed variation does not influence the results. The data for 0 MPa was performed to create a reference point, plus the results for actuation pressure of 0.69 MPa are overlapping each other. This proves that speed of 25.6 mm/min or less can be utilized to run the experiment without the results being influenced. Further investigation as shown in Figure 89, the work-displacement results illustrate that the strain rate is independent of the experiment at speeds less than or equal to 25.4 mm/min. The experimental error was at +/- 2.52, which is an acceptable range. The experimental error was calculated using Minitab to determine if there were any outliers – this can be viewed in Figure 90.

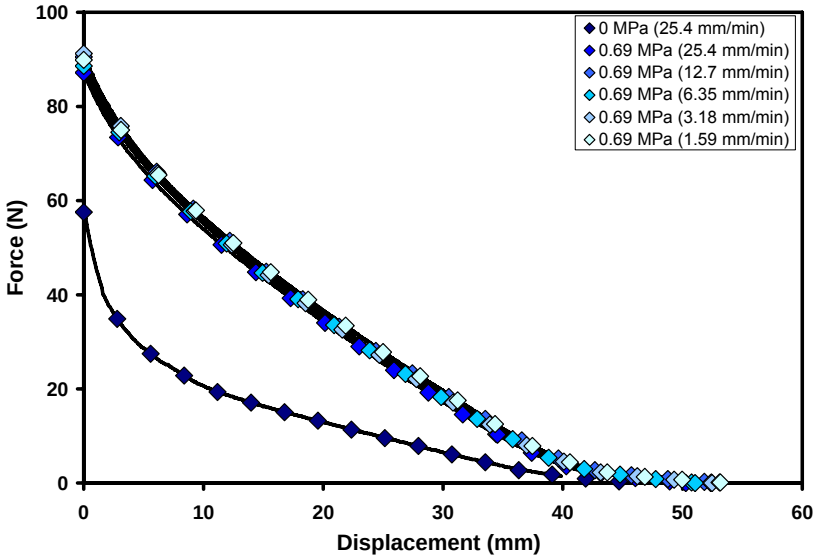

Figure 88. This graph shows that strain rate does not influence the force-displacement behavior of a single embedded muscle with an actuation pressure of 0.69 MPa. The 0 MPa performance appear for reference.

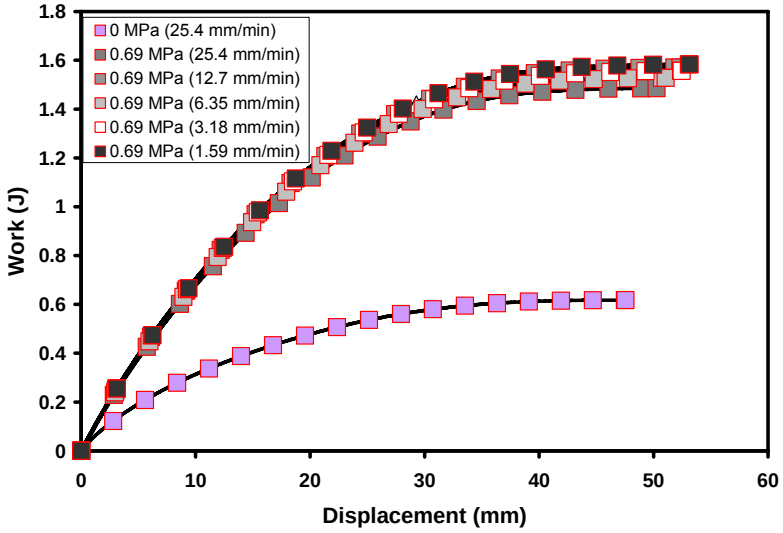

Figure 89. From this graph we do not expect the strain rate to affect the work output of a single embedded muscle for engineering strain rates between 0.0187 and 0.2988 min^{-1}. Average work output is 1.54 +/- 0.039 J, which is a reasonable experimental error at +/- 2.52 %.

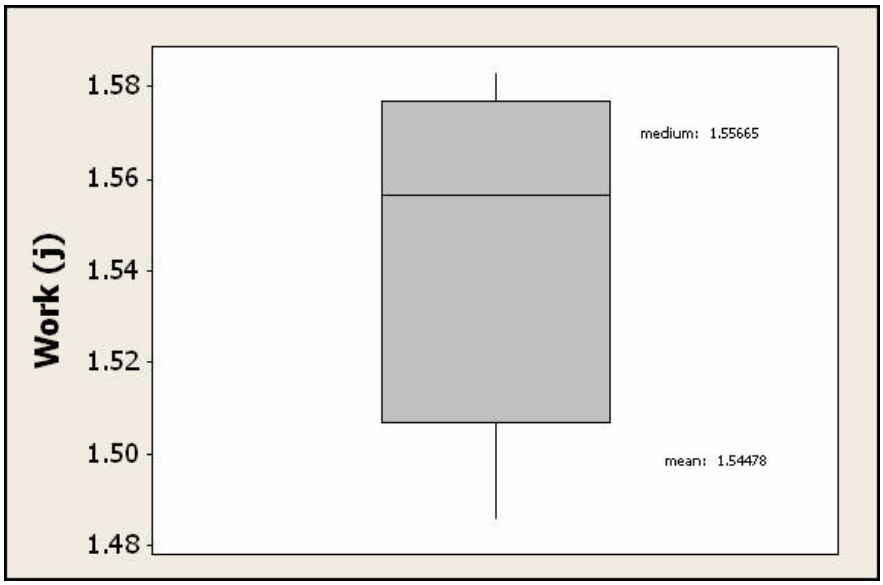

Figure 90. The average work output at 0.69 MPa actuation is 1.54 +/- 0.039 J, which is within typical experimental error. Therefore, the strain rate does not influence the work performed.

In Figure 91, the picture illustrates a dissected single-embedded McKibben muscle. The picture shows that the outer square shape is the polyurethane matrix that encloses the PET braided mesh sleeve of the McKibben muscle and inside the muscle is the latex rubber tube. The picture illustrates that the McKibben muscle did not collapse while being enclosed in the polyurethane matrix, plus the McKibben muscle was not filled with the polyurethane matrix.

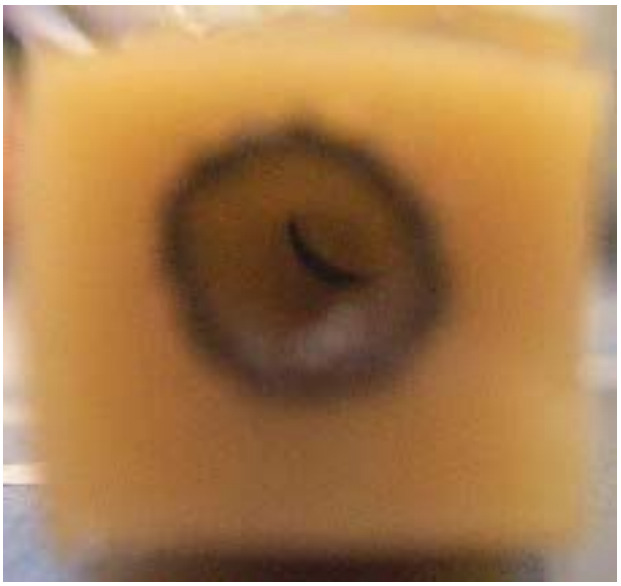

Figure 91. The dissected view of the single-embedded McKibben sheet.

6.5.2. Double Embedded Sheet

Tensile Test Experiment:

Data was acquired from three double-embedded McKibben muscle specimens, and the displacement graph is shown in Figure 92. Detailed information would be displayed for the mean of the three double-embedded McKibben sheet. The force-displacement results in Figure 92, were used to show the difference between all three sheets, plus it would be easier to calculate the mean from the graph. The graph depicts that all three sheets have the similar behavior especially when the hysteresis is pronounced in the graph. Comparing the force-displacement results from the single-embedded McKibben sheet to the double-embedded McKibben sheet, they both portray the same trends and characteristics – force output differs with the double-embedded McKibben sheet has a greater force output. Muscle one was chosen as the mean of all

three sheets.

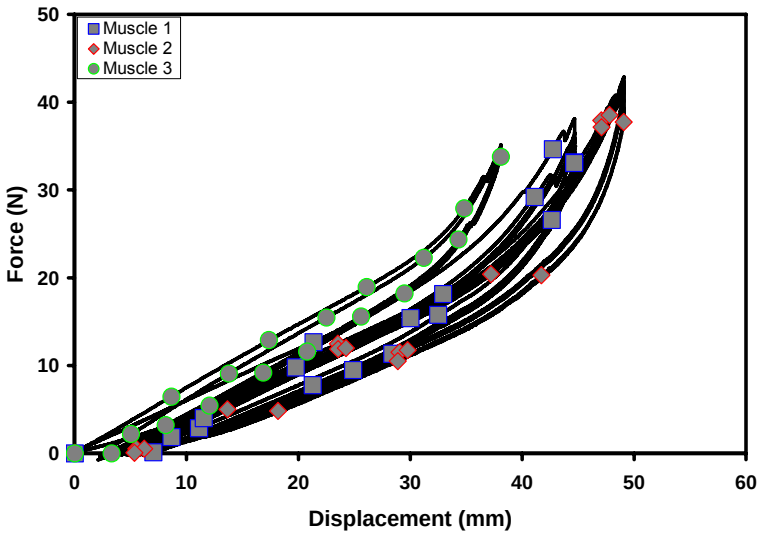

Figure 92. This graph represents force-displacement data for three double-embedded muscles.

Figures 94-97, display detailed results for the average double-embedded McKibben sheet from the three tested at 0 MPa – this is muscle one, which was chosen as the mean of the three single-embedded sheets. In Figure 93, the graph provides an overall trend of the double-embedded McKibben sheet. The peak force of the double-embedded McKibben sheet has increased from the peak force of the single – embedded McKibben sheet only. We performed three cycles on the specimen to acquire the true peak force that stabilizes after the 3rd cycle due to stress relaxation. In Figure 94, the graph focuses on the force-time process to illuminate the peak force changes due to stress relaxation. The force-displacement graph always illustrates if hysteresis has occurred or not, as shown in Figure 96. The lagging effect in the force-displacement

graph is close to the single-embedded McKibben sheet only, the 2nd and 3rd cycle do not return back to the 0 position but at 6 mm. Figures 95 and 97 provide an up-close view of the characteristics of the single-embedded McKibben. Both graphs prove that there is a consistent trend in regards to time and displacement due to the overlapping of all cycles of the unloading unactuated double-embedded McKibben muscle.

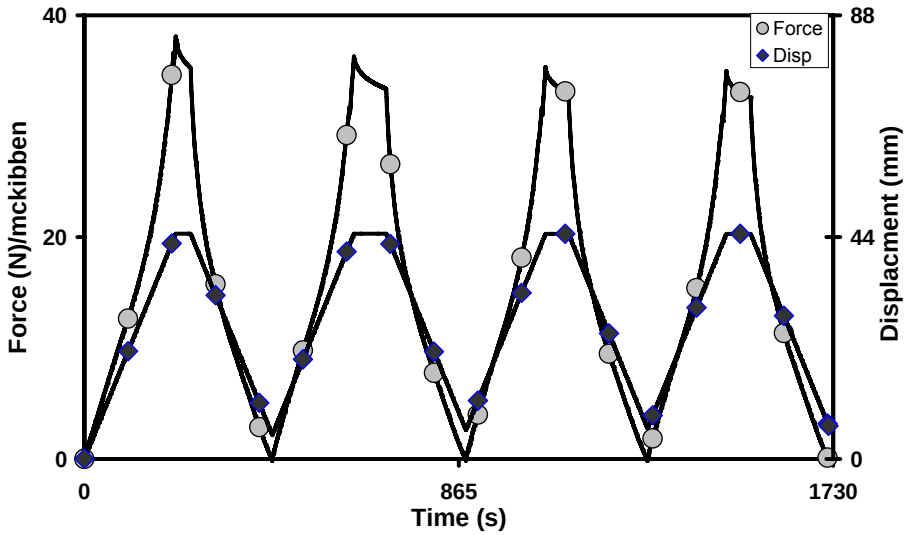

Figure 93. The data displayed is muscle one, which is the middle data at 0 MPa.

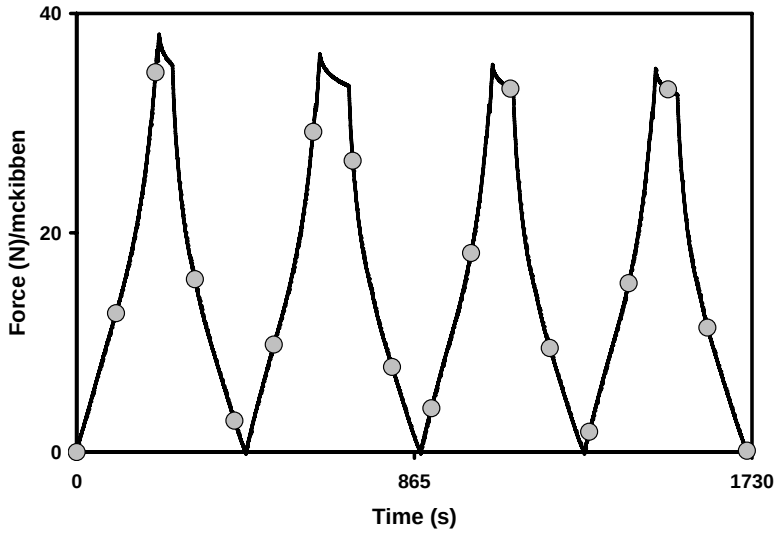

Figure 94. This graph conveys the cycle consistency of the double-embedded muscle.

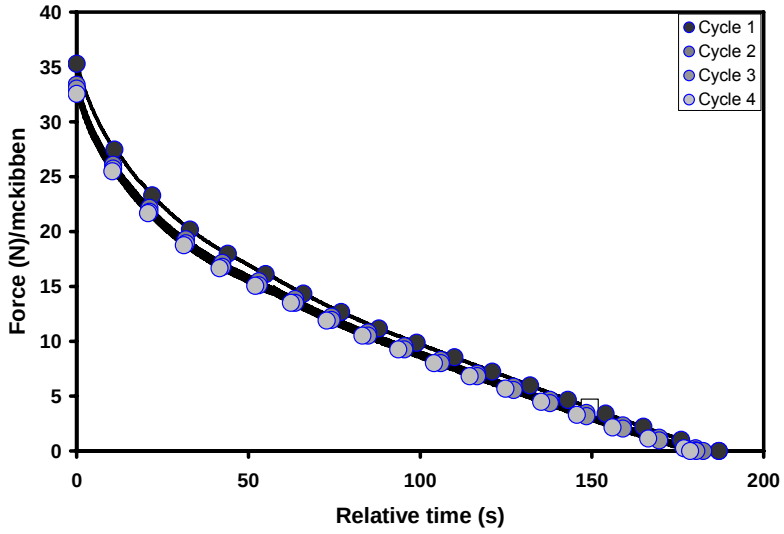

Figure 95. This graph conveys the double-embedded muscle consistency for the unloading time with all cycles.

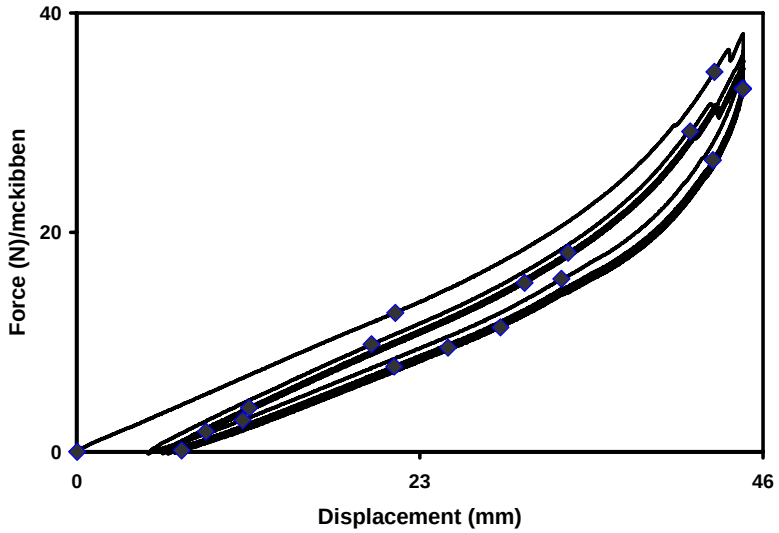

Figure 96. This graph conveys the how the force is dependent on displacement. The first cycle is separated from the other cycles.

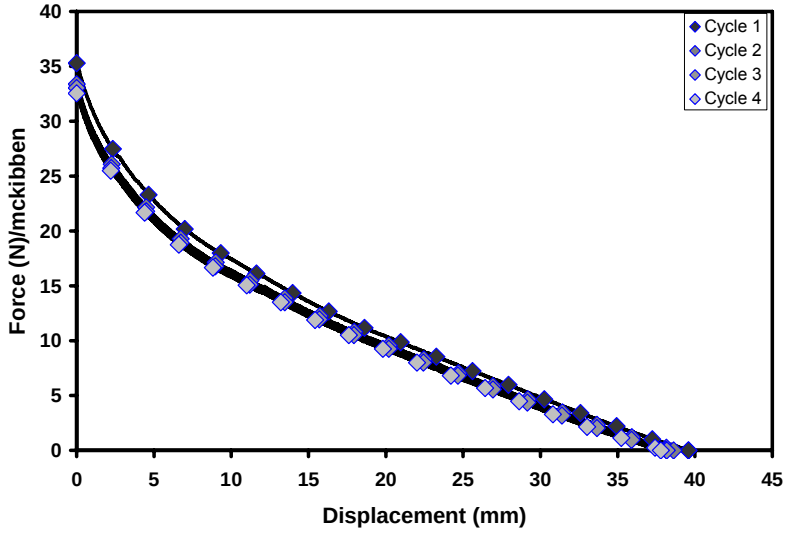

Figure 97. This graph conveys the consistency for all cycles of the unloading double-embedded muscle. The force gap between cycle 1 and cycle 2 is due to hysteresis.

Tensile Test at Variation of Actuation Pressure:

Figures 98 - 100, displays detailed information for the mean double-embedded McKibben muscle at all pressures from 0 to 0.69 MPa. This experiment is to determine if we can increase the force and work output by increasing the actuation pressure and to investigate what characteristics are affected. In Figure 98, the graph depicts the results of the double-embedded McKibben sheet as the actuation pressure varies from 0 MPa to 0.69 MPa. The initial test with actuation pressure of 0 MPa is cycled three times, to allow the sheet to undergo its stress relaxation – this allows us to perform one cycle with the changes of actuation pressure. The graph shows an interesting trend with the loading actuation process, for all actuation pressure on the double-embedded McKibben sheet the loading actuation process are equivalent to each other on the 1st cycle. Otherwise, their unloading actuation process differs because as the sheet contracts the actuation pressure determines how fast the muscle returns to its original state. In depth detail is provided in Figures 99 and 100, the graphs show how force behaves in regards to relative time and displacement, respectively. Both graphs, display the same characteristics in regards to actuation pressure. In a double-embedded McKibben sheet, as the actuation pressure increases the force increases as well, but the contraction rate decreases. Similar trend is shown in the force-displacement results of the unloading actuation process that as force increases with actuation pressure the displacement increases as well. The double-embedded McKibben sheet behaves similar to the single-embedded McKibben sheet specimen.

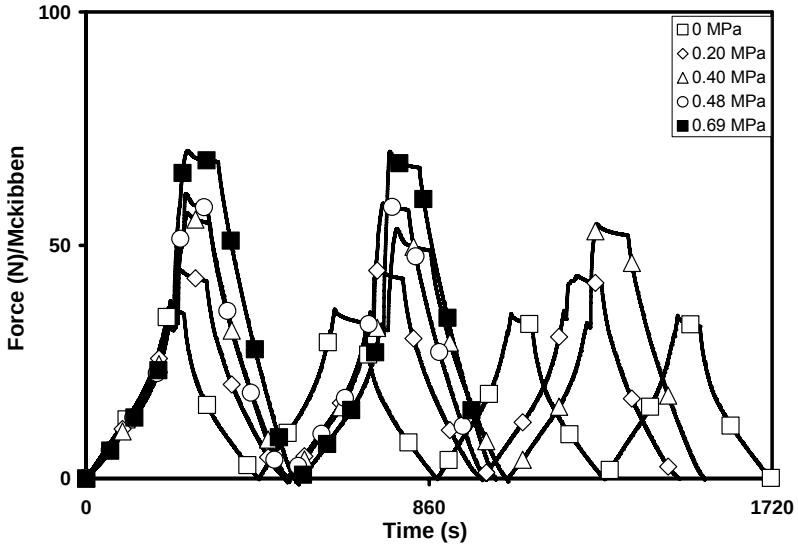

Figure 98. This graph conveys all pressures for the double-embedded muscle. It shows how force is dependent on pressure.

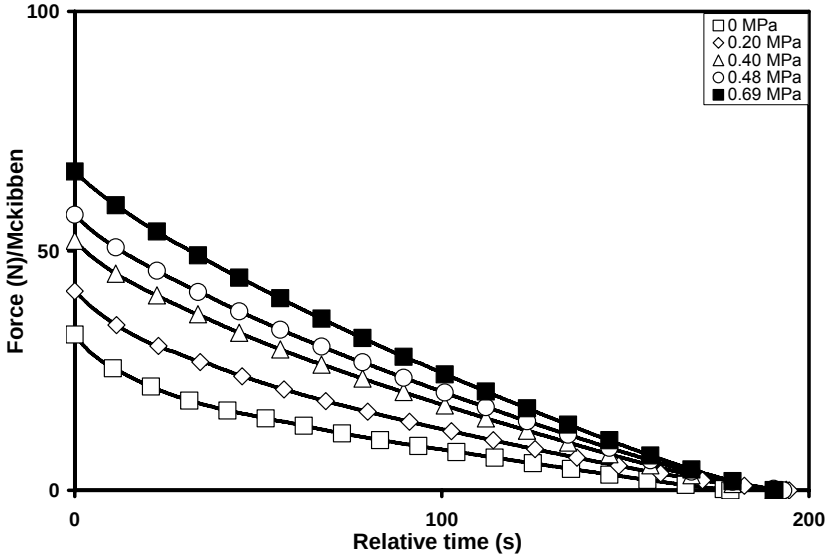

Figure 99. This graph represents the unloading of the double-embedded muscle for all pressure. It conveys how force is dependent on pressure.

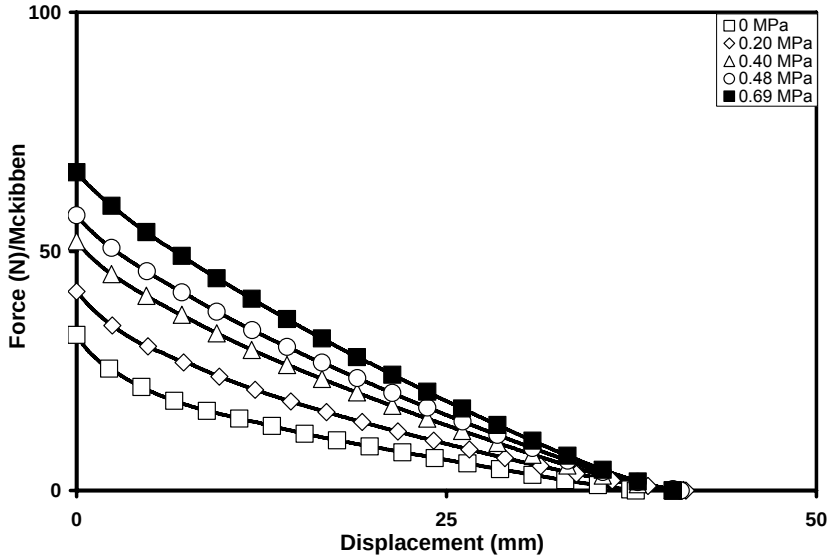

Figure 100. This graph represents the unloading of the double-embedded muscle for all pressure due to displacement. The displacement decreases as force increases.

In Figure 101, the stress-strain results illustrates that stress is influenced by the actuation pressure because as the actuation pressure increases stress increases. Note how the actuation pressure influences the stress-stain curve, the shape at 0 MPa is more of a parabolic form. As the actuation pressure increases the stress-strain curves become more linear.

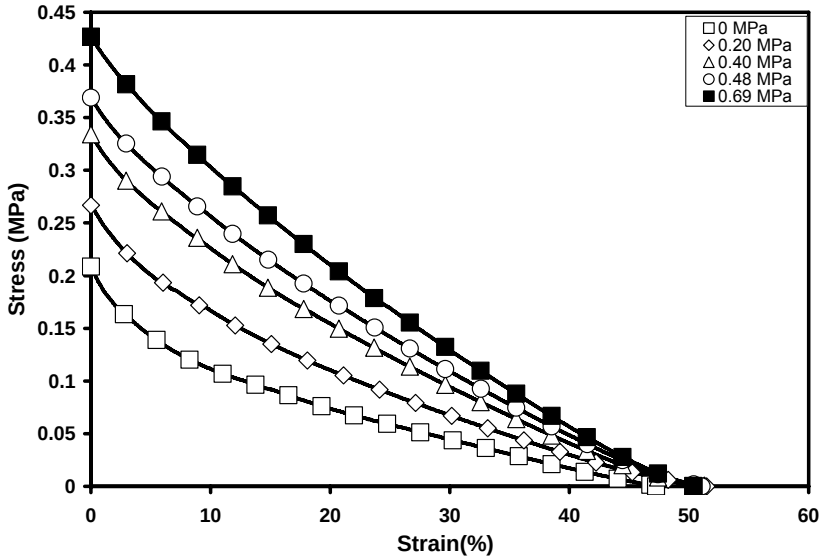

Figure 101. All pressures of the double-embedded muscle are represented by the stress-strain curve. Stress is dependent on pressure.

In Figure 102, the work-displacement results illustrate how the work output is influenced by the actuation pressure. As the actuation pressure increases the work output increases and displacement increases. We also calculated the work-density of the double-embedded McKibben sheet, by analyzing both the contraction and extended positions. In Figure 103, displays the result for the contraction process. It follows similar trend as the work-output, as the work-density increases with actuation pressure the displacement increases. The curve also shows that we can increase the work-density output, but the displacement will become constant after a while. The extended process is shown in Figure 104, it follows the same trend as the work and contraction work-density output. Comparing the contraction and extended process, the work-density output differs between positions. To acquire the correct data for the work-density output, interpolation would need to be performed in-between the contraction and extended

process.

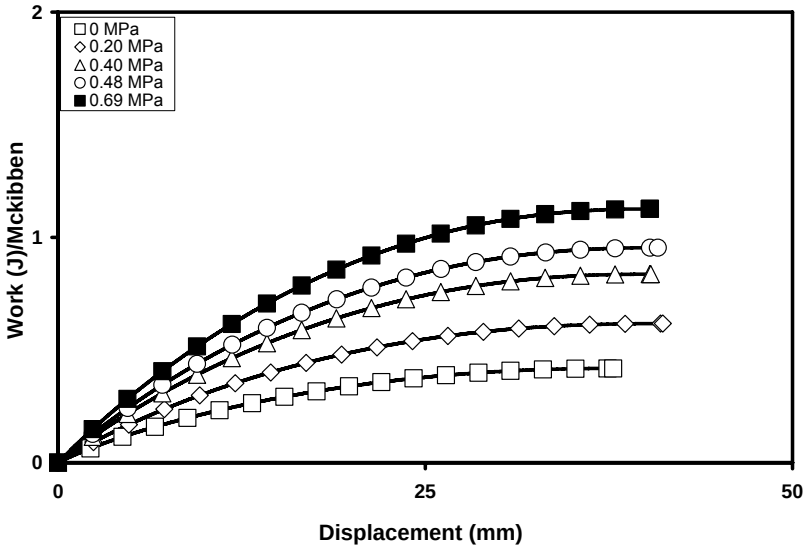

Figure 102. This graph conveys how work is dependent on pressure for a double-embedded muscle.

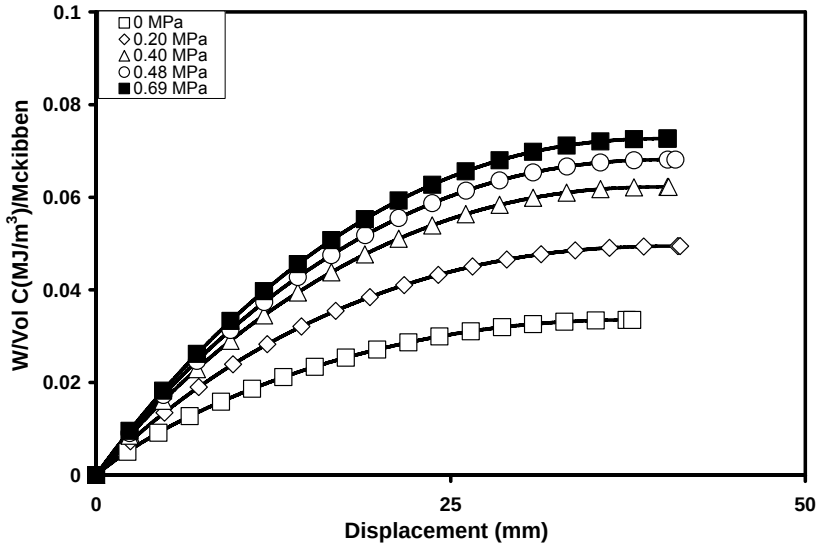

Figure 103. This graph conveys how density is dependent on pressure of a double-embedded muscle when it contracts.

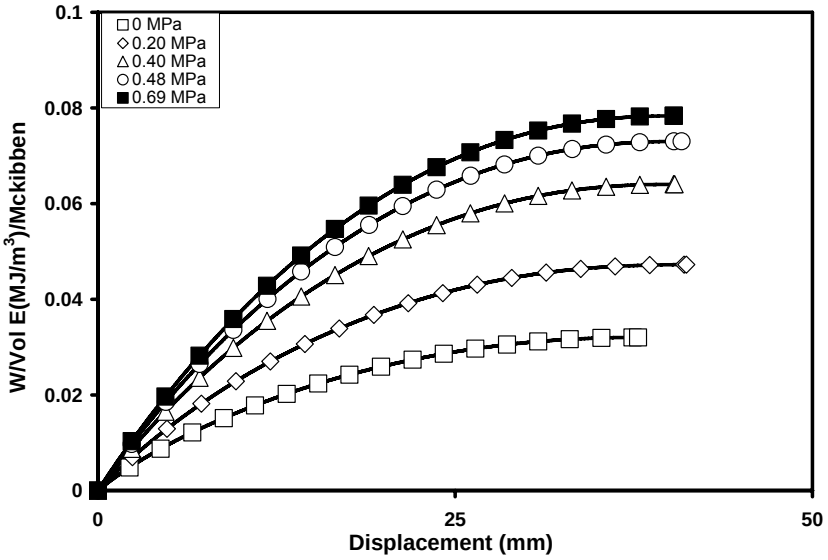

Figure 104. This graph conveys how density is dependent on pressure of a double-embedded muscle when it extends.

To understand how the actuation pressure influences the work and work-density output was calculated and the results are shown in Figures 105 and 106. The result in Figure 105 illustrates the work-density output in regards to the contraction and extension of the double-embedded McKibben sheet. To acquire the true work-density output of the double-embedded McKibben sheet, interpolation of the region in-between the contraction and extension result would need to be calculated. In Figure 106, the force-actuation pressure illustrates that as the actuation pressure increases the force output increases as well. The curve depicts a positive linear form that implies that there is a possibility of increasing the force output greater than 67 N by increasing the activation pressure.

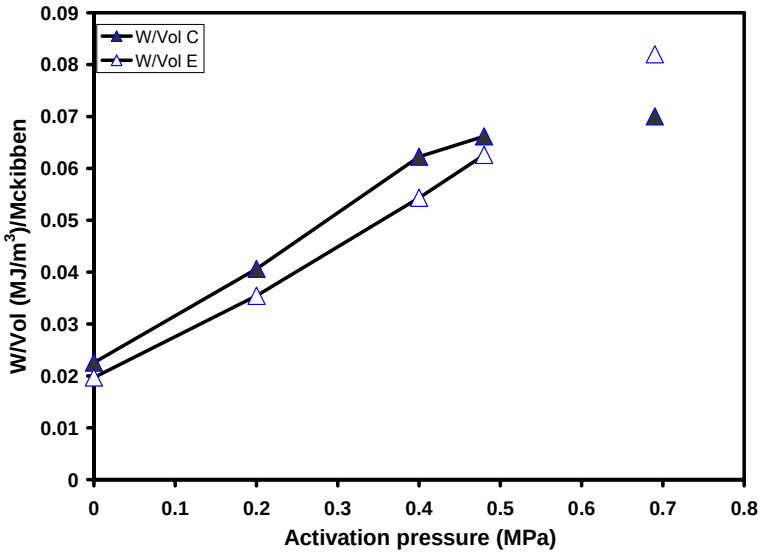

Figure 105. This is a detailed graph showing how work and density are dependent on pressure for a double-embedded muscle.

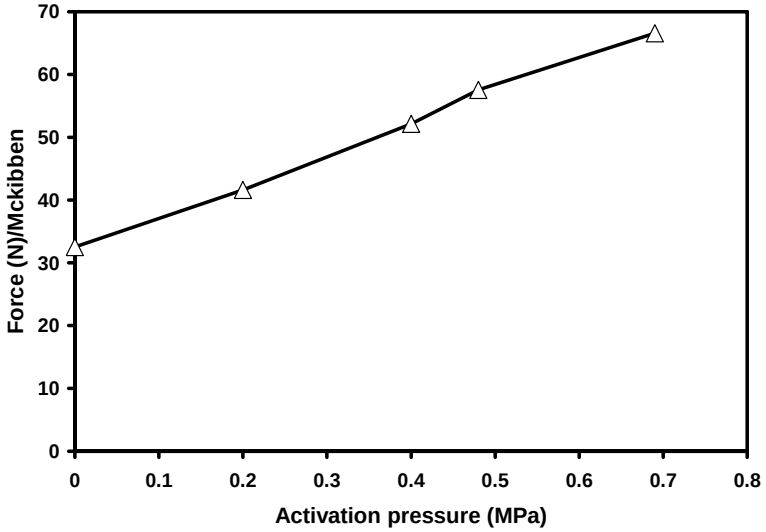

Figure 106. This is a detailed graph showing how force is dependent on pressure for a double-embedded muscle.

Stability Test by Variation in Speed:

The stability test by variation of speed was conducted to ensure if the experiment speed will influence the results acquired –it has to be confirmed with the double-embedded McKibben sheet due to additional factor of the polyurethane matrix. In Figure 107, the force-displacement results illustrates that the strain rate due to speed variation does not influence the results. The data for 0 MPa was performed to create a reference point, plus the results for actuation pressure of 0.69 MPa are overlapping each other. This proves that speed of 25.6 mm/min or less can be utilized to run the experiment without the results being influenced. Further investigation as shown in Figure 108, the work-displacement results illustrate that the strain rate is independent of the experiment at speeds less than or equal to 25.4 mm/min. The experimental error was at +/- 2.78, which is an acceptable range. The experimental error was calculated using Minitab to determine if there were any outliers – this can be viewed in Figure 109.

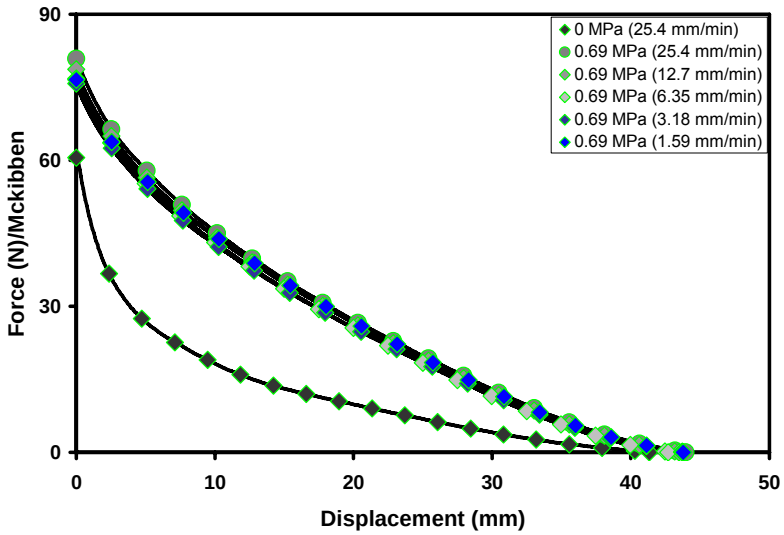

Figure 107. This graph shows that strain rate does not influence the force-displacement behavior of a double embedded muscle with an actuation pressure of 0.69 MPa. The 0 MPa performances appear for reference.

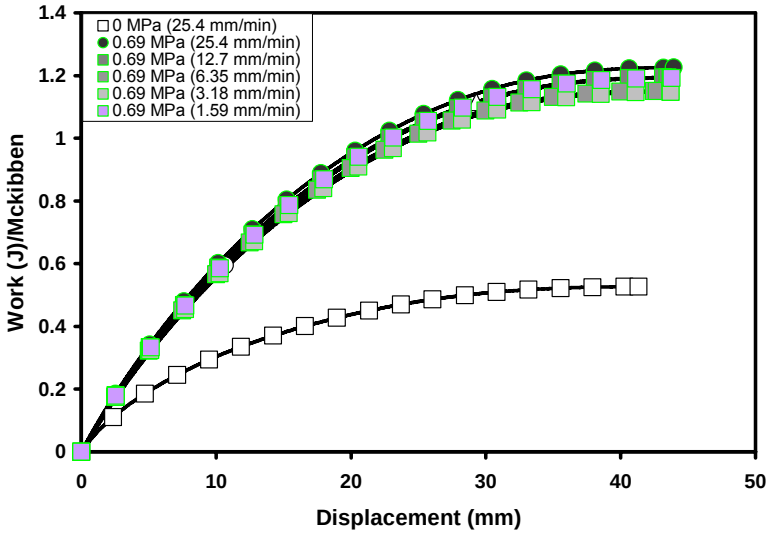

Figure 108. From this graph we do not expect the strain rate to affect the work output of a double embedded muscle for engineering strain rates between 0.0198 and 0.3175 min^{-1}. This graph conveys how speed influences work for double embedded muscle. The average work output is 1.18 +/- 0.033 J, which is a reasonable experimental error at 2.78 %.

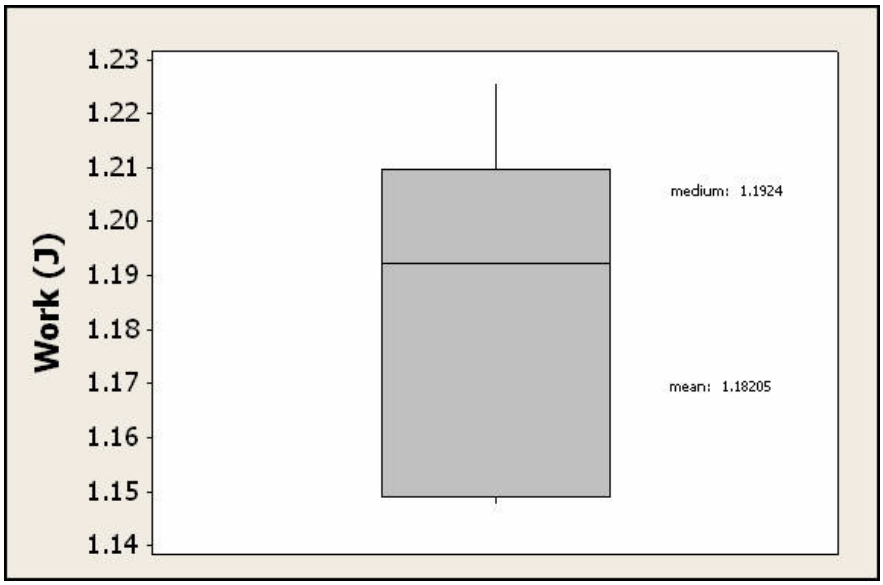

Figure 109. An average work output of 1.18 +/- 0.033 J which is within typical experimental error. Therefore, the strain rate does not influence the work performed.

The picture shown in Figure 110, illustrates a dissected part of the double-embedded McKibben sheet. The double-embedded McKibben sheet was created by enclosing two McKibben muscle in a polyurethane matrix, to act as an array. Note, the muscles were not centered properly to each other; this becomes a factor during the analysis.

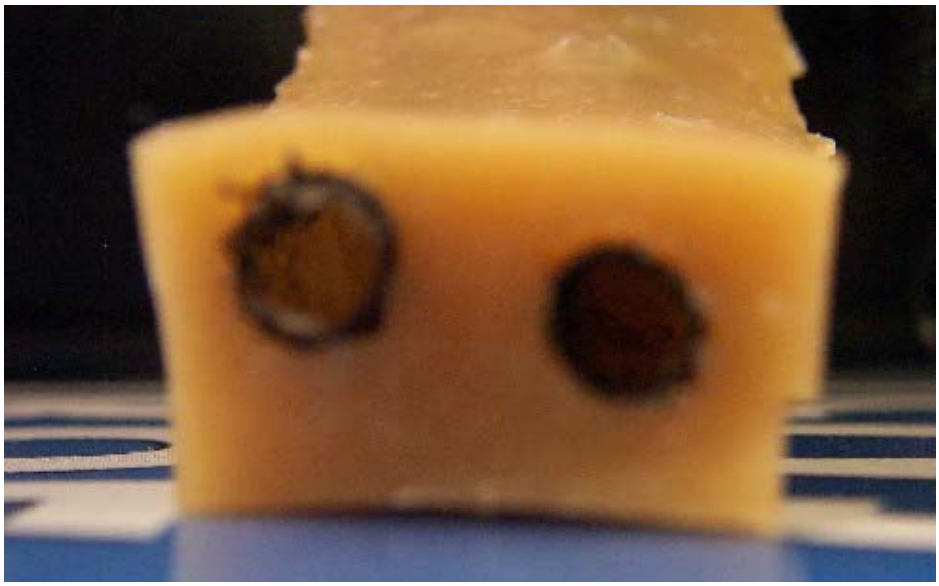

Figure 110. A dissected double-embedded McKibben sheet

Section 6.6.3 and 6.6.4 will provide details about the triple-embedded McKibben sheet and the quintuple-embedded McKibben sheet, respectively. Equivalent experiments were performed on these specimens and the results would show similar trends and characteristics but some differences. These experiments were important to determine how a McKibben muscle reacts being enclosed in a polyurethane matrix; and if one or more muscles being embedded would enhance its current characteristics and properties.

6.5.3. Triple Embedded Sheet

Tensile Test Experiment:

Data was acquired from three triple-embedded McKibben sheet specimens, and the displacement graph is shown in Figure 111. Detailed information would be displayed for the mean of the three double-embedded McKibben sheet. The force-displacement results in Figure 111, were used to show the difference between all three sheets, plus it would be easier to calculate the mean from the graph. Comparing the force-displacement results from the double-embedded McKibben sheet to the triple-embedded McKibben sheet, they both portray the same trends and characteristics – force output differs with the triple-embedded McKibben sheet has a greater force output. Muscle two was chosen as the mean of all three sheets.

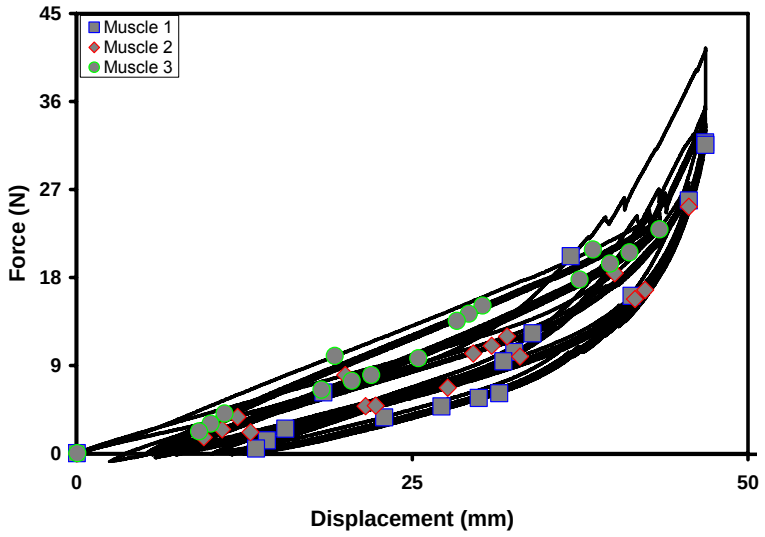

Figure 111. This graph represents force-displacement data for three triple embedded muscles.

Figures 112 - 116 display detailed results for the average triple-embedded McKibben sheet from the three tested at 0 MPa pressure – muscle sheet two was chosen as the mean of the three single-embedded sheets. In Figure 112, the graph provides an overall trend of the double-embedded McKibben sheet. We performed three cycles on the specimen to acquire the true peak force that stabilizes after the 3rd cycle due to stress relaxation. In Figure 113, the graph focuses on the force-time process to illuminate the peak force changes due to stress relaxation. The force-displacement graph always illustrates if hysteresis has occurred or not, as shown in Figure 115. Figures 114 and 116 provide an up-close view of the characteristics of the triple-embedded McKibben.

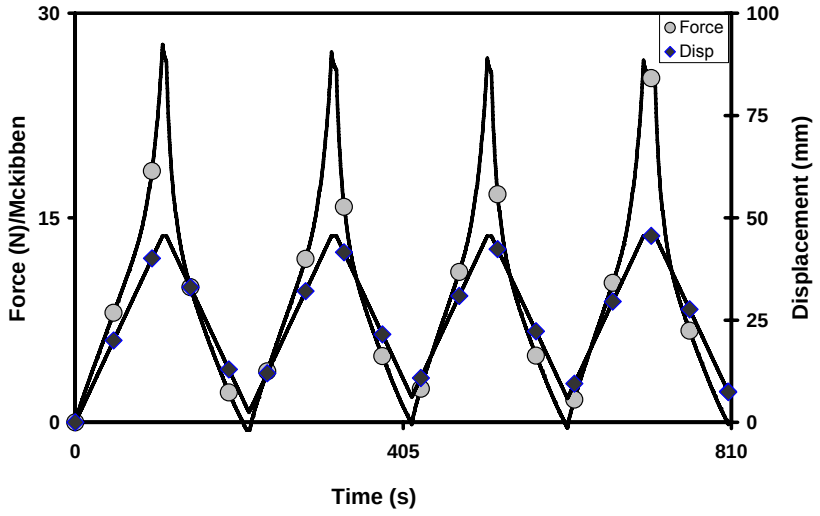

Figure 112. The data displayed is muscle two, which is the middle data at 0 MPa.

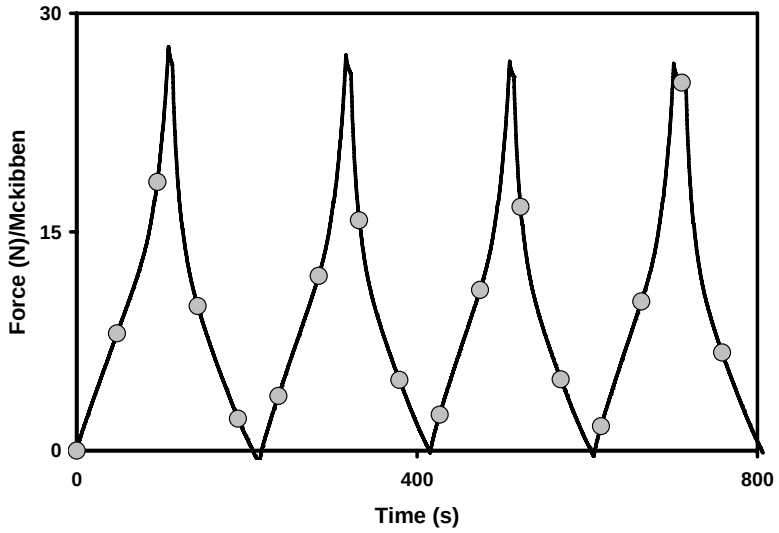

Figure 113. This graph conveys the cycle consistency of the triple-embedded muscle.

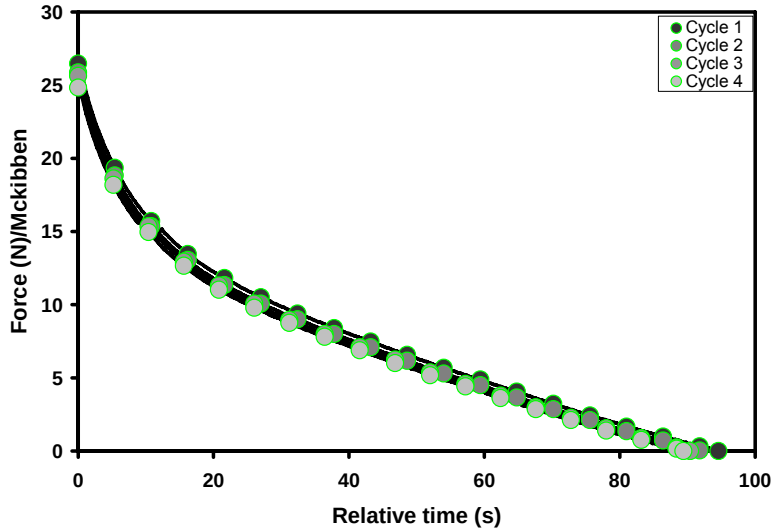

Figure 114. This graph conveys the triple-embedded muscle consistency for the unloading time with all cycles.

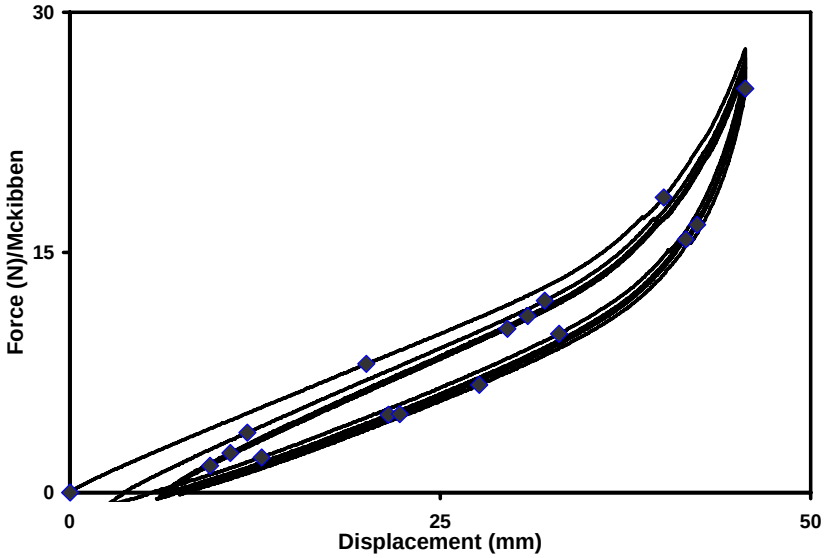

Figure 115. This graph conveys the how the force is dependent on displacement. The first cycle is separated from the other cycles.

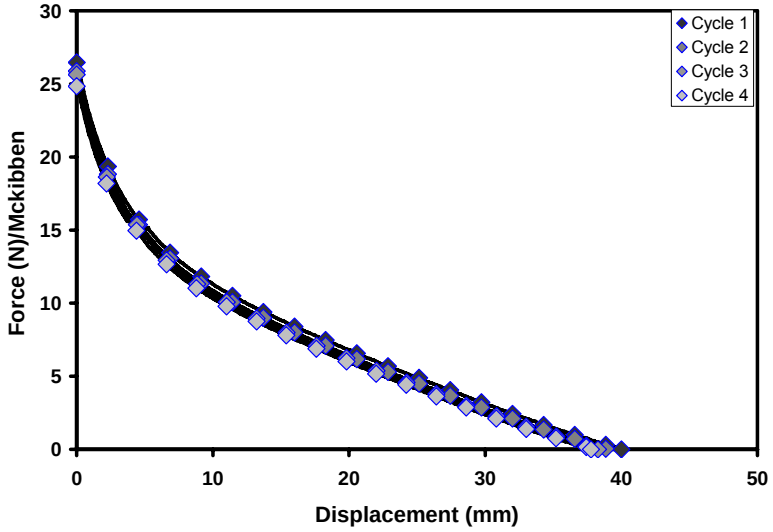

Figure 116. This graph conveys the consistency for all cycles of the unloading triple-embedded muscle.

Tensile Test at Variation of Actuation Pressure:

Figures 117 - 119, displays detailed information for the mean triple-embedded McKibben muscle at all pressures from 0 to 0.69 MPa. In Figure 117, the graph depicts the results of the triple-embedded McKibben sheet as the actuation pressure varies from 0 MPa to 0.69 MPa. In-depth detail is provided in Figures 118 and 119, the graphs show how force behaves in regards to relative time and displacement, respectively. In a triple-embedded McKibben sheet, as the actuation pressure increases the force increases as well, but the contraction rate decreases. Similar trend is shown in the force-displacement results of the unloading actuation process that as force increases with actuation pressure the displacement increases as well. In comparison, the triple-embedded McKibben sheet behaves similar to the double-embedded McKibben sheet specimen.

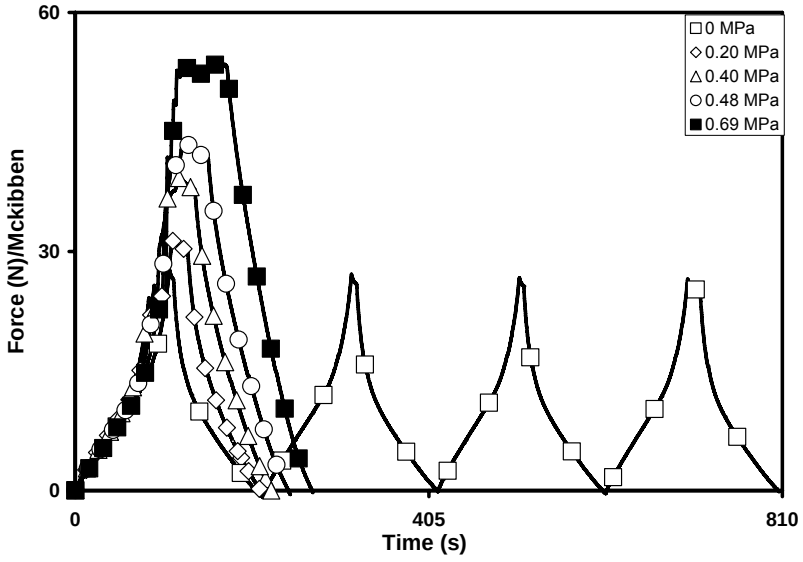

Figure 117. This graph conveys all pressures for the triple-embedded muscle. It shows how force is dependent on pressure.

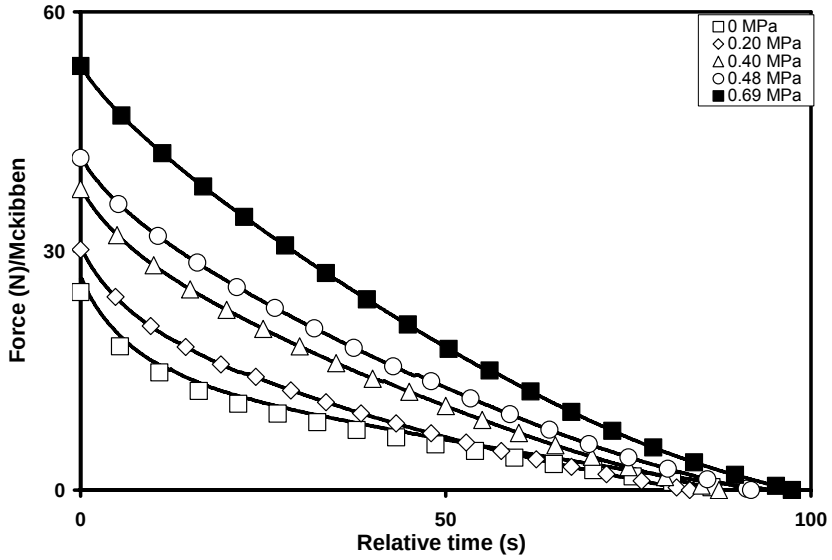

Figure 118. This graph represents the unloading of the triple-embedded muscle for all pressure. It conveys how force is dependent on pressure.

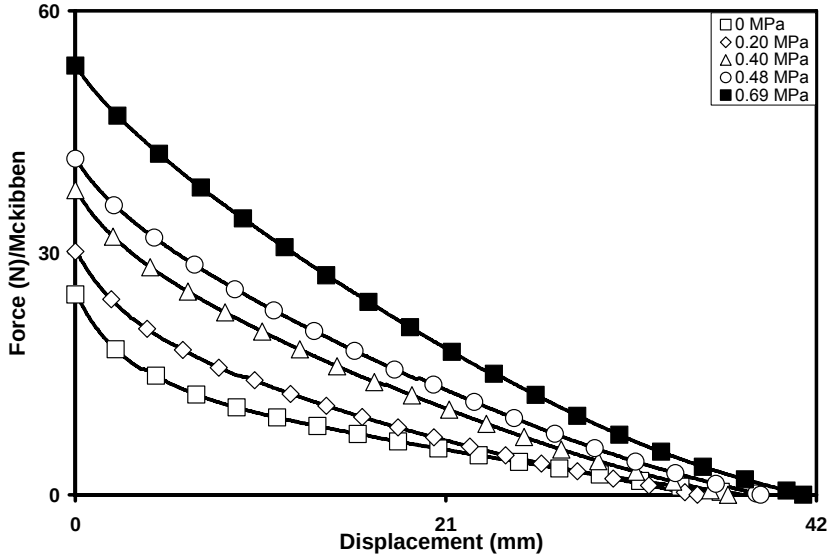

Figure 119. This graph represents the unloading of the triple-embedded muscle for all pressure due to displacement. The displacement decreases as force increases.

The stress-strain graph illustrated in Figure 120, provide continuance trend in regards to the activation pressure. The actuation pressure does influence the actuation stress and actuation strain. As the actuation pressure increases so do the stress and strain. In Figure 121, work-displacement results demonstrate that as the work output increases with activation pressure while the displacement decreases. The work output plateaus over a certain period. In Figures 122 and 123, the graph illustrates that the work-density in regards to the contraction and extension of the triple-embedded McKibben muscle increases as the activation pressure increases. The trend in both graphs does not show a significant difference between each other. This does not follow the same trend as the previous specimen, such as the double, single-embedded McKibben sheet and the McKibben muscle. This would need further investigation to determine why the work-density output reacts differently.

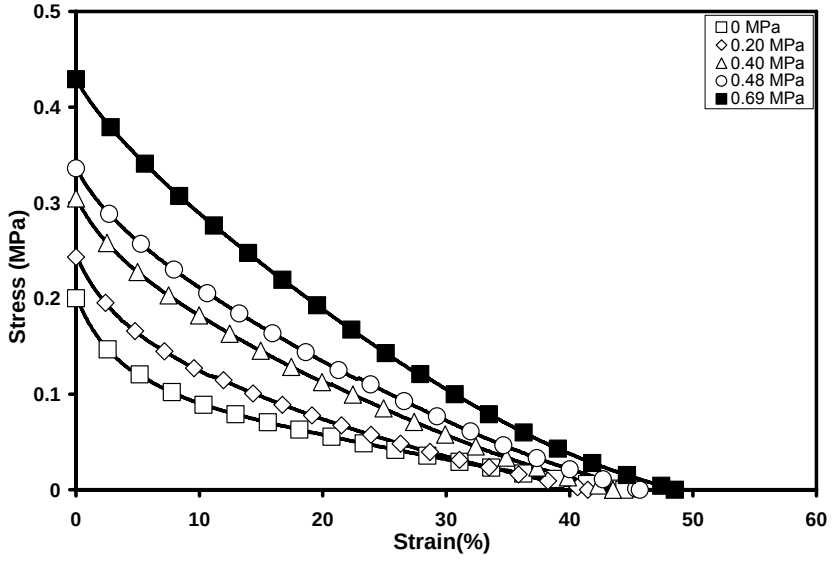

Figure 120. All pressures of the triple-embedded muscle are represented by the actuation stress-strain curve. Stress depends on pressure.

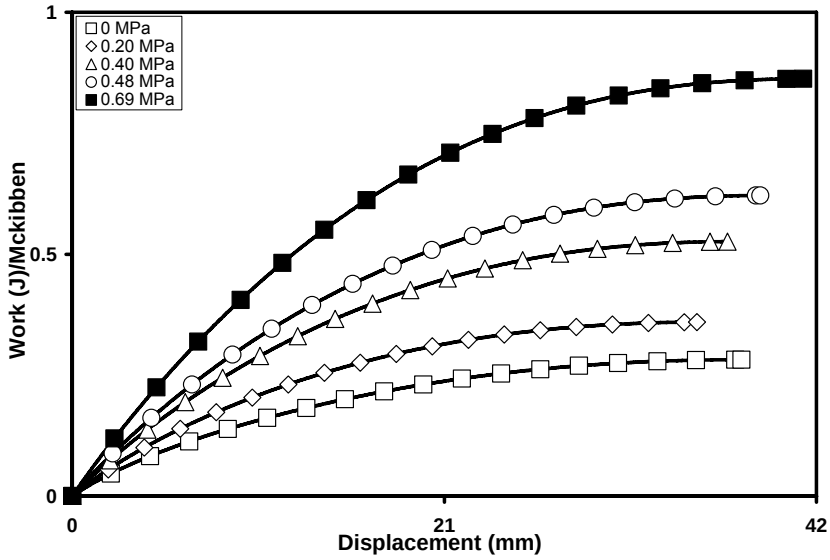

Figure 121. This graph conveys how work is dependent on pressure for a triple-embedded muscle.

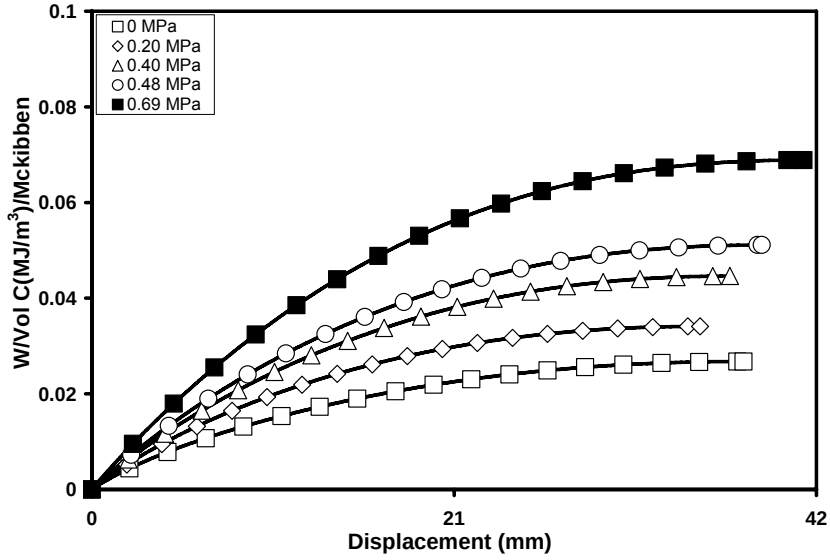

Figure 122. This graph conveys how density is dependent on pressure of a triple-embedded muscle when it contracts.

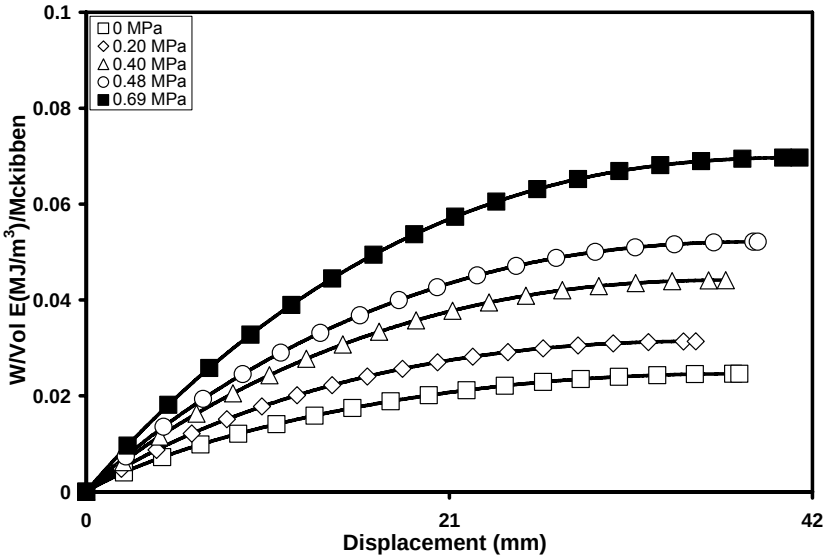

Figure 123. This graph conveys how density is dependent on pressure of a triple-embedded muscle when it extends.

In Figures 124 and 125, the graphs provide detail information in regards to the activation pressure. In Figure 124, the results show that the force increases as the activation pressure increases. Due to the positive linear trend of the curve, this informs us that we do have a possibility of increasing the force greater than what we found by increasing the activation pressure. In Figure 125, the work-density output is shown in the graph below – the triple-embedded McKibben sheet does not follow similar trend as the other specimens. This will require further investigation to determine why the characteristics behave differently..

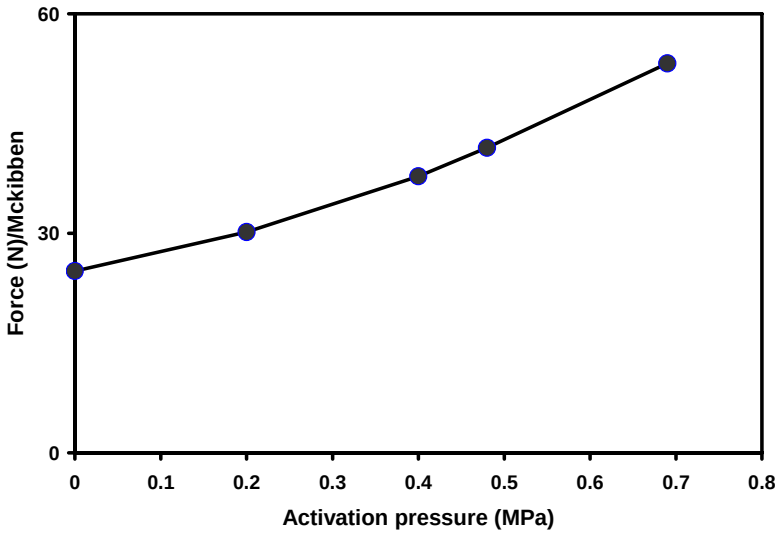

Figure 124. This is a detailed graph showing how force is dependent on pressure for a triple-embedded muscle.

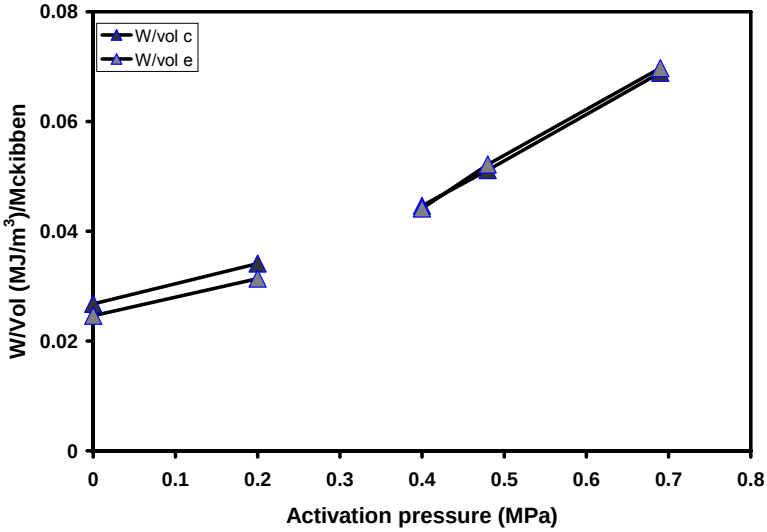

Figure 125. This is a detailed graph showing how work and density are dependent on pressure for a triple-embedded muscle.

Stability Test by Speed Variation:

Experiment has to be conducted to ensure that the speed variation of running the experiments does not influence the results. As shown in Figure 126, speed is not an influence on the results. The data for activation pressure of 0.69 MPa shows a consistent trend by the overlapping of each results due to different speed. As the strain rate decreases, the force output stays constant. Plus, the parabolic curvature of the line is pronounced more in the triple-embedded McKibben sheet than the double and single-embedded McKibben sheet. The work-displacement results, illustrates that the strain rate does not have any influence on the work output – in Figure 127. There was a slight change with an experimental error of 2.62%, which falls into the acceptable category. This informed us that we could run the experiment at 25.4 mm/min or lower without any changes to the results. In Figure 128, the experimental error calculation is provided to determine if any outliers exist.

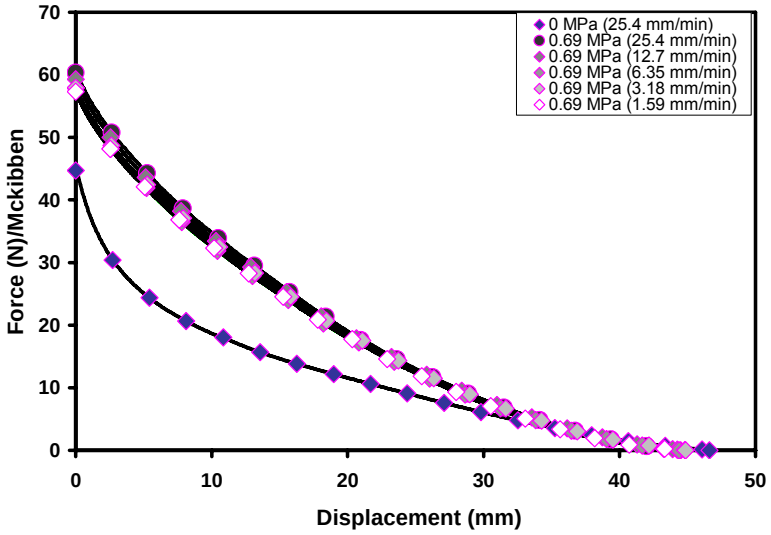

Figure 126. This graph shows that strain rate does not influence the force-displacement behavior of a triple embedded muscle with an actuation pressure of 0.69 MPa. The 0 MPa performances appear for reference.

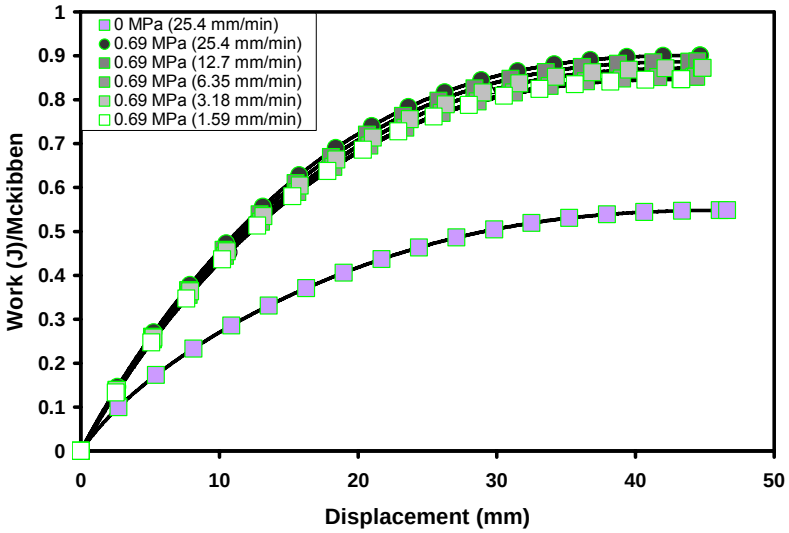

Figure 127. From this graph we do not expect the strain rate to affect the work output of a triple embedded muscle for engineering strain rates between 0.0198 and 0.3175 min^{-1}. This graph conveys how speed influences work for triple embedded muscle. The average work output is 0.87 +/- 0.023 J, which is a reasonable experimental error at 2.62 %.

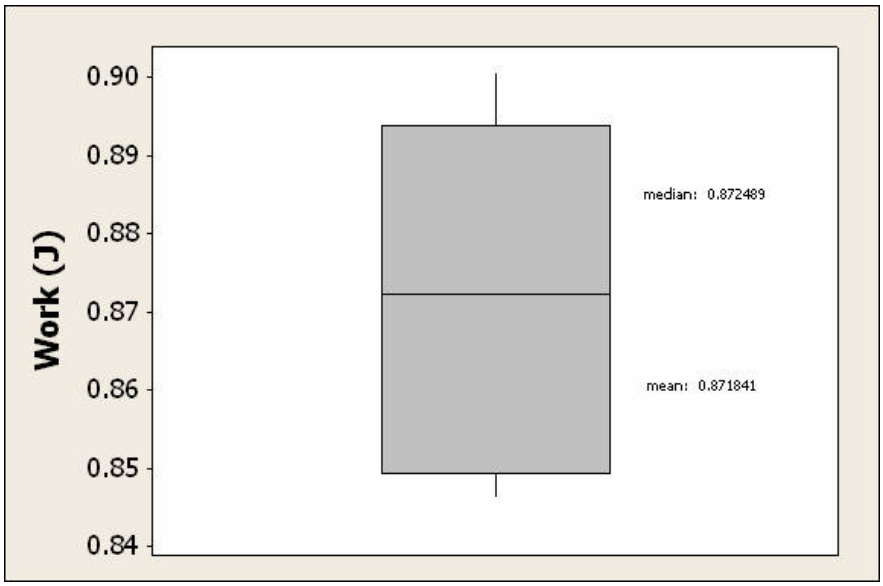

Figure 128. An average work output of 0.87+/- 0.023 J, which is within typical experimental error. Therefore, the strain rate does not influence the work performed.

The picture shown in Figure 129 is of a dissected portion of the triple-embedded McKibben sheet. The specimen consist of three McKibben muscle that should have been equally distance and centered – as you can see they are not centered to each other.

Figure 129. A dissected triple embedded sheet

6.5.4. Quintuple Embedded Sheet

Tensile Test Experiment:

Data was acquired from three quintuple-embedded McKibben sheet specimens, and the displacement graph is shown in Figure 130. Detailed information would be displayed for the mean of the three double-embedded McKibben sheet. The force-displacement results in Figure 111, was used to determine how consistent the quintuple-embedded McKibben sheets were designed – the graph proves that they were consistent. Muscle one was chosen as the mean of all three sheets.

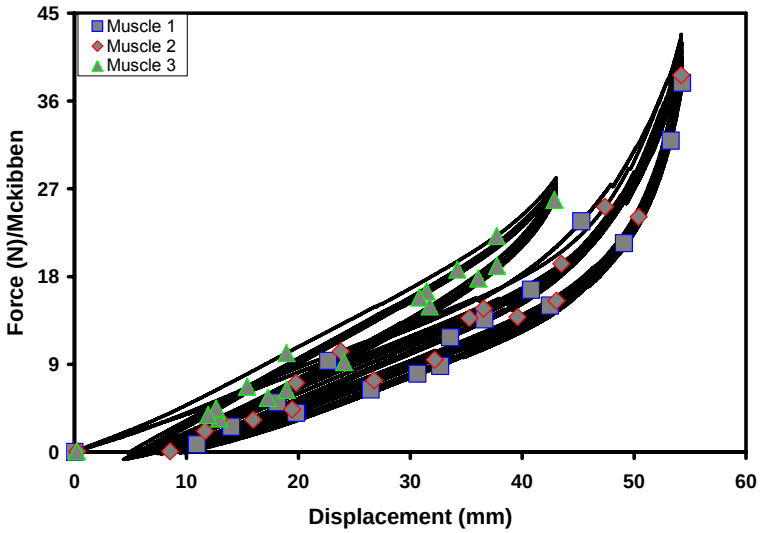

Figure 130. This graph represents force-displacement data for three quintuple-embedded sheets.

The next graphs shown will be detailed information of the quintuple-embedded McKibben muscle sheet that was calculated as the mean at 0 MPa – muscle one. The overall results for muscle one is displayed in Figure 131, which illustrates the behavior of the peak force and the displacement. As shown, the displacement has been staying constant while the sheet is undergoing its stress relaxation by the peak force's trend. A graph that displays only the force-time results in Figure 132, shows how the peak force stabilizes after the 3rd cycle. In Figure 133, the force-displacement result illustrates how hysteresis has a factor in the experiments. The quintuple-embedded McKibben sheet has a consistent cyclic response that allows the specimen to return to its original state as shown in cycles 2 to 4. The unloading actuation process is shown in the force-displacement in Figure 134. Due to the overlapping of all the data, it proves that there is a consistent.

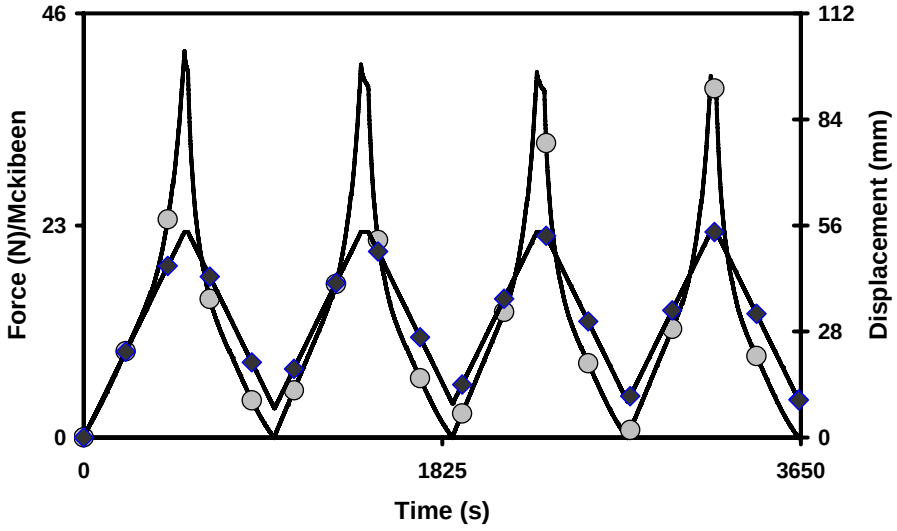

Figure 131. The data displayed is muscle one, which is the middle data at 0 MPa.

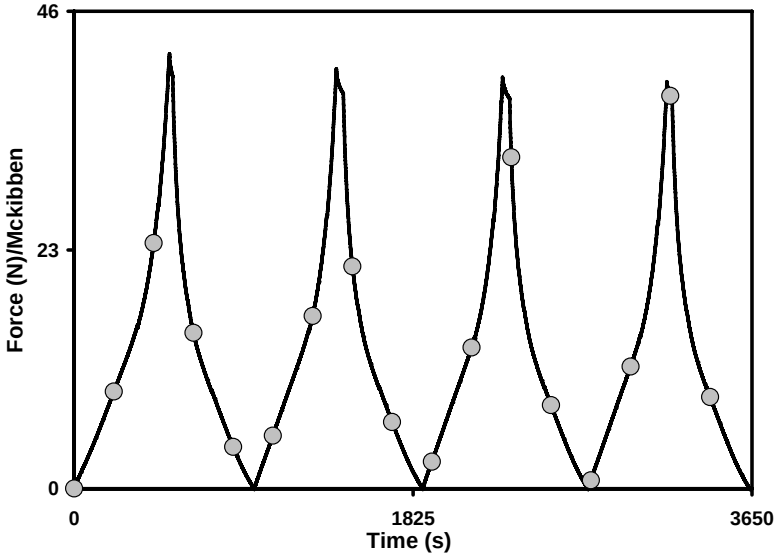

Figure 132. This graph shows that four cycles of extension/release are sufficient to break-in the material.

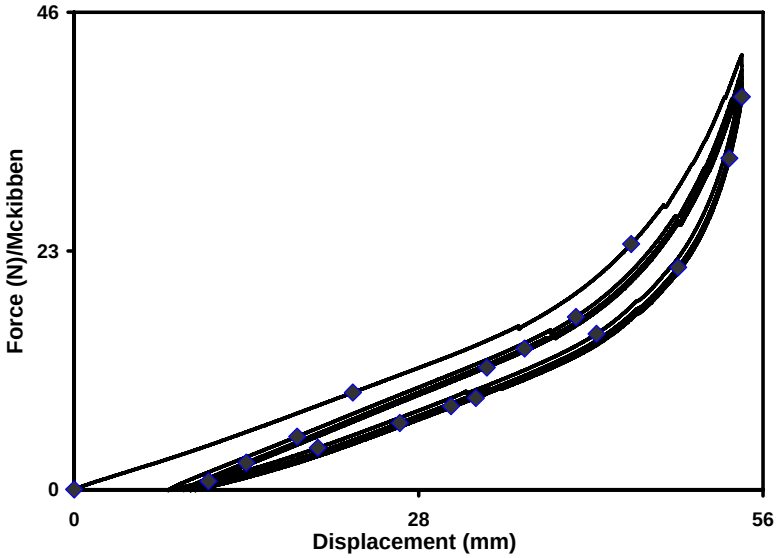

Figure 133. This graph shows that the force/displacement behavior showed typical response. During the first extension, which begins at zero displacement and force, the force rises to a peak. As the specimen unloads it follows the lowest curve and it goes slack at <54>mm. Further loading cycles follow the middle curve, which is marked with <diamonds>, during loading and the lowest curve during unloading..

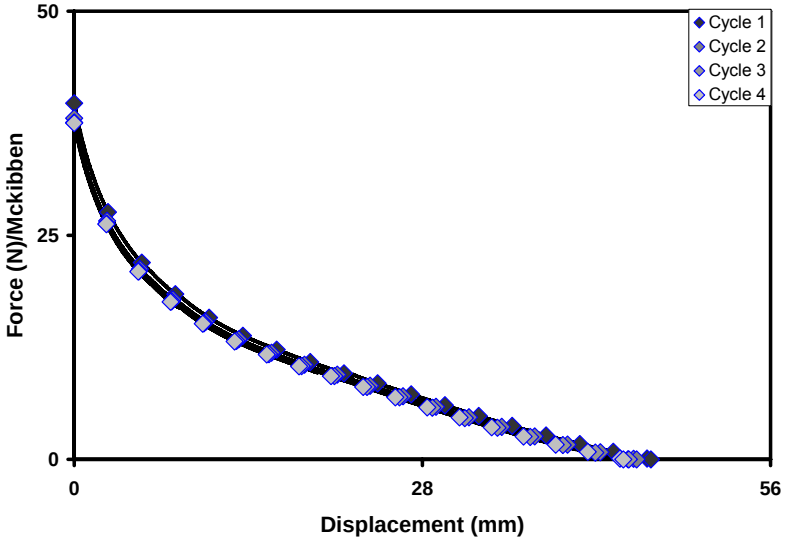

Figure 134. This graph conveys the consistency of the unloading force/displacement of the five muscle sheet during four cycles of extension/return.

Tensile Test at Variation of Activation Pressure:

Figures 135 - 136, display detailed information for the mean quintuple-embedded McKibben muscle at all pressures from 0 to 0.69 MPa. In Figure 135, the graph shows if the quintuple-embedded McKibben sheets were of consistent design. The loading actuation trend for all activation pressure has been consistent from the single-embedded McKibben sheet to the quintuple-embedded McKibben sheet. In-depth detail is provided in Figures 135 and 136, the graphs show how force behaves in regards to relative time and displacement, respectively. In a triple-embedded McKibben sheet, as the actuation pressure increases the force increases as well, but the displacement decreases. Similar trend is shown in the force-displacement results of the unloading actuation process that as force increases with actuation pressure the displacement increases as well.

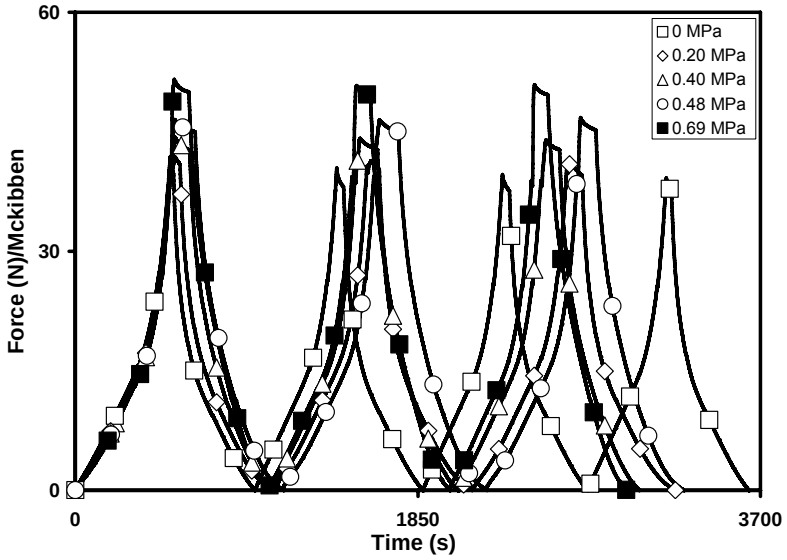

Figure 135. The force/time data shown is a record of the test history of each specimen tested. After stretching the specimens to the maximum extension, pressure was applied and the sample remained extended until the system reached full applied pressure.

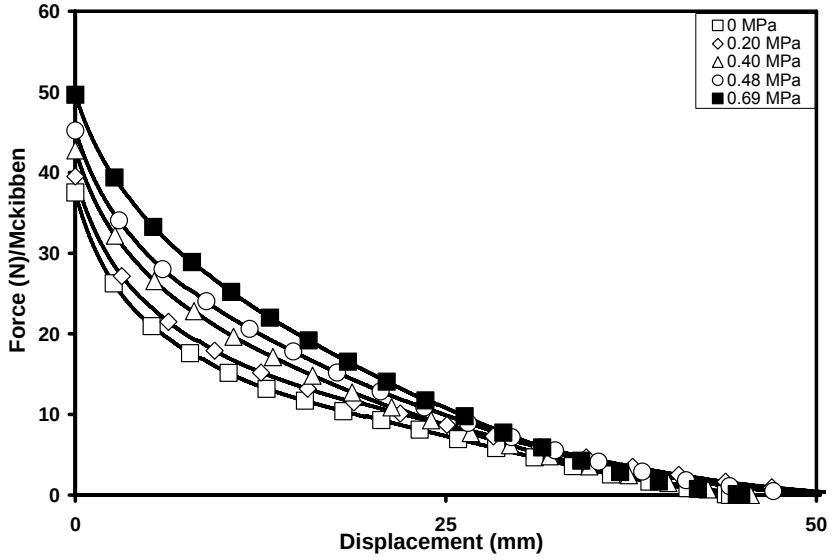

Figure 136. The force/displacement graph shows that the sheet with quintuple embedded muscles provides almost 50 mm of displacement regardless of the activation pressure. However, the maximum displacement decreases as the activation pressure increases.

In the stress-strain response in Figure 137, the strain is decreased as the activation pressure and the stress increases. The distance between the curves have decreased as we increase the activation pressure and compared to the previous specimen of single-embedded McKibben sheet. Work-displacement response is shown in Figure 138, where the work increases as the activation pressure increases. The curvature begins to stabilize over time, especially after it reaches a specific displacement amount – might be due to maximum length of extension. The work output has significantly dropped compared to the single-embedded McKibben sheet. We also calculated the work-density at the contraction and extension process; results are shown in Figures 139 and 140. The work-density response increased with the activation pressure.

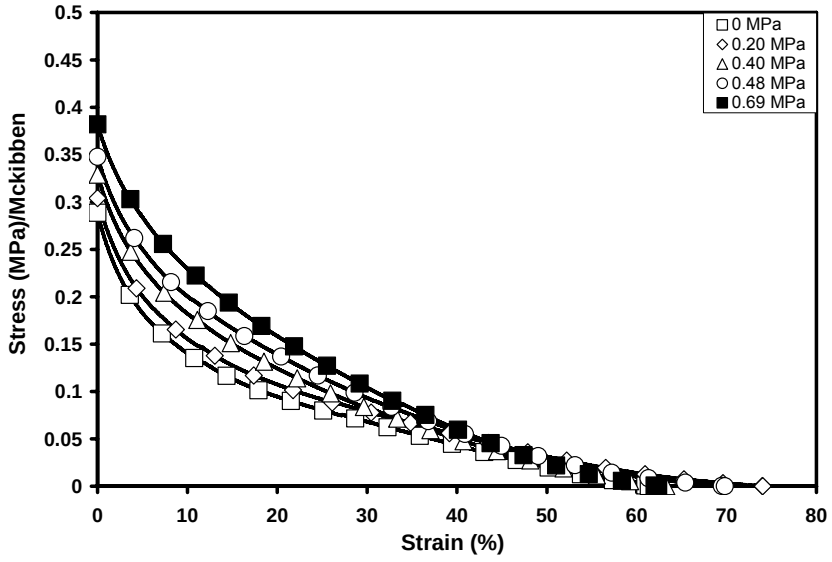

Figure 137. The stress/strain response of a quintuple-embedded muscle sheet actuator at four activation pressures. Increased activation pressure increases the initial stress; however, it decreases the total strain available.

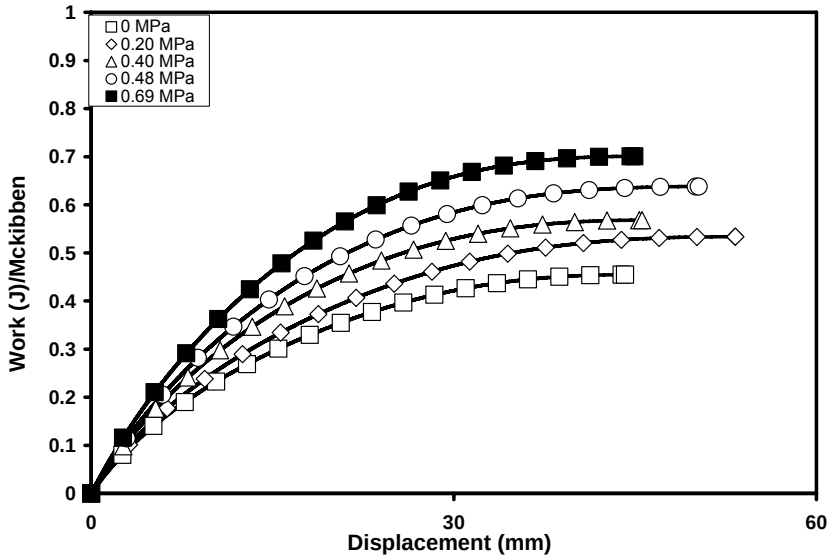

Figure 138. Normalized work produced by a quintuple embedded muscle sheet.

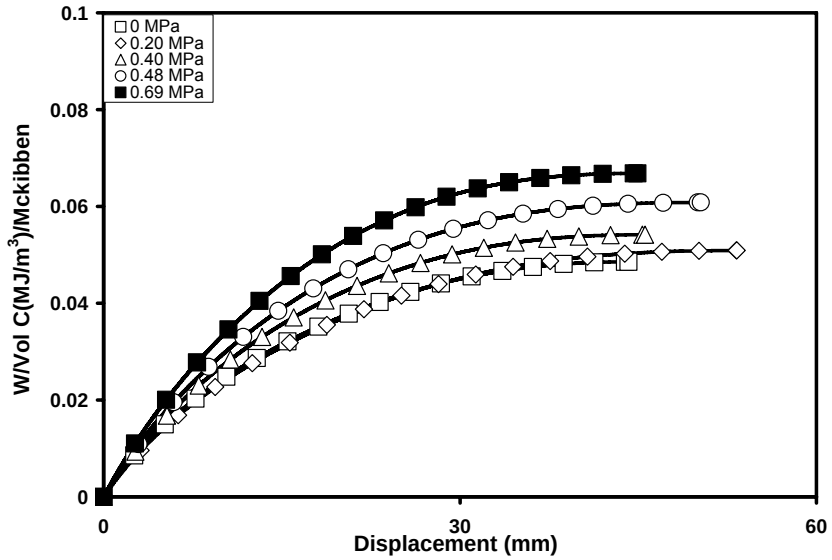

Figure 139. The work density of the sheet in this graph is based on the volume of the sheet after it has moved through the entire displacement range. The net output work density is the difference between any of the pressurized curves and the unpressurized work density curve indicated with the open square symbols.

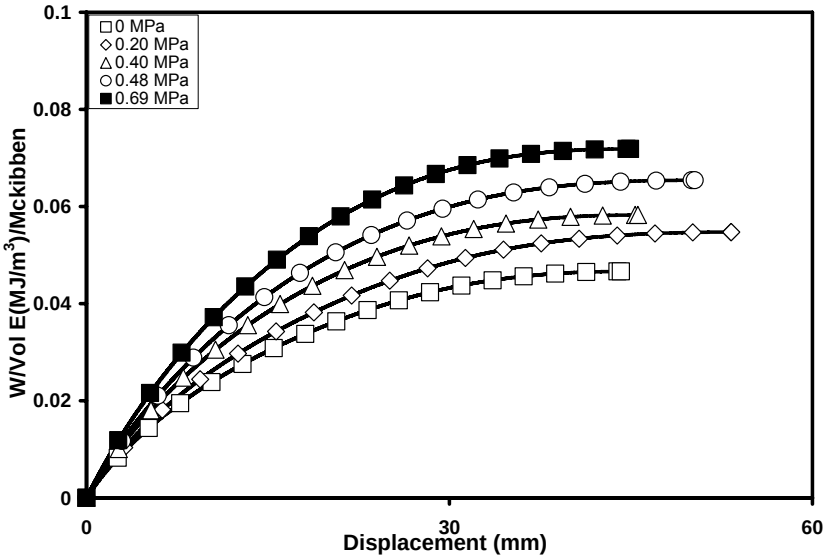

Figure 140. In this graph work density is estimated using the volume of the extended, unactuated sheet. The output work density of a sheet containing five muscles increases with increasing activation pressure and displacement. The net output work density is the difference between the un-actuated work density curve, which is noted by the open square symbols, and the curve shown for any of the activated experiments.

Influence of the activation pressure is shown in Figures 141 and 142 in regards to the force response and the work-density response, respectively. The curve for the force response is almost horizontal, but still shows a positive slope that allows us to increase force by increasing the activation pressure. The work-density of both the contraction and extension are shown in Figure 142, following the similar trend as the force response. Interesting area is that the initial point of the contraction work-density is almost overlapping the extension work-density response. This informs us that activation pressure at 0 MPa has little to no influence on the result whether it is contracted or extended. This trend behaves differently as the other specimen.

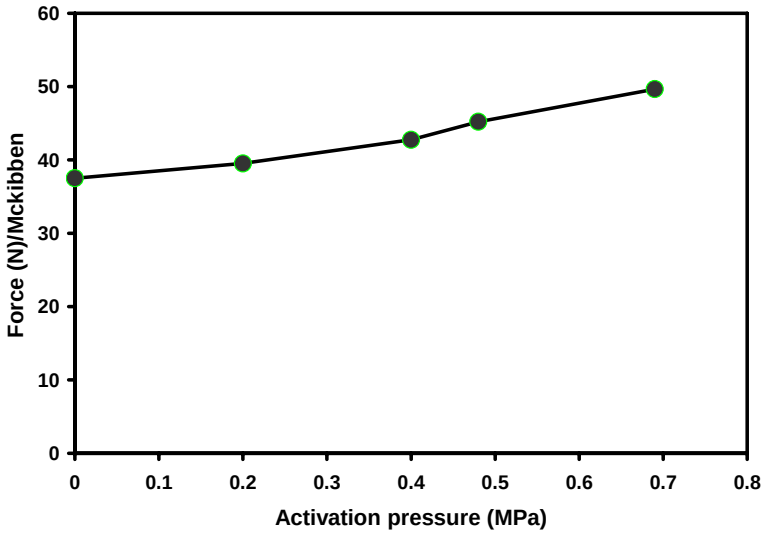

Figure 141. The normalized maximum force produced by the quintuple embedded sheet material increases with increasing activation pressure.

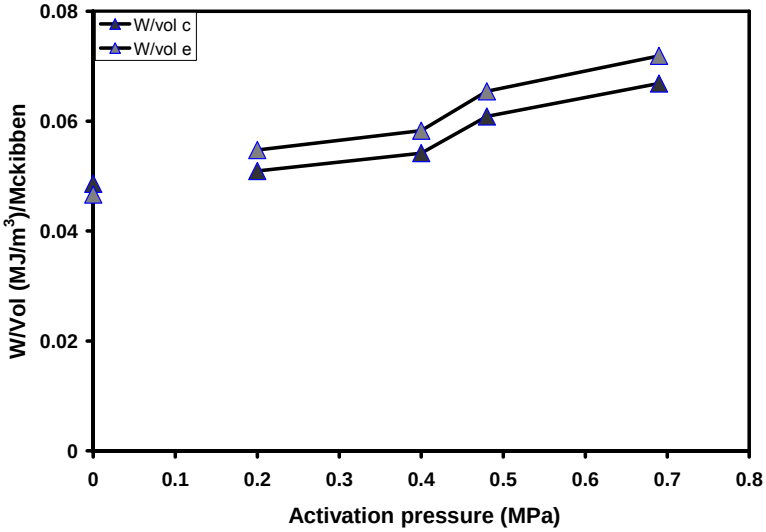

Figure 142. This graph shows how work density increases with increasing activation pressure for a sheet with quintuple embedded muscles.

Stability Test by Speed Variation:

Experiment has to be conducted to ensure that the speed variation of running the experiments does not influence the results. As shown in Figure 143, speed has a slight influence on the results. The data for activation pressure at 0.69 MPa with speed at 25.4 mm/min is slightly separated from the others. This is important because it informs us that we would need to run the experiments at a lower speed than 25.4 mm/min. The work-displacement results, illustrates that the strain rate does have a minuscule influence on the work output – in Figure 144. There was a slight change with an experimental error of 3.33%, which falls into the acceptable category. In Figure 145, the experimental error calculation is provided to determine if any outliers exist.

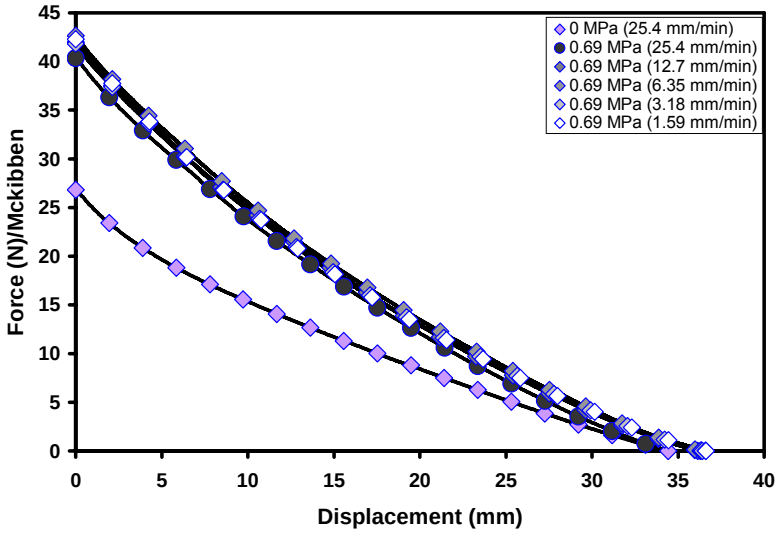

Figure 143. This graph shows that a strain rate of 25.4 mm/min slightly reduced the force-displacement behavior of a quintuple embedded muscle sheet at an actuation pressure of 0.69 MPa. The 0 MPa performance appears for reference.

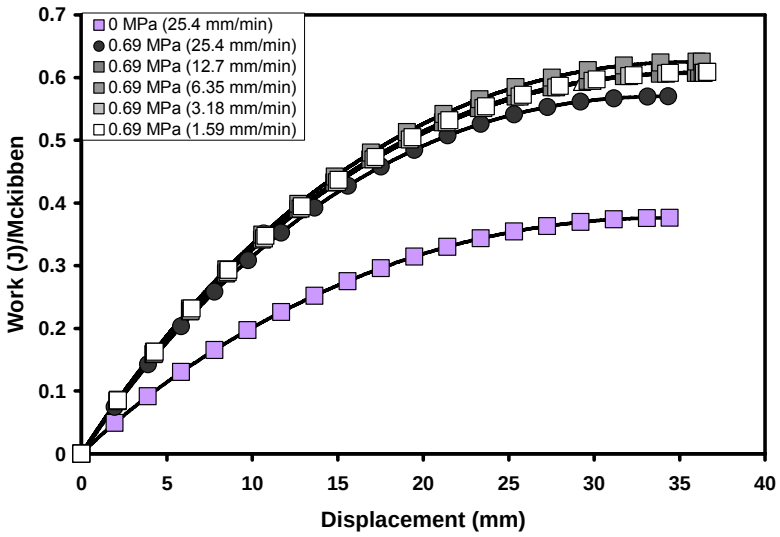

Figure 144. From this graph we see that strain rate to reduce slightly the work output of a quintuple embedded muscle sheet for engineering strain rates of 0.3175 min^{-1} or higher. At the 0.69 MPa activation pressure the average work output is 0.60 +/- 0.020 J. This variation—3.33 %—is a reasonable variation; however, the distinct drop in work output suggests that the experiment must occur that lower strain rates.

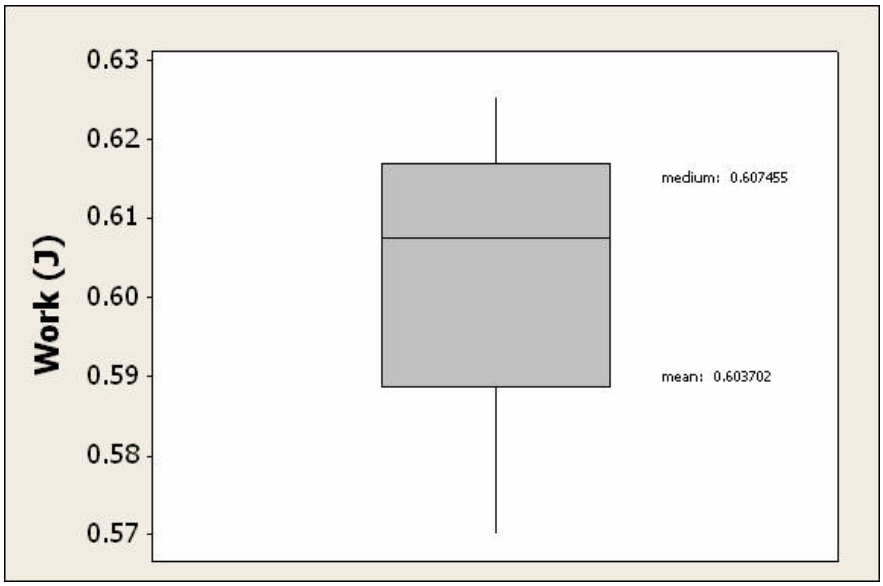

Figure 145. An average work output of 0.60 +/- 0.020 J. This is within typical experimental error. Therefore, the work performed is influenced slightly by the strain rate.

Specimens Comparison:

This section will focus compare each specimen to the others. The comparison covers the McKibben muscle and all the embedded McKibben sheets. Force responses of the specimens are compared to determine if a trend exist, in Figure 146. The embedded McKibben sheet with 0 McKibben muscle is referring to the McKibben muscle only. Our initial assumption was that as we increase the number of McKibben muscles in the embedded sheet, it would enhance all the characteristics of the McKibben muscle by acting as an array. The force response from zero to double-embedded McKibben sheet does prove this theory as true, but from the double to the triple-embedded McKibben sheet shows the opposite effect. At this time, this proves that there is no trend from the specimen, probably due to the batch to batch variation of the McKibben fabrication. Fabrication of the embedded sheets by not confirming, if each muscle is centered to each other and in the polyurethane matrix. Figure 147, illustrates the work output response; this response follows similar trend as the force response. The work-density response shows a decreasing trend from a McKibben muscle only to a quintuple-embedded McKibben sheet as shown in Figure 148. Our theory is completely wrong, because the more McKibben muscles added the closer the work-density response becomes constant. This would have to require more investigation to determine why the behavior acts differently. Of course, work-density depends on volume – did we create a constant matrix volume around each McKibben muscle in its sheet?

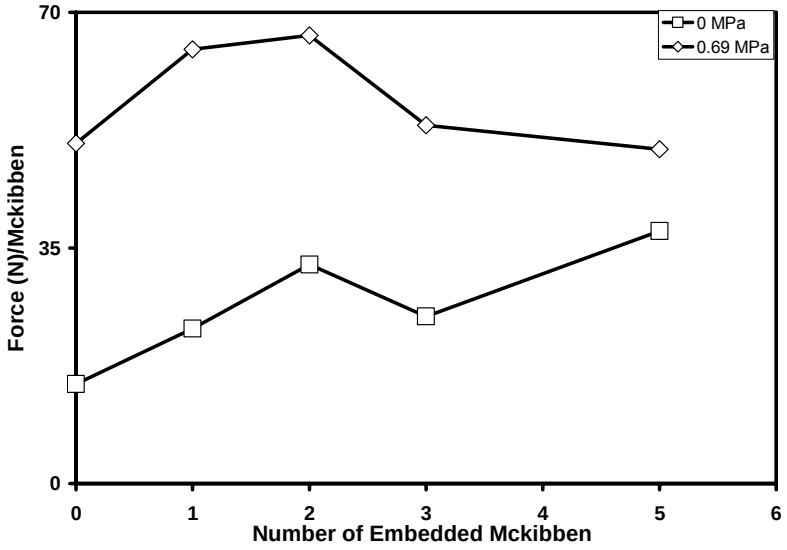

Figure 146. This graph conveys how the normalized maximum actuation force changes with the number of McKibbens embedded in a matrix. There is no trend in the maximum force/McKibben when the muscles are activated at 0.69 MPa. However, the unactuated materials show a definite increase in the force required to stretch them back into their activation configuration as the number of embedded muscles increases.

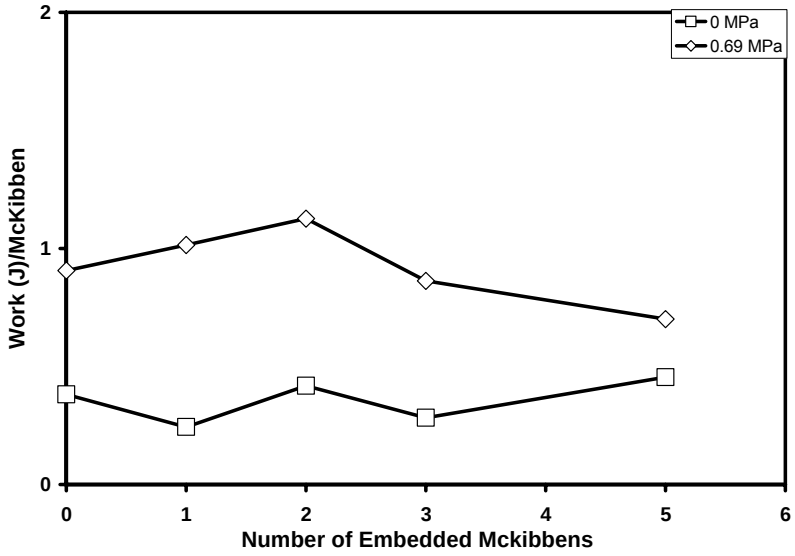

Figure 147. This graph shows that the total work output of both unactuated and actuated McKibben muscles and sheets are approximately constant, that is, no definite trend is obvious. This might reflect the 'batch-to-batch' variation of manual fabrication of McKibbens within the laboratory.

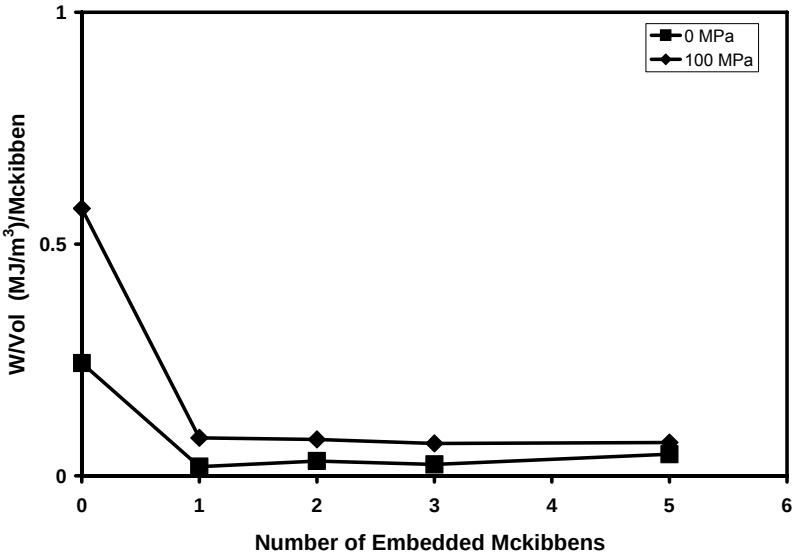

Figure 148. This graph shows that the work density of any embedded McKibben is less than that provided by a free McKibben. As the number of machines increases, the pressurized work density/muscle is constant.

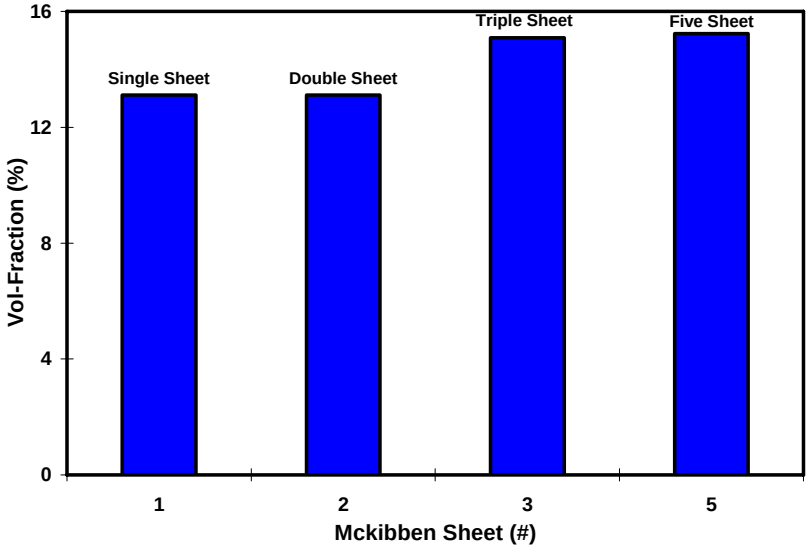

Figure 149. This graph shows the volume-fraction analysis of each specimen.

The volume-fraction analysis is displayed in figure 149. To confirm, that the McKibben muscles had free movement in the polyurethane matrix. The picture in Figure 150 provides the dissected view of a quintuple-embedded McKibben sheet. This Figure shows that every muscle was not centered in the surrounding matrix; therefore the matrix distribution was uneven. This is important because a muscle with fewer matrixes will work differently than one with slightly more matrix around it, meaning the muscle will probably have to perform less work to overcome the polyurethane surroundings. In Figure 151, we cut away some of the surrounding polyurethane matrix to prove that the McKibben muscle was not bonded to the matrix. We coated all McKibben muscles in the sheets with silicone gel to prevent bondage and prevent matrix from collapsing the muscle while the matrix gelled.

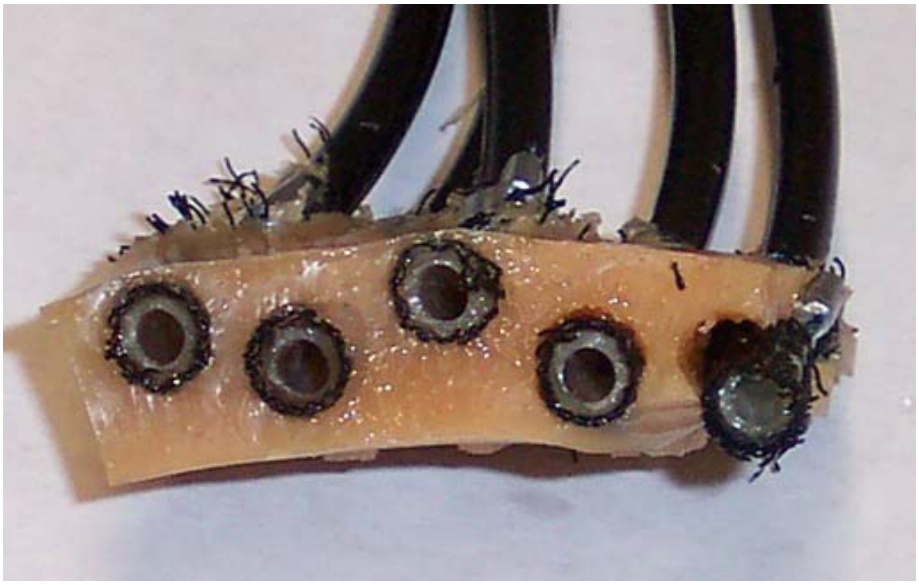

Figure 150. This photograph shows a dissected quintuple-embedded McKibben sheet. Note that the muscles were not encased uniformly along the centerline of the matrix. Muscles nearer to the outer surface of the matrix might not perform the same as those near the centerline. The muscle at the extreme right was twisted from the matrix to show that it was not bonded to the matrix.

Figure 151. This picture illustrates that the muscle was not bonded to the polyurethane matrix. The elastomer matrix was cut open. The braid and inner latex tube have no matrix bonded to them.

Results Conclusion:

The results provided in this chapter was for all the component of a McKibben muscle and the embedded sheet such as the latex rubber tube, the PET braided mesh sleeve, the polyurethane matrix. It also includes the experimental results for each specimen such as McKibben muscle, single-embedded McKibben sheet, double-embedded McKibben sheet, triple-embedded McKibben sheet and the quintuple-embedded McKibben sheet.

The subsequent chapter will provide further discussion and analysis of the results we acquired and determine what improvements or actions need to be taken.

CHAPTER VII

CONCLUSIONS AND SUGGESTED FUTURE WORK

7.1. CONCLUSION

We were able to make several observations from the experiments conducted on each specimen. In Table 13, we calculated the expected work-density of each specimen to compare with the actual work-density. The actual work-density for both the single and double-embedded sheets showed an increase to 7.82% and 2.96% consecutively. Though, both specimens had an equal muscle volume fraction per muscle at 0.1311, the matrix did not reduce the work-density at all. On the other hand, the actual work-density of both the triple and quintuple-embedded sheet had a decrease of 20.35% and 18.63% consecutively. The reduction in work-density allows us to conclude that the matrix had an effect on the specimen. This could also be due to the muscle volume fraction of both the tripe and quintuple-embedded sheets; there was an increase of muscle volume fraction from the double-embedded sheets to the triple and quintuple-embedded sheets. Another observation from the result shows a downward trend in the actual work-density whether the muscle volume fraction was either 13% or 15%. For example if we were to embed a decuple muscle into the polyutherane matrix the actual work-density of the decuple-embedded sheet would decrease to about double the amount of the quintuple-embedded sheet. The actual work-density of a centuple-embedded sheet would be a decrease ten times the decuple-embedded sheet.

Why was there a difference between the single and double-embedded sheets even

though they both had equal muscle volume fraction? One noticeable difference is that the double embedded sheet has an amount of space in-between both McKibben muscle. The muscle volume fraction around each muscle might not be as balanced as a single-embedded sheet.

In Table 13, the table shows a downward performance trend as the muscle volume fraction increases. For instance, the muscle volume fraction for both the single and double-embedded sheets were constant but the sheets performance decreased maybe due to the addition of a second muscle. As we increase the muscle volume fraction to about 15%, the sheets performance drastically decreases this could be in conjunction with the additional muscles added for the triple and quintuple-embedded sheets.

Overall, the unactuated sheets show a definite increase of the force/muscle needed to compensate for the enclosed matrix as the number of muscles increase. There is no trend of the actuated sheets for the force/muscle at the maximum pressure of 0.69 MPa. The results of both the actuated and unactuated sheets for the work/muscle shows a constant trend, meaning a noticeable trend is hard to determine. The results that we could not determine any trend might be due to the "batch to batch" variation of manual fabrication of the McKibben muscle in the laboratory. Table 13 proves that there is a muscle volume fraction variation from specimen to specimen. Any table or graphs that are present data for the triple-embedded sheet in comparison with the others, would be displayed a difference in the trend it should follow. This might also be due to the muscle volume fraction change and other factors of building this specimen.

Table 13. Comparison of the actual and expected work-density

# Muscles	Muscle Vol. Fraction	Work-density/ Muscle (MJ/m3)	Expected Work-Density (MJ/m3)	Diff %
0	0.000	0.58	0.0000	
1	0.1311	0.082	0.0761	7.82
2	0.1311	0.0783	0.0761	2.96
3	0.1509	0.0697	0.0875	-20.35
5	0.1523	0.0719	0.0884	-18.63

7.2. IMPLICATIONS AND SUGGESTED FUTURE WORK

The embedded sheets are being designed to have skeletal muscle characteristics due to the performance different stages, i.e. contraction, isometric and eccentric. Skeletal muscles have voluntary actions that the embedded muscles would also use.

Embedded sheets have been designed to have characteristics similar to synthetic shape changing materials. The McKibben muscle and the polyurethane matrix are both built from synthetic materials. Intertwine characteristics of the McKibben muscle and the polyurethane matrix has proven to be a contribution where it can be utilized in future applications. The McKibben muscle expands, due to energy from the compressed nitrogen; the muscle exerts pressure unto the polyurethane matrix which forces the matrix to change its shape accordingly. Most synthetic shape changing materials, such as copper-zinc (Cu-Zn) change shape due to various temperature.

The embedded McKibben sheets are designed similarly to the Machine Augmented Composites, which are simple machines, inside an elastomer matrix, used to create an external force. The experiment does show some promising results, especially if other improvements in regards to the manufacturing of the embedded McKibben

sheets, can be conducted. The experiments demonstrate that we did characterize the worst case scenario, due to embedding fully stretched McKibben muscle into a matrix, of an array of an embedded matrix. Once the specimens are removed from the mold, the McKibben muscle automatically tries to retract to its initial state while the polyurethane matrix tries to stay at its initial state. This causes the polyurethane matrix to counteract the McKibben muscle; they oppose each others motion.

There are other steps that can be used to improve the characteristics of the embedded McKibben sheets. One area is by embedding an unstretched McKibben muscle into a polyurethane matrix. This experiment would allow the polyurethane matrix to support or assist the activation of the McKibben muscle. Meaning the polyurethane matrix will work simultaneously with the muscle to enhance each others characteristics, this would allow the specimen to reach its full potential of the amount of work it can perform on an internal or external source. Our initial assumptions of increasing the force, work and work-density output should continuously increase in a positive trend either linearly or parabolically as we increase the array of McKibben muscle in a matrix should become true. If this experiment is successful, there would be data for the worst and best case scenario. In that sense, another experiment can be conducted of embedding a half-way stretched McKibben muscle into a polyurethane matrix. This would allow scientist and researchers to investigate at what point the specimen begins to provide the characteristics needed.

A second area of improvement on an embedded McKibben sheet is by assuring that the array of McKibben muscle(s) are properly centered inside the polyurethane

matrix – improvement can be made on the mold created to enclosed muscle. As shown by the pictures of the dissected embedded McKibben sheets, the McKibben muscles were not always centered in the middle of the polyurethane matrix. This could have influenced the outcome of the results, for example a McKibben muscle that is located closer to the edge of the matrix probably produced more work due to less or no constraint from the matrix. While, a McKibben muscle that was further away from the edge of the matrix had more constraint from the matrix. Another assumption is that this prevent the McKibben muscles to perform as an array to work as a single element of source if they were not properly balanced. The single-embedded McKibben sheet was centered properly in the matrix. Therefore, the results illustrate improved performance. The double-embedded McKibben sheet was centered well in the matrix. This explains the upward linear trend from the McKibben muscle.

A third area of improvement on an embedded McKibben sheet is by assuring that the McKibben muscle(s) are evenly surrounded by the polyurethane matrix – this can also be improved by redesign of the enclosing mold. This important because if the polyurethane matrix is overpowering or hindering the activation of the McKibben muscle, then the goals would not be achieved

A fourth area of improvement on an embedded McKibben sheet is by increasing, the volume-fraction of the McKibben muscle to about 50-60%. This would work together with the third area of improvement. The polyurethane or any polymer's volume is an important factor in regards to being used as a matrix because it can assist or hinder the activation of the source.

A fifth area of improvement on an embedded McKibben sheet is by creating another experiment without silicone coating of the McKibben muscle to determine if the silicone had an influence on the embedded McKibben sheets. We did not have the time to investigate this particular area, but it is important to determine if it has an influence on the outcome of the results. An assumption could be that the silicone is creating more friction between the McKibben muscle and the polyurethane matrix than needed. If this experiment does hold true, then a different type of coating or none would be needed to prevent muscle from being engulfed in the matrix.

A sixth area of improvement on an embedded McKibben sheet is to improve the muscle to matrix ratio, by designing the embedded McKibben sheets with smaller McKibben muscles than the original size – e.g. 2:1 ratio. This could be an important factor to determine how much of an improvement the polyurethane matrix was able to help activate.

There are several experiments that will need to be performed to verify all assumptions made thus far. For example, we assumed that the embedded McKibben sheets did not reach their full potential output work, meaning with a quintuple-embedded McKibben muscle the work output should have been greater than a McKibben muscle or a single-embedded muscle – the more muscle added should be able to increase its mechanical properties, due to the pre-stretched muscle. In this experiment, the McKibben muscle was fully stretched and embedded into the polyurethane matrix, which was cured at this initial state – this process limited the sheet's performance because the McKibben muscle works antagonistically to the polyurethane matrix during

contractions.

As the results from these experiments illustrate, we learned that the quantity of polyurethane matrix that is used to embed the McKibben muscle plays a role in determining the work output from the specimen. The matrix surrounding the single embedded muscle was at a lower volume fraction than that occurring in the other embedded sheets. This explains why the two, three and five muscles showed decreasing output per McKibben as more muscles. An experiment with different volume fractions could determine the largest work output possible and an application would use that volume fraction. It would be easier to use a polymer matrix that had the same characteristics as the polyurethane but in a clear form – this would allow for a visual form of how the muscle behaves, as well as confirms that the muscle is free in the matrix.

Future experiments should also be performed on embedded matrices that have multiple laminate muscles with +/-θ, in an embedded matrix to determine its performance; this would be beneficial to compare to the embedded sheets with straight McKibben muscles.

Experiments should be performed on a nano-scale of the embedded sheets to determine if they could produce characteristics of a smooth muscle; this might be useful with assisting women. The stomach is lined with smooth muscle, which is the muscle that is used to assist with giving birth. This muscle over time does deteriorate for several reasons, one reason is the when the doctors continue to slit open the same area of the stomach. If one could determine how to insert an embedded sheet into the stomach to

replace or assist with pregnancy or births, it might decrease the level of deterioration. The embedded sheet would have to be surgically implanted and removed; this could be beneficial for caesarean births, which are limited to no more than three births through this method.

These embedded sheets could be used by the veterinary field to assist animals with their skeletal system; it could be used to repair a bird or worms. Animals do have similar diseases as humans, for example if a bird's wing has deteriorate due to muscle problems, it can be repaired using an artificial muscle as an embedded McKibben sheet.

This thesis presented the experimental results that characterize a nastic sheet material's performance. We defined nastic sheet as a McKibben muscle designed from foundation that would be embedded as an array in an elastotmer matrix. The experiment was conducted with variation of array size embedded – we built several products with one McKibben muscle embedded into a polymer matrix to five pieces of McKibben muscles embedded into a polymer matrix. This sheet changes shape and provides actuation when subjected to internal pressure. The embedded sheets are subjected to an internal pressure similar to blowing up a balloon, the products shape will change from its original shape. Linking human technology and natural structures is and will continue to be important to society for several reasons, it would improve: (1) the lifestyle of humans in regards to artificial parts that mimic human parts (which will allow us to live longer), (2) artificial limb functionality, and (3) comfort and aesthetics. The goal of the research was to determine the characteristics that could be used as a replacement or improvement of current projects or process.

---

1 *History of biomechanics*, www.usd.edu

2 Aristotle. *Parts of Animals, Movement of Animals, Progression of Animals*. 1961

[3] *Muscles*. www.kidshealth.org reviewed by Steven Dowshen, M.D

[4] M.J. Farabee. *Muscular and Skeletal Systems*. www.emc.maricopa.edu/

[5] Lightner, S., and Lincoln, R. *The Fluidic Muscle: A 'New' Development*. The international Journal of Modern Engineering. 2002; 2(2)

[6] Campbell, Neil. *Biological Foundations*. Biology. 1996. 4th edition.

[7] Kanzawa, Nobuyuki and Tsuchiya, Takaide. *Seismonastic Movements in Plants, Reflexive Polymers and Hydrogels*. 2004: 17-31,

[8] R.C. Johnson. *Darpa Funds Working On Rigid Shape-Shifting Materials*. Electronic Engineering Times. Oct 2004; 1341: 22

[9] Herr, H., Whitley, G. and Childress, D. *Chapter V: Cyborg Technology – Biomimetic Orthotic and Prosthetic Technology*. Biologically Inspired Intelligent Robots. SPIE Press. Bellingham, Washington. 2003

[10] Woo, Gary. *Artificial Organs Produce Genuine Benefits*. Medical Device & Diagnostic Industry Magazine. May 1998.

[11] American Heritage® Dictionary of the English Language, Fourth Edition copyright ©2000 by Houghton Mifflin Company. Updated in 2003. Published by Houghton Mifflin Company.

[12] Caldwell, D.G. and Tsagarakis, N. *Bio-mimetric actuations in prosthesis and rehabilitation applications.* Technology and Health Care. 2002; 10: 107-120

[13] Clark, R. and Cowey, J. *Factors Controlling The Change Of Shape Of Certain Nemertran and Turbellarian Worms*. 1958: 731-748

[14] Freudenrich, Craig. *How Muscles Work*. www.health.howstuffworks.com

[15] http://library.thinkquest.org

[16] Gray, Henry. *Anatomy of the Human Body*. Philadelphia: Lea & Febiger, 1918; Bartleby.com, 2000; chapter IV. www.bartleby.com/107/ 10Jun06

[17] Suzuki, Madoka and Ishiwata, Shin'ichi. *Contractile Systems of Muscles*. 2004: 33-47

[18] Gasser, H. S. and Hill A.V. *The Dynamics of Muscular Contraction*. Proceedings of the Royal Society of London. Series B. Great Britain. 1922; 96: 398-437

[19] Lupton, H and Hill, A.V. *An analysis of the effects of speed on the mechanical efficiency of human muscular movement.* Journal of Physiology. 1923; 57(6): 337-353

[20] Ombrello, T. *The Sensitive Plant*. UCC Biology Department

[21] Ueda, M., Takada, N. and Yamamura, S. *Molecular Approach to the Nyctinastic Movement of the Plant Controlled by a Biological Clock*. International Journal of Molecular Sciences; 2001; 2: 156-164

[22] Baek, Namjin and Park, Kinam. *Natural Polymer Gels with Fast Responses*. 2004: 85 -96

[23] Hodgson, D., Wu, M. and Biermann, R. *Shape Memory Alloys*. ASM International , Metals Handbook – Properties and Selection: Nonferous Alloys and Special-Purpose Materials. 10th edition. 1990; 2: 897-902

[24] John, Reji. *Rise of Smart Materials and Structures*. The Hindu. 2001

[25] Chang L.C. and Read, T.A. *Plastic Deformation and Diffusionless Changes In Metals – The Gold-Cadmium Beta Phase*. American Institute of Mining and Metallurgical Engineers. 1951; 189: 47-52

[26] Kauffman, G. and Mayo, I. *The Story of Nitinol: The Serendipitous Discovery of the Memory Metal and Its Applications*. The Chemical Educator. Springer-Verlag, New York. 1996; 2(2)

[27] Simon et al, who designed the Simon Nitinol filter a vascular device (1977)

[28] Andreasen, G. and Barret, R. *An Evaluation of Cobalt-Substituted Nitinol Wire in Orthodontics.* American Journal of Orthodontics. May 1973; 63(5): 462-470

[29] Cutright, D. E, Bhaskar, S.N., Perez, B., Johnson, R.M. and Cowan Jr, G.S. M. *Tissue reaction to nitinol wire alloy.* Oral Surgery, Oral Medicine, Oral Pathology. 1973; 35, issue 4: 578-584

[30] Castleman, L.S., Motzkin, S.M. Alicandri, F. P. and Bonawit, V.L. *Biocompatibility of nitinol alloy as an implant material*. Journal of biomedical material research. 1976; 5:695-731

[31] Denoyer, K. K and Erwin, R. S. and Ninneman, R. R. *Advanced Smart Structures Flight Experiments for Precision Spacecraft.* Acta Astonautica. Elsevier Science. 2000; 2: 389-397

[32] Pacheco, P.M.C.L. and Savi, M.A. *Modeling and Simulation of a shape memory release device for aerospace application*. Brazil. 2000

[33] Webb, G., Wilson, L., Lagoudas, D. and Rediniots, O. *Adaptive Control of Shape Memory Alloy Actuators for Underwater Biomimetic Applications*. AIAA Journal. 2000; 38(2)

[34] Pfieffer, C., DeLaurentis, K and Mavroidis, C. *Shape Memory Alloy Actuated Robot Prosthesis: Initial Experiments*. IEEE International Conference on Robotics and Automation – Michigan. 1999

[35] Birman, V. *Theory and comparison of the effect of composite and shape memory alloy stiffeners on stability of composite shells and plates*. International Journal of Mechanical Science. 1997; 39(10): 1139-1149

[36] Mantovani, D. *Shape Memory Alloys: Properties and Biomedical Applications*. 2000

[37] Duerig, T., Stockel, P.D. *An overview of nitinol medical applications*. Materials Science and Engineering. 1999; A273-275: 149-160

[38] Machado, L.G. and Savi, M. A. "Medical Applications of Shape Memory Alloys". Brazilian Journal of Medical and Biological Research. June 2003; 36(6): 683-691

[39] Mantovani, Diego. *Shape Memory Alloys: Properties and Biomedical Applications.* Smart Materials. 2000

[40] Ryhanen, Jorma. *"Fundamental Characteristics of Nickel-Titanium Shape Memory Alloy". Biocompatibility Evaluation of Nickel-Titanium Shape Memory Metal Alloy.* Finland. 1999. Chapt 2-3

[41] *Introduction to Shape Memory Alloys*. www.smart.tamu.edu

[42] *Shape Memory Alloys*. SMA/MEMS Research Group. 2001

[43] Stalmans, R. and Humbeeck, J.V. *Shape Memory Alloys: Functional and Smart*. Smart materials and technology. Prague, Czech Republik. 1995.

[44] Hayashi, S., Hayashi, N., Tasaka, Y. and Akita, Y. *Development of Smart Polymer Materials and its Various Applications.* Mitsubishi Heavy Industries, Ltd. Technical Review. 2004; 41 (1)

[45] http://www.calo-mer.com

[46] Lendlein, A. and Langer, R. *Biodegradable, Elastic Shape-Memory Polymers for Potential Biomedical*

Applications. Science/AAAS. 2002; 296(5573): 1673-1676

[47] *Intelligent plastics change shape with light.* MIT tech talk. 2005

[48] Bar-Cohen, Y. "*Electroactive Polymers as Artificial Muscles – Capabilities, Potentials and Challenges* "Robotics and Space 2000. Albuquerque, NM

[49] Jang, B. *Advanced Polymer Composites*. ASM International. 1994; chapter 11

[50] McCutcheon, D. M., Reddy, J.N., O'Brien, M.J., Creasy, T.S. and Hawkins, G.F. *Damping composite materials by machine augmentation*. Journal of Sound and Vibration. 2006; 294: 828-840

[51] Kim, Jong Hyun. *Passive machine augmented composite for multifunctional properties*. TAMU Thesis. 2005

[52] Hawkins, G.F. *Augmenting the Mechanical Properties of Materials by Embedding Simple Machines.* Journal of Advanced Materials. 2002;34: 16

[53] Schulte Jr., H.F. *The Characteristics of the McKibben Artificial Muscle*. The Application of External Power In Prosthetics and Orthotics; a Report. 1961: 94-115

[54] Tondu, B. and Lopez, P. *The McKibben Muscle and its use in Actuating Robot-Arms Showing Similarities with Human Arm Behavior*. Industrial Robot. 1997: 432-439

[55] Laksanacharoen, S. *Artificial Muscle Construction Using Natural Rubber Latex in Thailand*. Bangkok

[56] Hannaford, B. and Winters, J. *Actuator Properties and Movement Control: Biological and Technological Models*. Multiple Muscle Systems. 1990

[57] Inoue, K. *Rubbertuators and applications for robot*. Robotics research: the fourth international symposium. 1987: 57-63

[58] Chou, CP and Hannaford, B. "*Measurement and Modeling of McKibben Pneumatic Artificial Muscles*". Robotics and Automation. IEEE. 996; 1(12): 90-102

[59] Bertetto, M. and Ruggiu, M. *Characterization and modeling of Air Muscles*. Mechanics Research Communication. 2004; 31: 185-194

[60] Klute, G. and Hannaford, B. *Fatigue characteristics of McKibben Artificial Muscle Actuators. Intelligent Robots and Systems.* 1998; 3: 1776-1783

[61] Winters, J. M. and Tannous, R. E. *Novel Artificial Muscle Design*: Development and testing. IEEE. 1993.

[62] Davis, S. *Enhanced Modeling and Performance in Braided Pneumatic Muscle Actuators*. The international Journal of Robotics Research. 2003; 22(3-4): 213-227

[63] Nakamura, T., Saga, N., and Yaegashi, K. *Development of a Pneumatic Artificial Muscle based on Biomechanical Characteristics*. IEEE. 2003

[64] Daerden, F and D. Lefeber. "*The Concept and Design of Pleated Pneumatic Artificial Muscles"*. The International Journal of Fluid Power. 2001; 2(3): 41-50

[65] Daerden, F., Lefeber, D., Verrelst, B. and Van Ham, R. *Pleated pneumatic artificial muscles: actuators for automation and robotics*. Advanced Intelligent Mechatronics. 2001

[66] Verrelst, B., Daerden, F., Lefeber, D., Van Ham, R., and Fabri, T. *Introducing Pleated Pneumatic Artificial Muscles for the Actuation of Legged Robots: a One-dimensional Set-up*. CLAWAR 2000

[67] Verrelst, B., Van Ham, R., Daerden, F., and Lefeber, D. *Design of a Biped Actuated by Pleated*

Pneumatic Artificial Muscles. CLAWAR 2002

[68] http://www.shadowrobot.com/

[69] *Air-bug – Artificial Muscles as Joint Actuators for a Six-Legged Walking Machine*; 2001

[70] http://www.festo.com

[71] Bar-Cohen, Y. Biologically *Inspired Robots as Artificial Inspectors.* NDT. 2002; 7(1)

[72] Caldwell, D. *Natural and Artificial Muscle Elements as Robot Actuators*. Mechatronics. 1993; 3(3): 269-283

[73] Klute, G., Czerniecki, J., Hannaford, B. *McKibben Artificial Muscles: Pneumatic Actuators with Biomechanical Intelligence*. IEEE/ASME. 1999

[74] Caldwell, D., Tsargarakis, N., Medrano-Cerda, G.A. *Bio-mimetic actuators: polymeric pseudo muscular actuators and pneumatic muscle actuators for biological emulation*. Mechatronics. 2000; 10: 499-530

[75] Ferris, D. Czerniecki, J. and Hannaford, B. *An Ankle-Foot Orthosis Powered by Artificial Pneumatic Muscles. Journal of Applied Biomechanics.* 2005; 21: 189-197

[76] L. Mullins. *Softening of Rubber by Deformation.* Rubber Chemistry and Technology (RC&T). February 1969; 1 (42): 339-361

NOMENCLATURE

ASTM	American Society of Testing and Materials
Au-Cd	Aluminum-cadmium alloy
CuAlNi	Copper-aluminum-nickel
Cu-Sn	Copper-tin alloy
Cu-Zn	Copper-zinc alloy
CuZnAl	Copper-zinc-aluminum
FEM	Finite element analysis
MAC	Machine augmented composites
Ni-Ti	Nickel-titanium
Nitinol	Nickel-Titanium Naval Ordinance Laboratory
PAM	Pneumatic muscle actuator
PET	Polyethylene terephthalate
pH	A measure of acidity or alkalinity
PPAM	Pleated pneumatic artificial muscle
SMA	Shape memory alloy
SMP	Shape memory polymer
Tg	Glass transitions

REFERENCES

1. History of biomechanics and kinesiology, Available at http://www.usd.edu/~jarichar/HIST.html. Access date: October 2006.
2. Aristotle. Translated by Peck, A., Forster, E. Volume XII. Parts of Animals, Movement of Animals, Progression of Animals. Loeb Classical Library. Cambridge, MA: Havard University Press. 1961; 8.
3. Muscles. Available at http://www.kidshealth.org/kid/body/muscles_noSW.html reviewed by Steven Dowshen, M.D. Access date: April 2006.
4. Farabee, M.J. Muscular and skeletal systems. Available at http://www.emc.maricopa.edu/faculty/farabee/biobk/BioBookMUSSKEL.html. Access date: April 2006.
5. Lightner, S., Lincoln, R. The fluidic muscle: A 'new' development. The International Journal of Modern Engineering. 2002; 2(2).
6. Campbell, N. Biological foundations. Biology 4th edition. San Fransicsco: Benjamin Cummings. 1996.
7. Kanzawa, N., Tsuchiya, T. Seismonastic movements in plants, Reflexive Polymers and Hydrogels. 2004: 17-31.
8. Johnson, R. C. Darpa funds working on rigid shape-shifting materials. Electronic Engineering Times. Oct 2004; 1341: 22.
9. Herr, H., Whitley, G., Childress, D. Cyborg technology – biomimetic orthotic and prosthetic technology. In: Biologically Inspired Intelligent Robots.

Bellingham, Washington: SPIE Press. 2003: 2-31

10. Woo, G. Artificial organs produce genuine benefits. Medical Device & Diagnostic Industry Magazine. May 1998.
11. American Heritage® Dictionary of the English Language, Fourth Edition copyright ©2000 by Houghton Mifflin Company. Updated in 2003. Published by Houghton Mifflin Company.
12. Caldwell, D.G. and Tsagarakis, N. Bio-mimetric actuations in prosthesis and rehabilitation applications. Technology and Health Care. 2002; 10: 107-120.
13. Clark, R., Cowey, J. Factors Controlling The Change Of Shape Of Certain Nemertran and Turbellarian Worms. 1958: 731-748.
14. Freudenrich, C. How Muscles Work. Available at http://health.howstuffworks.com/muscle.htm. Access date: October 2006.
15. The basic muscle structure. Available at http://library.thinkquest.org/3379/basic.htm. Access date: October 2006.
16. Gray, H. Anatomy of the Human Body. Philadelphia: Lea & Febiger, 1918; Bartleby.com, 2000; chapter IV. Available at www.bartleby.com/107/. Accessed on 10Jun06.
17. Suzuki, M., Ishiwata, S. Contractile Systems of Muscles. In Reflexive polymers and hydrogels: Understanding and designing fast-responsive polymeric systems. (ed. by N. Yui, R. Mrsny and K. Park), CRC Press LLC. 2004: 33-47.
18. Gasser, H. S., Hill A.V. The dynamics of muscular contraction. Proceedings of

the Royal Society of London. Series B. Great Britain. 1922; 96: 398-437.

19. Lupton, H., Hill, A.V. An analysis of the effects of speed on the mechanical efficiency of human muscular movement. Journal of Physiology. 1923; 57(6): 337-353.

20. Ombrello, T. The Sensitive Plant. UCC Biology Department. Available at http://faculty.ucc.edu/biology-ombrello/POW/sensitive_plant.htm. Access date: October 2005.

21. Ueda, M., Takada, N., Yamamura, S. Molecular approach to the nyctinastic movement of the plant controlled by a biological clock. International Journal of Molecular Sciences; 2001; 2: 156-164.

22. Baek, N., Park, K. Natural Polymer Gels with Fast Responses. Reflexive Polymers and Hydrogels: In: Nobuhiko Yui, Randall J Mrsny and Kinam Park, editors. Culinary and Hospitality Industry Publications Services.2004: 85 -96.

23. Hodgson, D., Wu, M., Biermann, R. Shape memory alloys. ASM International , Metals Handbook – Properties and Selection: Nonferous Alloys and Special-Purpose Materials. 10th edition. 1990; 2: 897-902.

24 John, Reji. Rise of Smart Materials and Structures. The Hindu. November 22nd, 2001.

25. Chang L.C., Read, T.A. Plastic deformation and diffusionless changes in metals – the gold-cadmium beta phase. American Institute of Mining and Metallurgical Engineers. 1951; 189: 47-52.

26. Kauffman, G., Mayo, I. The story of nitinol: The serendipitous discovery of the

memory metal and its applications. The Chemical Educator. New York: Springer-Verlag. 1996; 2(2).

27. Simon, M. Blood Clot Filter. US Patent. January 1984.

28. Andreasen, G., Barret, R. An evaluation of cobalt-substituted nitinol wire in orthodontics. American Journal of Orthodontics. May 1973; 63(5): 462-470.

29. Cutright, D. E, Bhaskar, S.N., Perez, B., Johnson, R.M., Cowan Jr, G.S. M. Tissue reaction to nitinol wire alloy. Oral Surgery, Oral Medicine, Oral Pathology. 1973; 35, issue 4: 578-584.

30. Castleman, L.S., Motzkin, S.M. Alicandri, F. P., Bonawit, V.L. Biocompatibility of nitinol alloy as an implant material. Journal of Biomedical Material Research. 1976; 5:695-731.

31. Denoyer, K. K., Erwin, R. S. and Ninneman, R. R. Advanced smart structures flight experiments for precision spacecraft. Acta Astonautica. Elsevier Science. 2000; 2: 389-397.

32. Pacheco, P.M.C.L., Savi, M.A. Modeling and simulation of a shape memory release device for aerospace application. Available at http://www.lavi.coppe.ufrj.br/~savi/Publicacoes/SMASep_Unesp00.pdf. Brazil. 2000.

33. Webb, G., Wilson, L., Lagoudas, D., Rediniots, O. Adaptive control of shape memory alloy actuators for underwater biomimetic applications. AIAA Journal. 2000; 38(2).

34. Pfieffer, C., DeLaurentis, K., Mavroidis, C. Shape memory alloy actuated robot

prosthesis: initial experiments. IEEE International Conference on Robotics and Automation – Michigan. 1999.

35. Birman, V. Theory and comparison of the effect of composite and shape memory alloy stiffeners on stability of composite shells and plates. International Journal of Mechanical Science. 1997; 39(10): 1139-1149.

36. Mantovani, D. Shape memory alloys: Properties and biomedical applications. Smarts Materials. Journal of the Minerals, Metals and Materials Society. October 2000.

37. Duerig, T., Stockel, P.D. An overview of nitinol medical applications. Materials Science and Engineering. 1999; A273-275: 149-160.

38. Machado, L.G., Savi, M. A. Medical applications of shape memory alloys. Brazilian Journal of Medical and Biological Research. June 2003; 36(6): 683-691.

39. Mantovani, D. Shape memory alloys: Properties and biomedical applications. Smart Materials. Journal of Minerals, Metal and Materials Society. October 2000.

40. Ryhanen, J. Fundamental characteristics of nickel-titanium shape memory alloy. In: Biocompatibility Evaluation of Nickel-Titanium Shape Memory Metal Alloy. Oulu University Library. Finland. 1999.

41. Detailed introduction to Shape Memory Alloys. http://smart.tamu.edu/overview/smaintro/detailed/detailed.html. Access date: April 2006.

42. SMA/MEMS Research group. Shape Memory Alloys. Available at http://www.cs.ualberta.ca/~database/MEMS/sma_mems/sma.html. 2001.

43. Stalmans, R., Humbeeck, J.V. Shape Memory Alloys: Functional and Smart. Smart materials and technologies – sensors, control systems and regulators. Prague, Czech Republic. 1995. Available at http://www.colorado.edu/ASEN/asen4012/MaterialsPapers/SMA%20functional%20and%20smart.pdf. Access date: October 2006.

44. Hayashi, S., Hayashi, N., Tasaka, Y., Akita, Y. Development of smart polymer materials and its various applications. Mitsubishi Heavy Industries, Ltd. Technical Review. 2004; 41 (1).

45. Calo-MER. Available at http://www.polymertech.com/materials/calomer.html. Access date: April 2006

46. Lendlein, A., Langer, R. Biodegradable, elastic shape-memory polymers for potential biomedical applications. Science/AAAS. 2002; 296(5573): 1673-1676.

47. Thomson, E. Intelligent plastics change shape with light. MIT tech talk. Available at http://web.mit.edu/newsoffice/2005/smart-plastics.html. 2005.

48. Bar-Cohen, Y. Electroactive Polymers as Artificial Muscles – Capabilities, Potentials and Challenges. Robotics 2000 and Space 2000. Albuquerque, NM. Available at http://ndeaa.jpl.nasa.gov/ndeaa-pub/Japan/biomimetic-polymers-handbook.pdf.

49. Jang, B. Advanced polymer composites. ASM International. Portland, OR:

Annotation Copyright Book News, Inc. 1994.

50. McCutcheon, D. M., Reddy, J.N., O'Brien, M.J., Creasy, T.S., Hawkins, G.F. Damping composite materials by machine augmentation. Journal of Sound and Vibration. 2006; 294: 828-840.

51. Kim, J-H. Passive machine augmented composite for multifunctional properties. M.S. Thesis, Texas A&M University. College Station, 2005.

52. Hawkins, G.F. Augmenting the mechanical properties of materials by embedding simple machines. Journal of Advanced Materials. 2002;34: 16.

53. Schulte Jr., H.F. The characteristics of the McKibben artificial muscle. The Application of External Power In Prosthetics and Orthotics; a Report. 1961: 94-115.

54. Tondu, B., Lopez, P. The McKibben muscle and its use in actuating robot-arms showing similarities with human arm behavior. Industrial Robot. MCB UP Ltd. 1997; 24(6): 432-439.

55. Laksanacharoen, S. Artificial muscle construction using natural rubber latex in Thailand. Bangkok. Available at http://biobot.kmitnb.ac.th/publications/msat.pdf. Access date: February 2006.

56. Hannaford, B., Winters, J. Actuator Properties and Movement Control: Biological and Technological Models. In: J.M. Winters, editor. Multiple Muscle Systems, J.M. Winters, Ed., Placellocation: Springer Verlag, 1990.

57. Inoue, K. Rubbertuators and applications for robot. Robotics Research: The Fourth International Symposium. University of California, Santa Clara,

California. 1987: 57-63.

58. Chou, CP., Hannaford, B. Measurement and modeling of McKibben pneumatic artificial muscles. Robotics and Automation. IEEE. 996; 1(12): 90-102.

59. Bertetto, M. and Ruggiu, M. Characterization and modeling of air muscles. Mechanics Research Communication. 2004; 31: 185-194.

60. Klute, G., Hannaford, B. Fatigue characteristics of McKibben artificial muscle actuators. Intelligent Robots and Systems. 1998; 3: 1776-1783.

61. Winters, J. M., Tannous, R. E. Novel artificial muscle design: development and testing. IEEE Journal. 1993. 940-941.

62. Davis, S. Enhanced modeling and performance in braided pneumatic muscle actuators. The International Journal of Robotics Research. 2003; 22(3-4): 213-227.

63. Nakamura, T., Saga, N., Yaegashi, K. Development of a pneumatic artificial muscle based on biomechanical characteristics. IEEE Journal. 2003; 2: 729-734.

64. Daerden, F., Lefeber, D. The concept and design of pleated pneumatic artificial muscles. The International Journal of Fluid Power. 2001; 2(3): 41-50.

65. Daerden, F., Lefeber, D., Verrelst, B., Van Ham, R. Pleated pneumatic artificial muscles: actuators for automation and robotics. Advanced Intelligent Mechatronics. 2001; 2: 738-743.

66. Verrelst, B., Daerden, F., Lefeber, D., Van Ham, R., Fabri, T. Introducing Pleated Pneumatic Artificial Muscles for the Actuation of Legged Robots: a One-dimensional Set-up. CLAWAR 2000

67. Verrelst, B., Van Ham, R., Daerden, F., Lefeber, D. Design of a Biped Actuated by Pleated Pneumatic Artificial Muscles. CLAWAR 2002.

68. Air Muscle. Available at http://www.shadowrobot.com/airmuscles/overview.shtml. Access date: October 2005.

69. Kerscher, T., Albiez, J., Berns, K. Air-bug – Artificial Muscles as Joint Actuators for a Six-Legged Walking Machine; Available at http://www.fzi.de/KCMS/kcms_file.php?action=link&id=257. 2001

70. FESTOs.Available at https://enep.festo.com/irj/servlet/prt/portal/prtroot/festo.guest?NavigationTarget=ROLES://portal_content/com.festo.portal/sap40/v/cr/ssp/rl/com.festo.portal.sap40.v.cr.ssp.rl.ssp_pub/com.festo.portal.sap40.v.cr.ssp.ws.gnt_ssp_1/sho/cat/com.festo.portal.sap40.v.cr.ssp.iv.cat.cat&j_user=ano_ep_customer_us. Access date: October 2005.

71. Bar-Cohen, Y. Biologically inspired robots as artificial inspectors. Proceeding of the SPIE Smarts Structures and Materials. NDE. 2002; 7(1).

72. Caldwell, D. Natural and artificial muscle elements as robot actuators. Mechatronics. 1993; 3(3): 269-283.

73. Klute, G., Czerniecki, J., Hannaford, B. McKibben artificial muscles: pneumatic actuators with biomechanical intelligence. IEEE/ASME. 1999.

74. Caldwell, D., Tsargarakis, N., Medrano-Cerda, G.A. Bio-mimetic actuators: polymeric pseudo muscular actuators and pneumatic muscle actuators for

biological emulation. Mechatronics. 2000; 10: 499-530.

75. Ferris, D. Czerniecki, J., Hannaford, B. An ankle-foot orthosis powered by artificial pneumatic muscles. Journal of Applied Biomechanics. 2005; 21: 189-197.

76. L. Mullins. Softening of rubber by deformation. Rubber Chemistry and Technology (RC&T). February 1969; 1 (42): 339-361.

APPENDIX

1. Calculate the extended displacement that would be used for the cyclic test by following these calculations:

   a. (ε) Strain (%):

$$\left(\frac{l_f}{l_i}\right) * 100 \qquad (1)$$

   Where, l_i = initial gage length

   l_f = final gage length (failure displacement)

   b. Find 90 percent of strain (%):

$$straing \Rightarrow \left(\frac{90}{100}\right) * strain \qquad (2)$$

   Where, $strain_g$ = 90 percent of strain

   c. Extended displacement (mm):

$$le \Rightarrow \frac{(li * straing)}{100} \qquad (3)$$

   Where, l_e = extended gage length

2. Conversion of force and displacement:

   a. $N \Rightarrow (lbs * 4.4482216)$

   $mm \Rightarrow (in * 25.4)$

3. Calculations used to determine work, work-density, stress, strain.

a. Example for the double embedded McKibben muscle sheet

i. area of double embedded muscle sheet:

$$area = \left(\frac{width * depth}{n} \right) \quad (4)$$

where, n = 2 (number of McKibben muscle)

ii. volume of double embedded muscle sheet:

$$volumeC = \left(\frac{width * depth * gagelength}{n} \right) \quad (5)$$

$$volumeE = \left(\frac{width * depth * extendedgagelength}{n} \right) \quad (6)$$

where, n = 2 (number of McKibben muscle)

C = contraction

E = extended

iii. stress of double embedded muscle sheet:

$$stress = \left(\frac{force}{area} \right) \quad (7)$$

iv. strain of double embedded muscle sheet:

$$strain = \left(\frac{\mathrm{l}_{n\,ew}}{l_i} \right) \quad (8)$$

where, l_{new} = new gage length while its loading and unloading

v. output work of the double embedded muscle sheet:

$$Work = \left(\sum_{i=1}^{m} \left(\frac{\left(\frac{f_{m-1} + f_m}{2} \right) * \left(l_m - l_{m-1} \right)}{1000} \right) + W_{m-1} \right) \quad (9)$$

where, m = number of data point

vi. work-density of the double embedded muscle sheet when contracted and extended:

$$work - densityC = \left(\frac{\frac{Work}{volC}}{10\text{^}6} \right) \quad (10)$$

$$work - densityE = \left(\frac{\frac{Work}{volE}}{10\text{^}6} \right) \quad (11)$$

VITA

Omotayo Folasade Ewumi acquired her Bachelor of Science degree in Mechanical Engineering from the University of Wisconsin-Madison in August of 1997. After working in industry for seven years with John Deere and the U.S. Coast Guard, Omotayo decided to the academic. Omotayo began her graduate research in September 2004 at Texas A&M University and acquired her Master of Science degree in Mechanical Engineering focusing on Polymers in August 2007. Her graduate research was focused on muscles, nastic, and the biomedical field.

Ms. O. F. Ewumi can be reached at c/o Dr. Creasy, Department of Mechanical Engineering, Texas A & M University, 309 Engineering/Physics building, College Station, TX 77843-3123. Her email address is ofewumi@yahoo.com.